NATIONAL ADVISORY COMMITTEE FOR AERONAUTICS

TECHNICAL NOTE 2966

PROPELLER-PERFORMANCE CHARTS FOR TRANSPORT AIRPLANES

By Jean Gilman, Jr.

Langley Aeronautical Laboratory
Langley Field, Va.

Washington
July 1953

NATIONAL ADVISORY COMMITTEE FOR AERONAUTICS

TECHNICAL NOTE 2966

PROPELLER-PERFORMANCE CHARTS FOR TRANSPORT AIRPLANES

By Jean Gilman, Jr.

SUMMARY

The preliminary selection of a propeller on the basis of cruising and take-off performance for application to transport airplanes at flight Mach numbers up to 0.8 can be accomplished by the use of the charts and methods presented. The charts are of sufficient scope to permit a fairly rapid evaluation of the propeller performance for engine power ratings of 1,000 to 10,000 horsepower. The method is presented primarily in the interest of propeller-noise abatement.

INTRODUCTION

Increasing engine power ratings, together with expanding airport operations and greater concentrations of people near airports, have led to serious complaints in regard to airplane noise. Inasmuch as the airplane propeller is a major offender as a producer of high noise levels, a general study of the propeller-noise problem has been undertaken by the National Advisory Committee for Aeronautics. The initial phase of this study concerned quiet propeller operation for the light personal-owner airplane and the results have been presented in references 1 and 2. The propeller-noise investigation has now been extended to include transport airplanes having engines with power ratings of 1,000 to 10,000 horsepower.

Reference 3 presents methods and charts for estimating propeller noise, and indicates the factors which govern the intensity of the noise. The present paper is concerned with the performance of propellers selected on the basis of quiet operation. This paper and reference 3 are intended to be used in conjunction with each other. Presented herein are charts by means of which the performance of various propeller configurations at cruising and take-off conditions can be quickly analyzed.

It is presupposed that the preliminary airplane design has progressed to the point where the cruising velocity, altitude, and engine power ratings have been determined. It is also presumed that the airplane

weight, the velocity required for take-off, and the lift-drag ratio of the airplane for take-off have been established. With these factors known, the propeller analysis can proceed along the lines suggested in the paper.

SYMBOLS

AF	activity factor per blade
B	number of blades
b	blade width (chord), ft
C_L	airplane lift coefficient
C_P	power coefficient, $P/\rho n^3 D^5$
$C_{P_X} = \frac{C_P}{X}$	
C_T	thrust coefficient, $T/\rho n^2 D^4$
c_d	section drag coefficient
c_l	section lift coefficient
c_{l_d}	design section lift coefficient
D	propeller diameter, ft; drag, lb
E_r	rotational energy per unit time in slipstream, ft-lb/sec
h	blade section maximum thickness, ft
J	advance ratio, V/nD
K_s	coefficient for take-off run
L	airplane lift, lb
M	flight Mach number

M_R	rotational tip Mach number
N	propeller rotational speed, rpm
n	propeller rotational speed, rps
P	power, ft-lb/sec
P_{C_V}	power coefficient, $P/\rho V^3 D^2$
R	propeller tip radius, ft
r	radius to a blade element, ft
S	wing area, sq ft
s	take-off distance, ft
T	thrust, lb
T_o	static thrust, lb
T_1	net static thrust, lb
V	velocity of advance, ft/sec or mph
W	airplane weight, lb
X	power-coefficient adjustment factor
x	fraction of propeller tip radius, r/R
η	efficiency, JC_T/C_P or TV/P
η_a	efficiency of ideal actuator disk
η_i'	basic induced efficiency
η_i	induced efficiency
η_o	profile efficiency
μ	ground friction coefficient

ρ air density, slugs/cu ft

σ propeller-element solidity, $Bb/\pi Dx$

σc_l propeller-element load coefficient

Subscripts:

0.7R at 0.7-radius station

D profile drag

i induced

t take-off

DISCUSSION

The selection of propellers from performance considerations is a twofold problem. First of all, a reasonable cruising efficiency must be maintained. Secondly, the take-off run must remain within the limitations of practical airport runways. The selection of a propeller to meet both conditions usually involves consideration of a number of propellers in order to arrive at a suitable compromise. A series of propeller charts covering ranges of parameters suitable for quiet operation is presented herein and should give fairly rapid estimates of suitable propeller dimensions and the associated performance.

The discussion begins with a presentation of charts which are used in selecting propellers for the cruising condition. Then follows a consideration of the factors affecting the take-off run. To complete the discussion, charts for obtaining the thrust for calculating the take-off run are presented.

Performance in Cruising Condition

The selection of a propeller to satisfy the requirements of the cruising condition is accomplished through the use of four charts. Figure 1 is a composite plot, conveniently arranged to show the interrelationship of the major propeller design variables, which gives the basic induced efficiency η_i'. (The construction of this chart is explained in appendix A.) Figure 2 is an adjustment chart to account for various numbers of propeller blades. Figure 3 is an adjustment chart to be used when needed to accommodate dual-rotating propellers. Figure 4 gives the

profile efficiency, and thus accounts for blade profile drag. The overall efficiency is simply the product of the induced efficiency and the profile efficiency.

The procedure for using figure 1 is indicated by the arrows in the figure. The example shown involves a 3,800-horsepower engine for operation at an altitude of 25,000 feet with 400 miles per hour as the airplane cruising velocity (M = 0.54). The propeller is to be operated at a relatively low tip speed (say 700 feet per second) in an effort to obtain a low propeller-noise level. The combination of airplane forward speed (587 feet per second) and the tip speed just cited gives an advance ratio V/nD of 2.64. The arrows in figure 1 show that a trial diameter of 16 feet leads to a total activity factor of about 600. The basic induced efficiency is about 91 percent.

In working the problem in figure 1, the assumption has been made that the approximate required engine horsepower has been established. By a trial-and-error process, however, the application of the results in figure 1 could be extended to the problem of estimating the required engine horsepower, provided that the drag horsepower (airplane velocity multiplied by airplane drag) has been established.

Choice of number of blades and associated adjustment factor.- The basic induced efficiency of the propeller is subject to an adjustment which is dependent on the advance ratio, the total activity factor, and the number of blades, as shown in figure 2. The choice of the number of blades would ordinarily be governed by the obvious desirability of using blades of standard design that are available from the various propeller manufacturers. Such blades generally have activity factors varying from about 80 to approximately 150. A simple division of the total activity factor obtained from figure 1 by various numbers of blades gives required blade activity factors for the cruising condition.

The activity factor as obtained from figure 1 need not be exactly matched. The curves of figure 1 for total activity factor are based on propellers of optimum load distribution having the lift coefficient at the 0.7R station equal to 0.5. This is a desirable value, at least for flight Mach numbers up to about 0.8, but actually this lift coefficient can vary from about 0.4 to about 0.6 without undue harm to the propeller efficiency. Inasmuch as the induced efficiency is in reality a function of the product of the total activity factor and the operating lift coefficient, it is sufficient to match the total activity factor from figure 1 within approximately 20 percent.

The total activity factor for the example indicated by the arrows in figure 1 is about 600. The propeller configuration might consist of four blades having an activity factor of 150 each, for which figure 2 gives an adjustment value $\Delta\eta_i = -0.018$, or it might consist of six blades

having an activity factor of 100 each, for which $\Delta\eta_i = 0$. A choice of eight blades having an activity factor of 75 each would result in a positive $\Delta\eta_i$ adjustment but might lead to structurally undesirable blades.

In any event, the adjusted induced efficiency is given by

$$\eta_i = \eta_i' + \Delta\eta_i$$

Thus, in the example, the induced efficiency of the four-blade propeller is 0.892, and that of the six-blade propeller is 0.91.

Adjustment for dual rotation.- An examination of the lower right-hand corner of figure 1 shows that rather low values of η_i' are obtained at the higher values of V/nD and total activity factor. Figure 3 is a plot of the quantity E_r/P against J at various constant values of total activity factor and blade number. This quantity is the fractional energy loss due to rotation of the slipstream. Experience has shown that about 60 percent of this loss is recoverable through the use of dual-rotating propellers. Thus, the adjusted induced efficiency for a dual-rotating propeller is

$$\eta_i = \eta_i' + \Delta\eta_i + 0.6\,\frac{E_r}{P}$$

In the example of figure 1 a six-blade dual-rotating propeller would have an over-all induced efficiency of 0.946 as compared with 0.910 for the six-blade single-rotating propeller.

The results of reference 3 show that a dual-rotating propeller is noisier than a single-rotating propeller at a given power loading, propeller tip speed, diameter, and number of blades. Thus, for a given sound-intensity level, the dual-rotating propeller would require a lower tip speed than would the single-rotating propeller.

Adjustment for propeller blade drag.- Figure 4 is a plot of estimated profile efficiency as a function of flight Mach number with $J = \frac{V}{nD}$ as parameter. The curves correspond to a propeller having a thickness-ratio distribution as shown in figure 5. The approximate over-all propeller efficiency is given by the product

$$\eta = \eta_i \eta_o$$

for either single- or dual-rotating propellers.

For the sample problem indicated by the arrows in figure 1, where the conditions of the problem resulted in an advance ratio of 2.64 and a flight Mach number of 0.54, the corresponding value of η_o from figure 4 is 0.96. Thus the over-all efficiency η of the four-blade configuration would be $\eta_i\eta_o = 0.856$. The over-all efficiency of the six-blade configuration would be 0.874 for single rotation or 0.908 for dual rotation.

Summary outline of propeller selection procedure for cruising condition.- The foregoing discussion may be summarized by the following step-by-step procedure:

1. For the given cruising velocity, altitude, and shaft horsepower, choose a desired value of rotational tip speed πnD. Calculate V/nD from the equation

$$\frac{V}{nD} = \pi \frac{V}{\pi nD}$$

2. From figure 1, obtain the basic induced efficiency η_i' and the total activity factor for various propeller diameters.

3. Select a suitable number of blades for each case and use figure 2 to obtain the appropriate adjustment $\Delta\eta_i$. Compute η_i from the equation

$$\eta_i = \eta_i' + \Delta\eta_i$$

4. If dual rotation appears desirable, obtain the quantity E_r/P from figure 3 and compute η_i from

$$\eta_i = \eta_i' + \Delta\eta_i + 0.6 \frac{E_r}{P}$$

5. For the required flight Mach number and the trial value of V/nD, obtain η_o from figure 4. Compute η from the equation

$$\eta = \eta_i\eta_o$$

Performance in Take-Off

Factors governing take-off run.- A discussion of the factors affecting the take-off run is given in reference 4. It is pointed out that the major factors affecting the take-off run, aside from such factors as pilot technique, engine power variations, and presence or absence of wind, are weight of the plane, ground friction, air drag, and variation of thrust during the take-off run. By assuming a straight-line variation of thrust, which will be seen later to be a reasonable assumption, Diehl, in reference 4, obtained a simplified formula for the take-off run. In the notation of the present paper, the formula is:

$$s = \frac{K_s V_t^2}{\frac{T_1}{W}}$$

where

$$\frac{T_1}{W} = \frac{T_o}{W} - \mu$$

and where K_s is a function of the ratio

$$\frac{\frac{T_t}{W} - \frac{D}{L}}{\frac{T_o}{W} - \mu}$$

A plot of K_s against this ratio is reproduced from reference 4 and is given herein as figure 6.

Evaluation of the take-off run in a calm requires the value of static thrust and the value of thrust at take-off velocity; the other quantities in the take-off formula are presumed to be known. Before proceeding to methods for estimating these thrusts, typical values of μ and D/L will be cited. Reference 4 gives the value of μ for hard-surfaced runways as 0.02, which would be typical of normal commercial airports, and gives a range of values of μ for other types of runways. In this reference the suggestion is made that the maximum value of L/D for the airplane can be used with satisfactory accuracy in calculating the take-off run. Now that partially deflected flaps are commonly used in the take-off, the use of such a value in making

the calculation does not seem advisable. The value of L/D at take-off velocity for modern transport airplanes with flaps partially deflected is shown by some unpublished NACA data to be about 8 or 9.

Charts for determination of thrust for take-off run.- A convenient chart for estimating the thrust for the take-off run is given in figure 7. This chart is reproduced from reference 5. Figure 8 is an auxiliary chart (also reproduced from ref. 5) used to account for variations in activity factor. Figure 7 shows the ratio $C_T/C_P^{2/3}$ as a function of the quantity $J/C_P^{1/3}$ with the power coefficient C_{P_X} as parameter. The quantity C_{P_X} is obtained from

$$C_{P_X} = \frac{C_P}{X}$$

where X is a function of total activity factor as shown in figure 8.

In order to obtain the static thrust T_o it is necessary first to calculate C_P from the formula

$$C_P = \frac{P}{\rho n^3 D^5}$$

where P is the power in foot-pounds per second rather than the horsepower, and then to calculate C_{P_X}. This value of C_{P_X} is used to obtain $C_T/C_P^{2/3}$ for $\frac{J}{C_P^{1/3}} = 0$ and the static thrust is given by

$$T = \frac{C_T}{C_P^{2/3}} \frac{P}{nDC_P^{1/3}}$$

It should be noted that the power P and propeller rotational speed n in the above equations are likely to be different from the values used for the cruising condition. The difference between cruising and take-off engine power and rotational speed depends on the engine characteristics and on how the engine is operated.

The thrust at take-off velocity is obtained from the same equations used to obtain the static thrust except that the ratio $C_T/C_P^{2/3}$ is obtained for the value of $J/C_P^{1/3}$ corresponding to the take-off velocity. The velocity for take-off is given by

$$V_t^2 = \frac{2W}{\rho C_{L_t} S}$$

Although the propeller data used in preparing figure 7 were obtained from the results of tests of a relatively thick propeller having cylindrical blade shanks, values of static thrust obtained from figure 7 apply very well to more modern thinner propellers having airfoil shank sections, provided that moderately cambered blades $\left(c_{l_d} = 0.4 \text{ to } 0.6\right)$ are used. The results in figure 7 do not apply at all well for uncambered blades, but such blades are not suitable for operations involving the low section speeds necessary to reduce noise.

Take-off is usually accomplished at a constant value of C_{P_X}. Inasmuch as $J_t/C_P^{1/3}$ rarely exceeds a value of about 1.5, an inspection of the variation of $C_T/C_P^{2/3}$ with $J/C_P^{1/3}$ at a constant value of C_{P_X} between the limits $\frac{J}{C_P^{1/3}} = 0$ and $\frac{J}{C_P^{1/3}} \approx 1.5$ (fig. 7) shows that the assumption of a linear variation of thrust for calculating the take-off run (ref. 4) gives a reasonably accurate approximation of the actual variation of thrust.

Round-shank propeller blades undergo progressively larger drag losses as the airspeed is increased. For this reason, the results in figure 7 give values of thrust which are from 3 to 5 percent lower than the thrust of more modern propeller blades at airspeeds as low as 100 miles per hour. The error becomes even more pronounced at the higher airspeeds. For this reason, a series of charts has been prepared to show the efficiency of propellers having the thickness distribution of figure 5 for airspeeds from 100 to 250 miles per hour at NACA standard sea-level atmospheric conditions. The results for single-rotating propellers are given in figures 9 to 14 and the results for dual-rotating propellers are given in figures 15 to 18. For take-off velocities of 100 miles per hour or greater, these charts can be used to obtain closer estimates of the take-off thrust for propellers having airfoil shank sections than is given by figure 7. The efficiencies for

the higher velocities can be used for calculating initial rates of climb at sea level. The construction of these charts is explained in appendix B.

Summary outline of procedure for estimating take-off run.- The procedure for estimating the take-off run can be summarized as follows:

1. For each trial propeller, using take-off horsepower and rotational speed, compute C_P from

$$C_P = \frac{P}{\rho n^3 D^5}$$

2. Use figure 8 to find the quantity X as a function of the total activity factor determined from the preliminary calculation for the cruising condition. Compute C_{P_X} from the formula

$$C_{P_X} = \frac{C_P}{X}$$

3. Obtain from figure 7 the value of $C_T/C_P^{2/3}$ at $\frac{J}{C_P^{1/3}} = 0$ for the given value of C_{P_X}. Using this value, compute the static thrust:

$$T_o = \frac{C_T}{C_P^{2/3}} \frac{P}{nDC_P^{1/3}}$$

4. Compute the quantity $J_t/C_P^{1/3}$, where

$$J_t = \frac{V_t}{nD}$$

The velocity at take-off is given by

$$V_t^2 = \frac{2W}{\rho C_{L_t} S}$$

From figure 7 obtain the value of $C_T/C_P^{2/3}$ that corresponds to the quantities $J_t/C_P^{1/3}$ and C_{P_X}, and use this value to compute the take-off thrust:

$$T_t = \frac{C_T}{C_P^{2/3}} \frac{P}{nDC_P^{1/3}}$$

If V_t is equal to or greater than 100 miles per hour a more accurate value of take-off thrust can be obtained from figures 9 to 18. A value of η is obtained from the appropriate figure by direct reading or by interpolation, whereupon

$$T_t = \frac{(\eta P)_t}{V_t}$$

where V_t is in feet per second.

5. Calculate the quantity

$$\frac{\frac{T_t}{W} - \left(\frac{D}{L}\right)_t}{\frac{T_o}{W} - \mu}$$

and obtain K_s from figure 6.

6. Compute the take-off distance from

$$s = \frac{K_s V_t^2}{\frac{T_1}{W}}$$

where

$$\frac{T_1}{W} = \frac{T_o}{W} - \mu$$

CONCLUDING REMARKS

The present paper has been prepared with the idea of giving a reasonably short procedure for determining the effect of the major propeller variables on the cruising and take-off performance of propellers. The procedure consists of a trial-and-error process for arriving at a suitable propeller to meet both the cruising and take-off requirements. Additional data are given to aid in the estimation of initial rates of climb.

Langley Aeronautical Laboratory,
National Advisory Committee for Aeronautics,
Langley Field, Va., April 24, 1953.

APPENDIX A

CONSTRUCTION OF PROPELLER SELECTION CHARTS

References 1 and 6 present propeller selection charts in which the basic propeller parameters are interrelated in such a manner as to facilitate the selection of a propeller for a given design condition. For the purposes of the present paper, it was found convenient to rearrange these charts as propeller performance charts, as shown in figure 19. These charts show the optimum induced efficiency η_i as a function of $C_{P_i}{}^{-1/3}$ with $(\sigma c_l)_{0.7R}$ and J as parameters. Also included are lines of constant $P_{c_{v_i}}{}^{-1/3}$. There is a separate chart for each blade number because η_i is a function of blade number.

The induced efficiency η_i and the propeller-element load coefficient $(\sigma c_l)_{0.7R}$ are primarily functions of the power due to lift P_i rather than the total power P, and there is also some dependency on the distribution of lift along the blades. This latter dependency can be ignored in many cases with only a small loss in accuracy. For cases where the propeller operates near peak efficiency, η_i can be considered as being dependent on P rather than on P_i as a first approximation with sufficient accuracy for preliminary propeller analyses.

The parameter $C_P{}^{-1/3}$ is a convenient form of the power coefficient because it is directly proportional to the term nD as shown by the definition

$$C_P{}^{-1/3} = nD\left(\frac{\rho D^2}{P}\right)^{1/3}$$

The term nD has a direct bearing on the propeller-noise problem.

For normal transport-airplane cruising conditions it is desirable to operate the propeller with $c_{l_{0.7R}}$ at a value in the neighborhood of 0.5, the propeller being properly cambered for this lift coefficient in order to attain a maximum value of section lift-drag ratio. The induced efficiency is shown by the charts of figure 19 to be dependent on the

product $(\sigma c_l)_{0.7R}$. Thus, if the required value of $(\sigma c_l)_{0.7R}$ has been determined, an arbitrary assignment of a value to $c_{l_{0.7R}}$ gives the required value of $\sigma_{0.7R}$ by simple division. It can be seen that for a series of arbitrarily assigned values of $c_{l_{0.7R}}$ a corresponding series of values of $\sigma_{0.7R}$ results with no change in the induced efficiency. By keeping the range of lift coefficients in the approximate limits 0.4 to 0.6, there is also very little change in the section lift-drag ratio, and hence the over-all efficiency remains nearly constant.

Although the solidity $\sigma_{0.7R}$ is usually used as a measure of total blade width in theoretical investigations, the propeller industry has found it convenient to refer to the blade width in terms of activity factor. Reference 6 gives an approximate conversion factor:

$$\text{Total activity factor} \approx 2{,}600\sigma_{0.7R}$$

Thus, $(\sigma c_l)_{0.7R}$ can be expressed in terms of the product

$$\text{Total activity factor} \times c_{l_{0.7R}}$$

or, if $c_{l_{0.7R}}$ is given an arbitrary value of 0.5, then

$$\text{Total activity factor} \approx 2{,}600\,\frac{(\sigma c_l)_{0.7R}}{0.5} = 5{,}200(\sigma c_l)_{0.7R}$$

This definition of total activity factor was used in constructing figure 1.

The lower left-hand corner of figure 1 was constructed by plotting the quantity $(D^2/P)^{1/3}$ against shaft horsepower for constant values of D. The upper left-hand corner is a plot of $\rho^{1/3}(D^2/P)^{1/3}$ at constant values of ρ, where ρ is expressed in terms of NACA standard density altitude. The upper right-hand corner is a plot of $nD(\rho D^2/P)^{1/3}$ where nD is expressed in terms of the tip rotational speed πnD. The lower right-hand corner is obtained by plotting η_i' against $nD(\rho D^2/P)^{1/3}$

with V/nD and $(\sigma c_l)_{0.7R}$ (expressed in terms of total activity factor with $c_{l_{0.7R}} = 0.5$) as parameters. Figure 1 is based on a six-blade propeller. The adjustment factors in figure 2 are obtained by subtracting η_i' for a six-blade propeller from η_i for the same loading and V/nD for other numbers of blades.

The adjustment factors for dual-rotating propellers are derived from charts in reference 6 which show E_r/P in terms of $(\sigma c_l)_{0.7R}$, the number of blades, and V/nD. Figure 3 was constructed by expressing $(\sigma c_l)_{0.7R}$ in terms of total activity factor in the manner used for constructing figure 1.

APPENDIX B

CONSTRUCTION OF CHARTS OF PROPELLER EFFICIENCY AND TIP MACH NUMBER AT SEA LEVEL

The propeller-performance curves in figures 9 to 18 were obtained for most of the range by a method similar to that of references 1 and 6. The present method differs only in that the induced losses are obtained from figure 19, which is merely a rearrangement of the induced-loss charts of references 1 and 6, and values of the drag loss to correspond to the thickness distribution of figure 5 are used. The thickness distribution of figure 5 is considered to be more nearly typical of the thickness distribution of propellers currently in use than that of references 1 and 6. In particular, the round shanks have been eliminated.

The short method of estimating propeller performance is applicable for a range of $c_{l_{0.7R}}$ from approximately 0.15 to 0.8. For operating conditions not in this range it is necessary to make strip calculations as in reference 7, or to use experimental data if available.

In preparing figures 9 to 18, the element solidity per blade at the 0.7R station was taken to be 0.045. This value corresponds to an activity factor of about 120.

The variation with advance ratio of C_{T_D} and C_{P_D}, expressed in terms of $\sigma_{0.7R}$, is shown in figure 20. The distribution of the section drag coefficient used in calculating C_{T_D} and C_{P_D} is as follows:

Blade station, x	Section drag coefficient, c_d
0.30	0.010
.45	.009
.60	.008
.70	.007
.80	.006
.90	.006
.95	.006

The values listed for c_d are representative of minimum values for the thickness distribution of figure 5. Under actual operating conditions, some variations from the values listed are encountered, but these variations are not of importance unless the propeller is stalled or partially stalled. Because of these variations, it was considered to be sufficiently accurate to base the calculations of C_{T_D} and C_{P_D} on a propeller blade having a rectangular plan form.

As a matter of interest, figures 9 to 14 include curves of η_i for $B = 4$. These curves are representative of the upper limit of the efficiency (single-rotating propellers) for each operating condition. Values of η_a are given in the legends of figures 15 to 18 to indicate the upper limit for dual-rotating propellers.

REFERENCES

1. Crigler, John L., and Jaquis, Robert E.: Propeller-Efficiency Charts for Light Airplanes. NACA TN 1338, 1947.

2. Hubbard, Harvey H., and Regier, Arthur A.: Propeller-Loudness Charts for Light Airplanes. NACA TN 1358, 1947.

3. Hubbard, Harvey H.: Propeller-Noise Charts for Transport Airplanes. NACA TN 2968, 1953.

4. Diehl, Walter S.: The Calculation of Take-Off Run. NACA Rep. 450, 1932.

5. Uddenberg, R.: A General Propeller Chart Suitable for a Wide Range of Propellers. Rep. No. D-4842, Boeing Aircraft Co., May 12, 1943.

6. Crigler, John L., and Talkin, Herbert W.: Charts for Determining Propeller Efficiency. NACA WR L-144, 1944. (Formerly NACA ACR L4I29.)

7. Crigler, John L.: Comparison of Calculated and Experimental Propeller Characteristics for Four-, Six-, and Eight-Blade Single-Rotating Propellers. NACA WR L-362, 1944. (Formerly NACA ACR 4B04.)

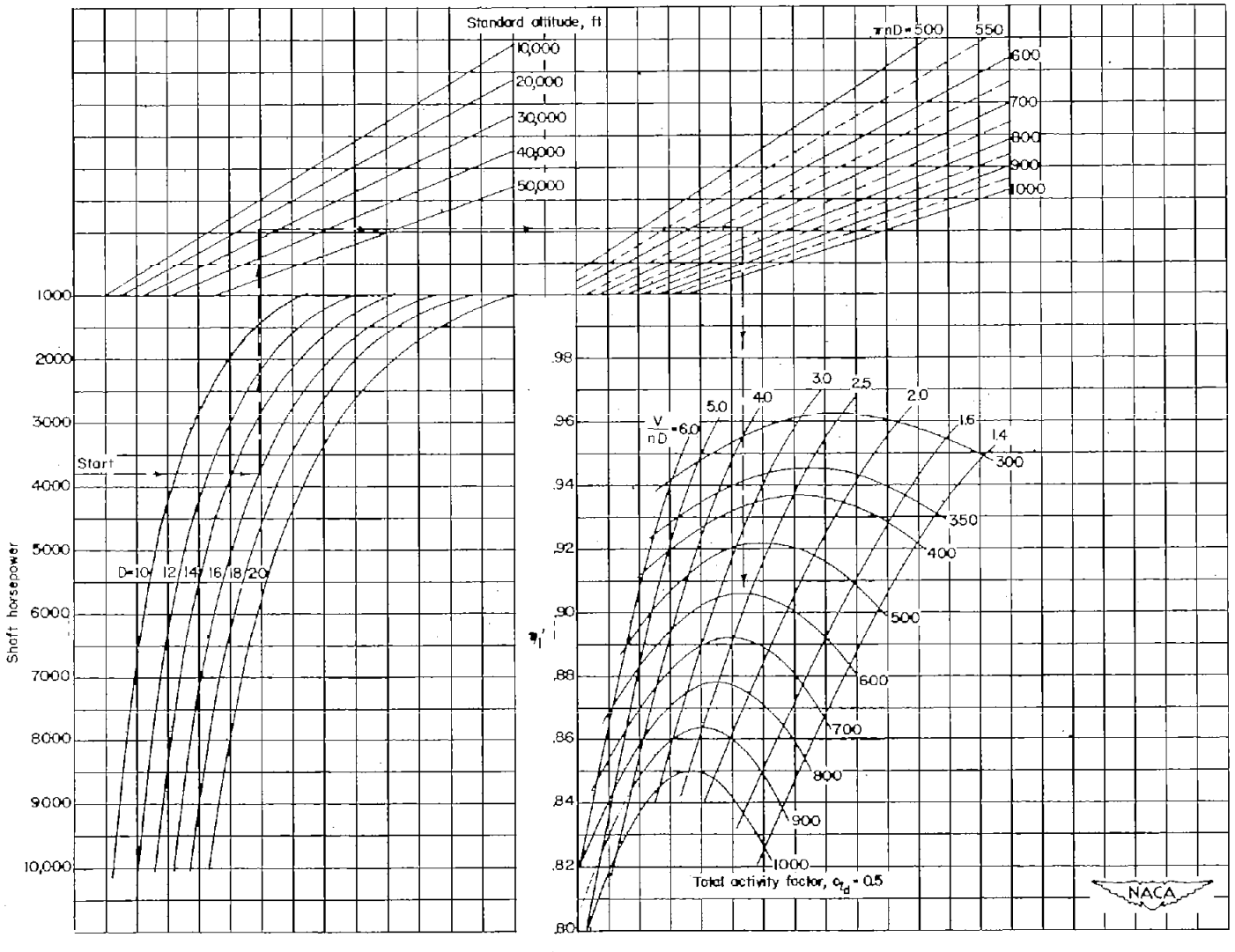

Figure 1.- Basic propeller selection chart for cruising condition. Six-blade propeller.

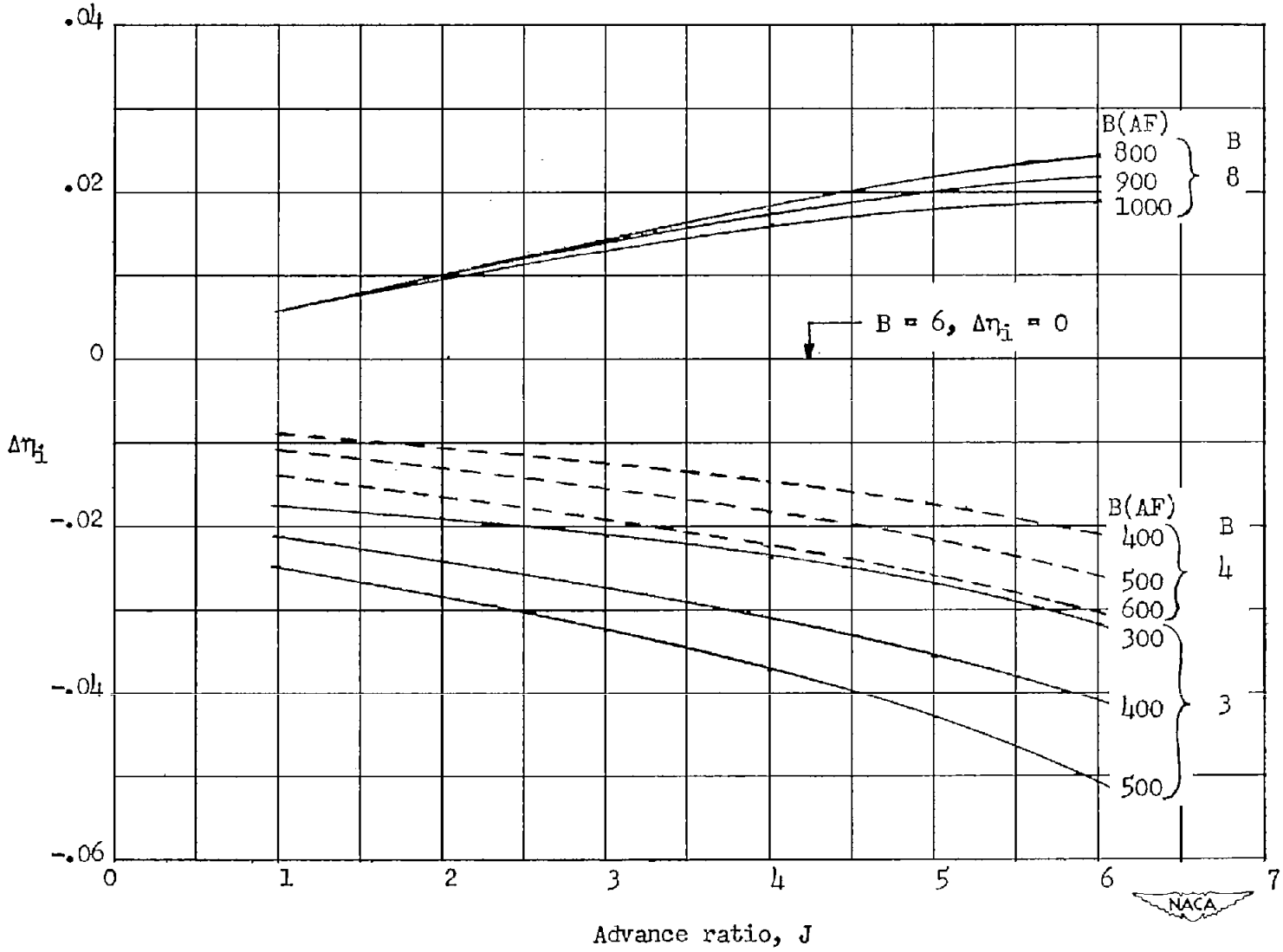

Figure 2.- Blade-number adjustment to basic induced efficiency η_i' for cruising condition.

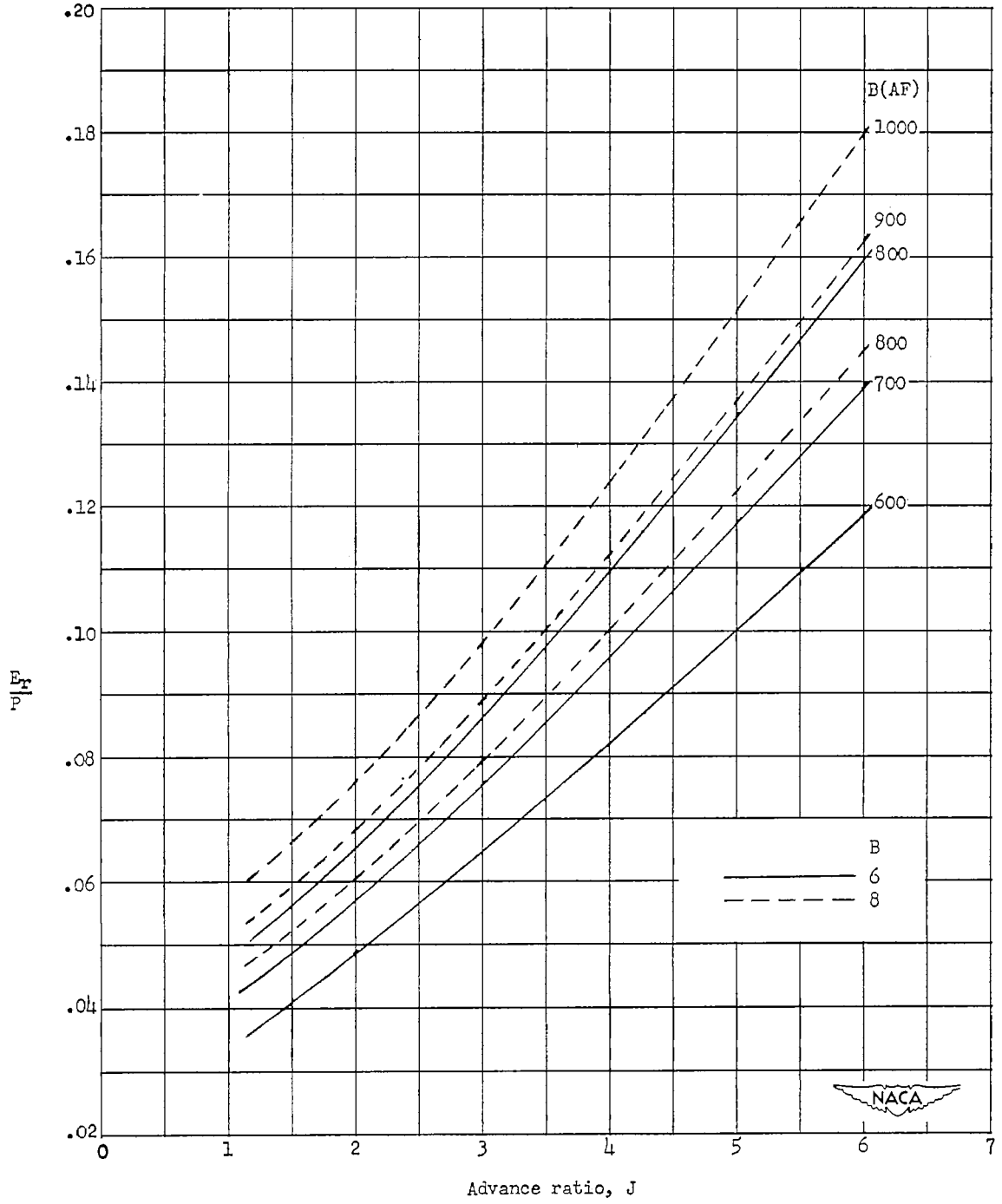

Figure 3.- Fractional energy loss due to slipstream rotation, to be used in adjusting basic induced efficiency of dual-rotating propellers.

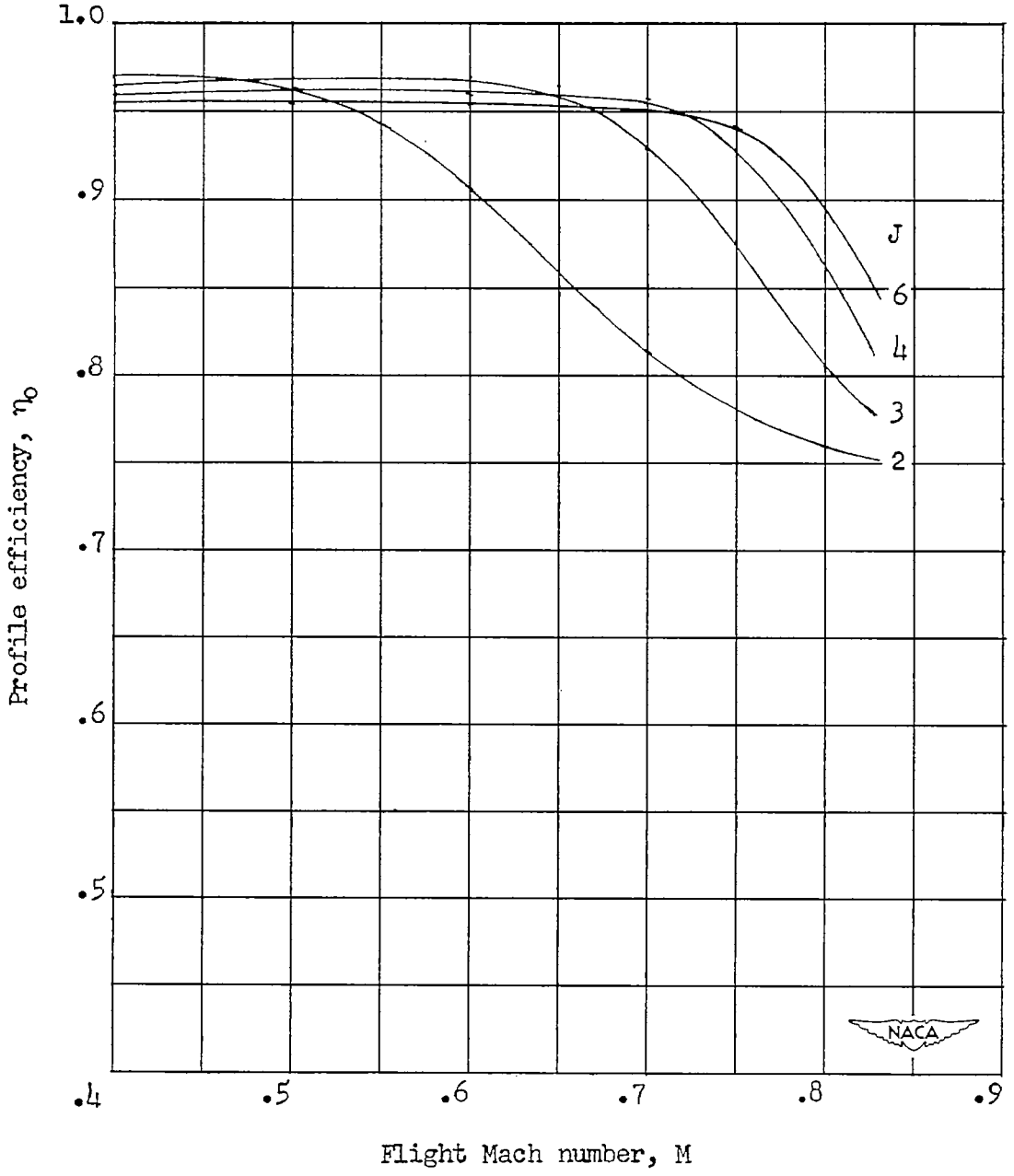

Figure 4.- Estimated variation of peak profile efficiency with flight Mach number for various advance ratios.

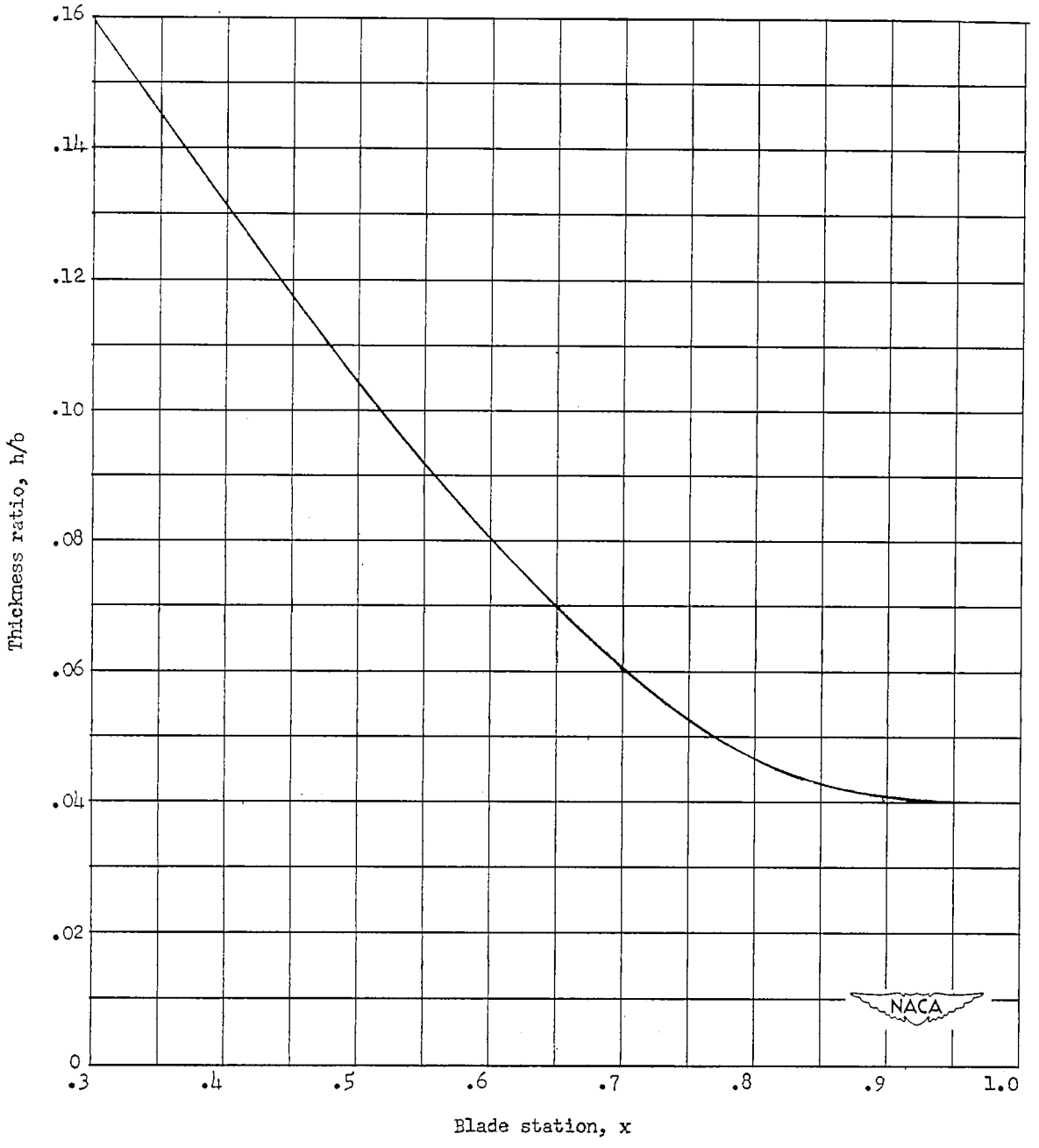

Figure 5.- Thickness distribution for representative transport propeller.

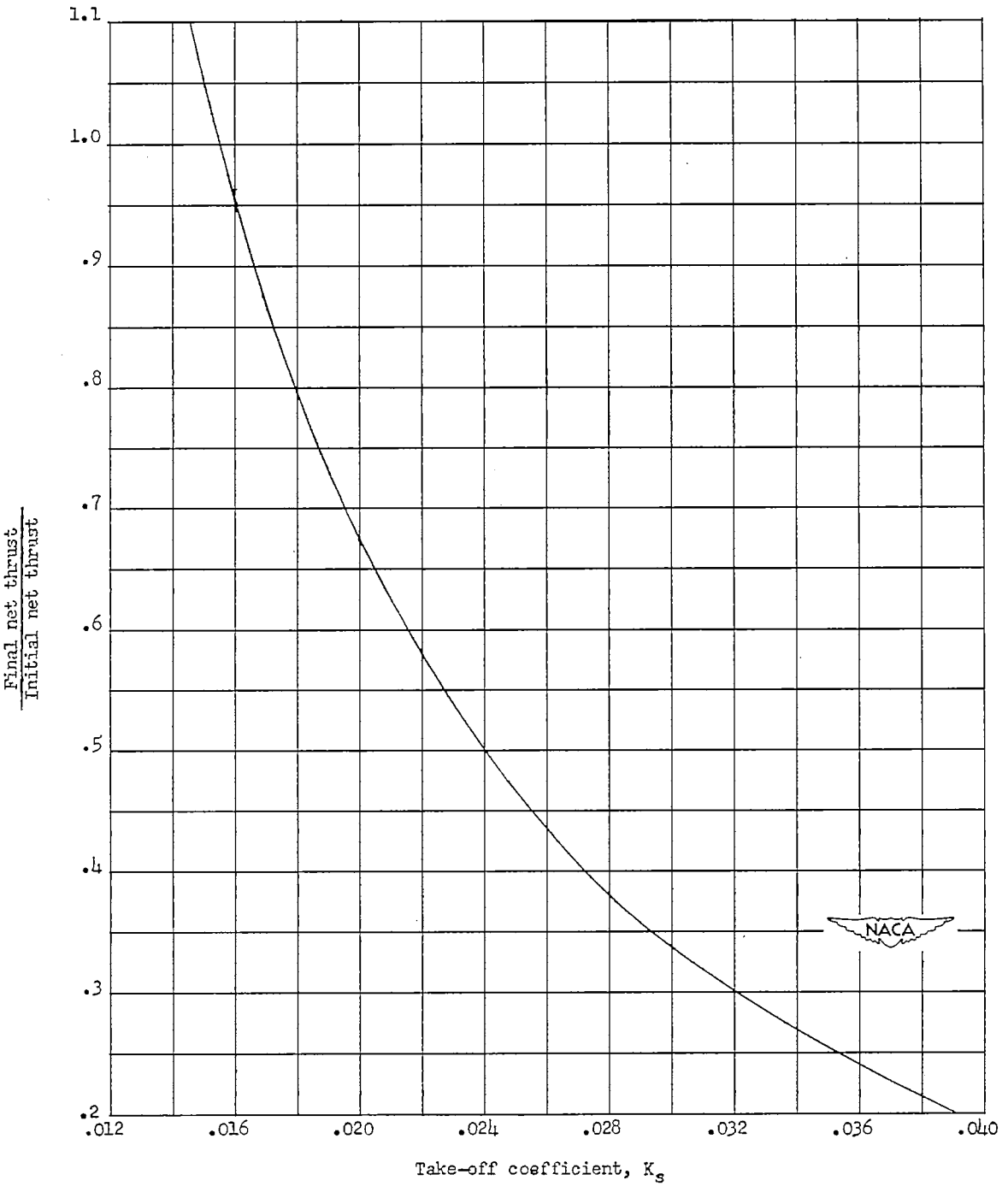

Figure 6.- Coefficient for take-off run in a calm. Reproduced from reference 4. $\frac{\text{Final net thrust}}{\text{Initial net thrust}} = \frac{\frac{T_t}{W} - \frac{D}{L}}{\frac{T_o}{W} - \mu}$.

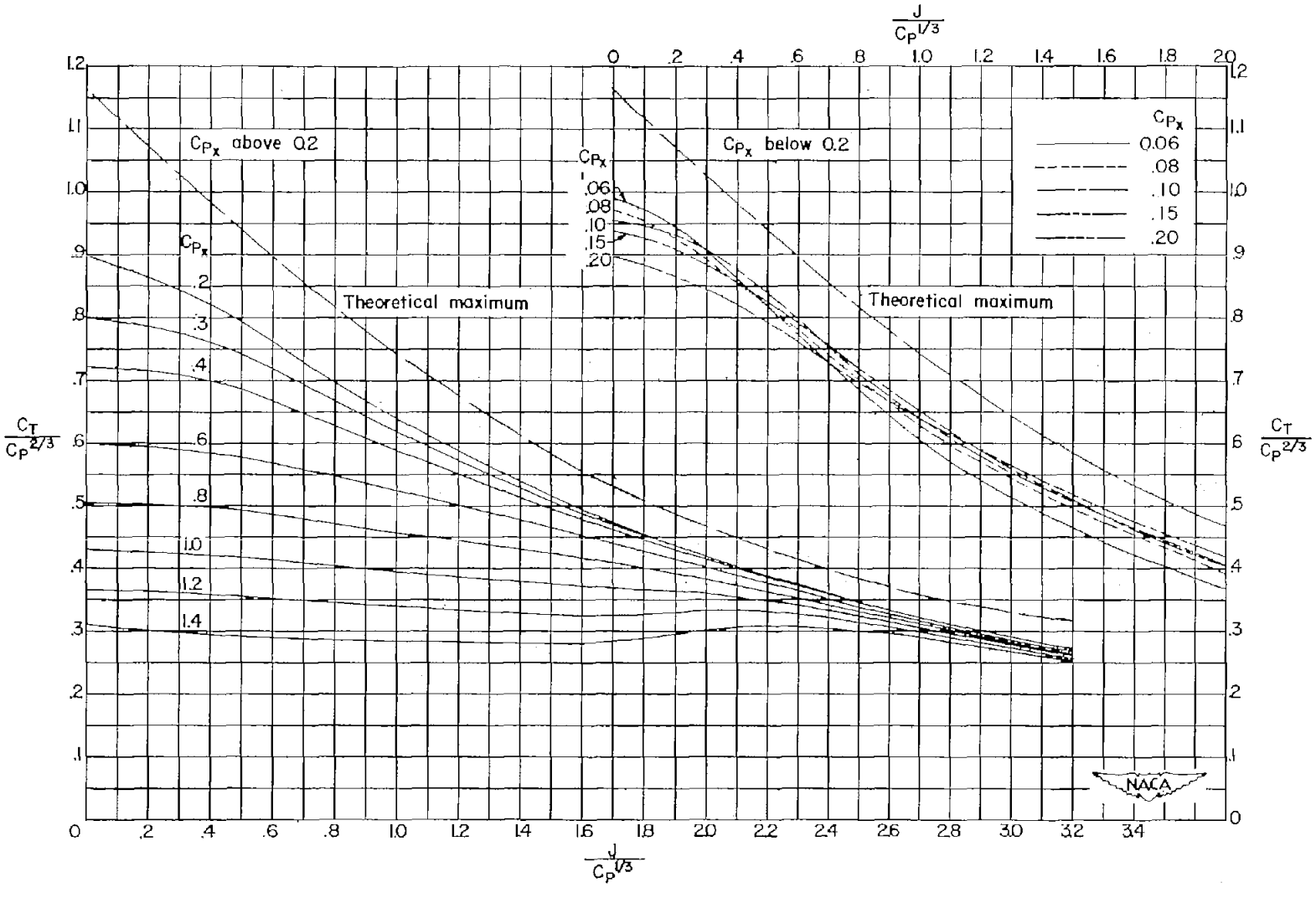

Figure 7.- General propeller chart for take-off. Reproduced from reference 5.

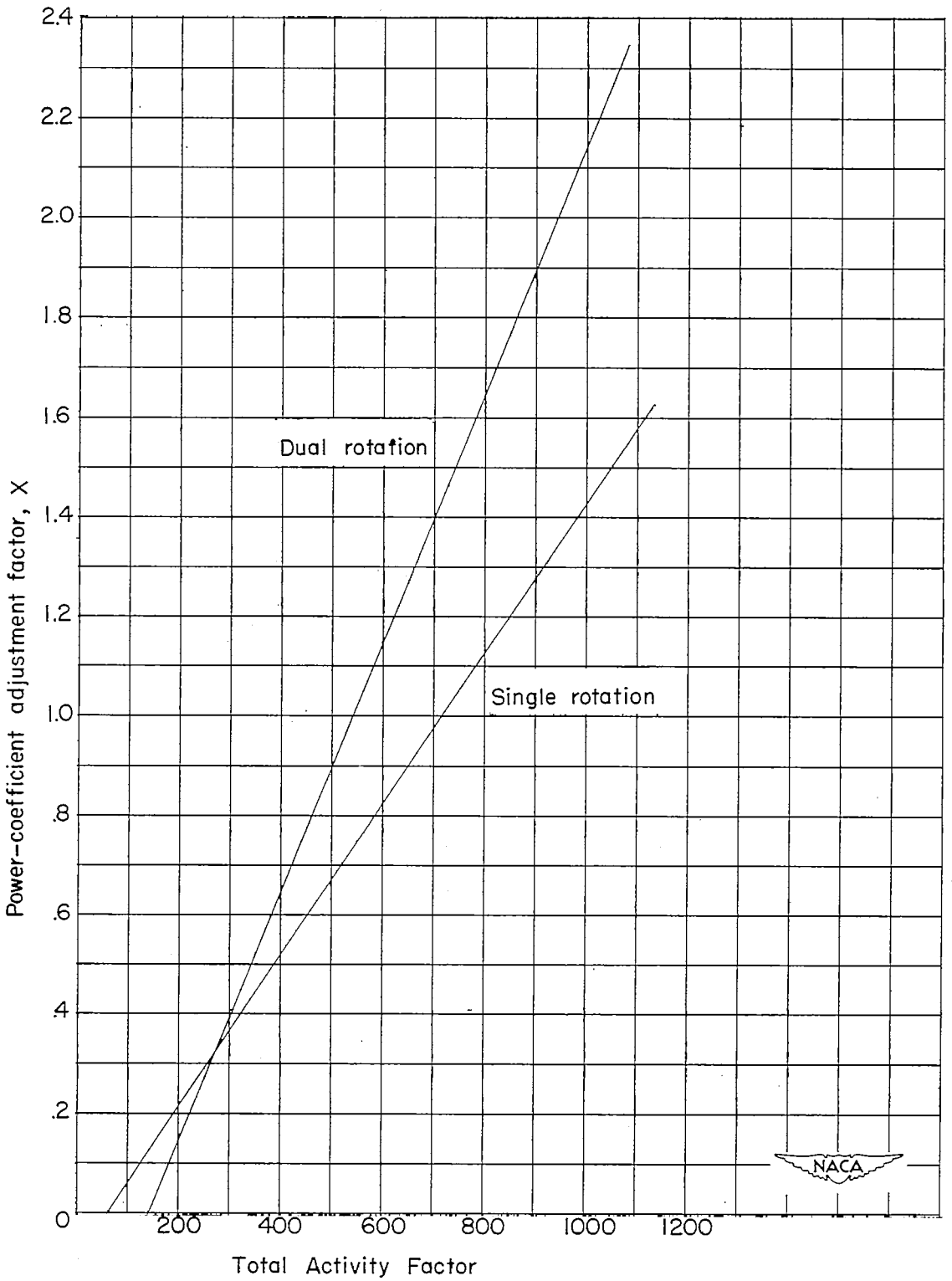

Figure 8.- Variation of power-coefficient adjustment factor X with total activity factor. Reproduced from reference 5.

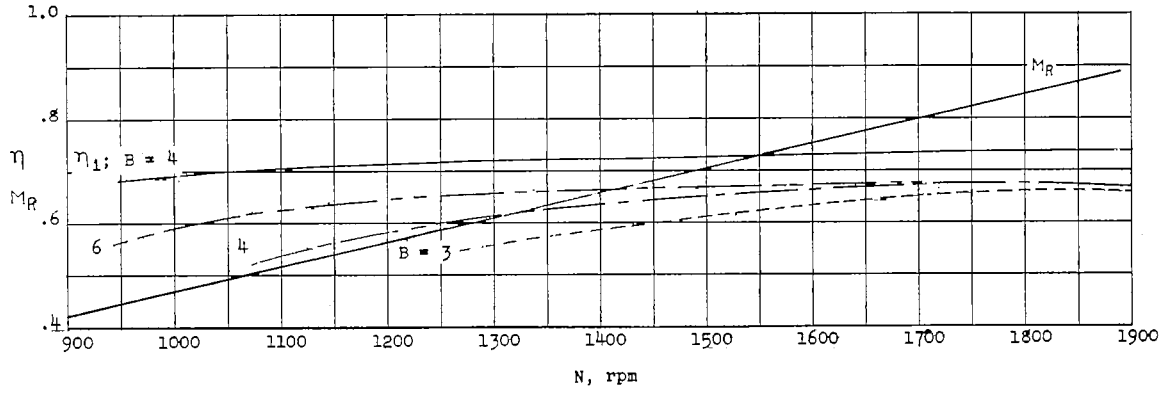

(a) D = 10.0; V = 100 mph.

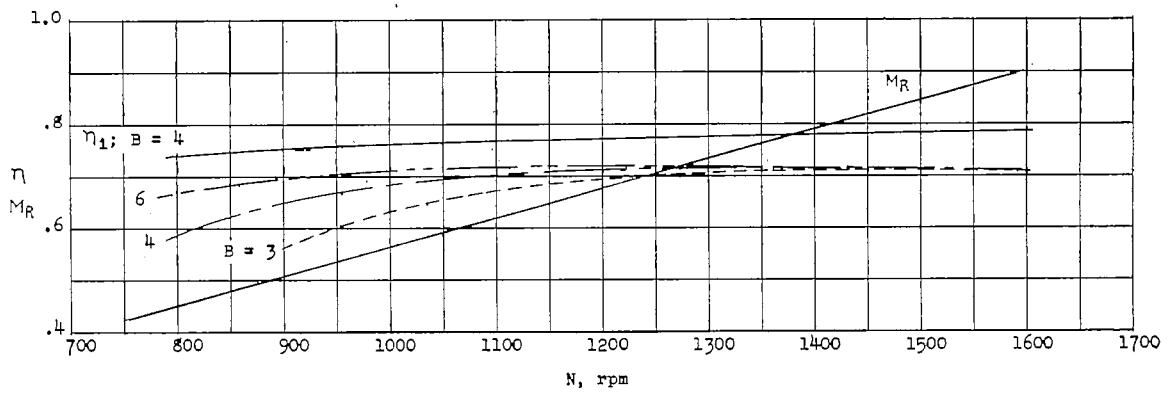

(b) D = 12.0; V = 100 mph.

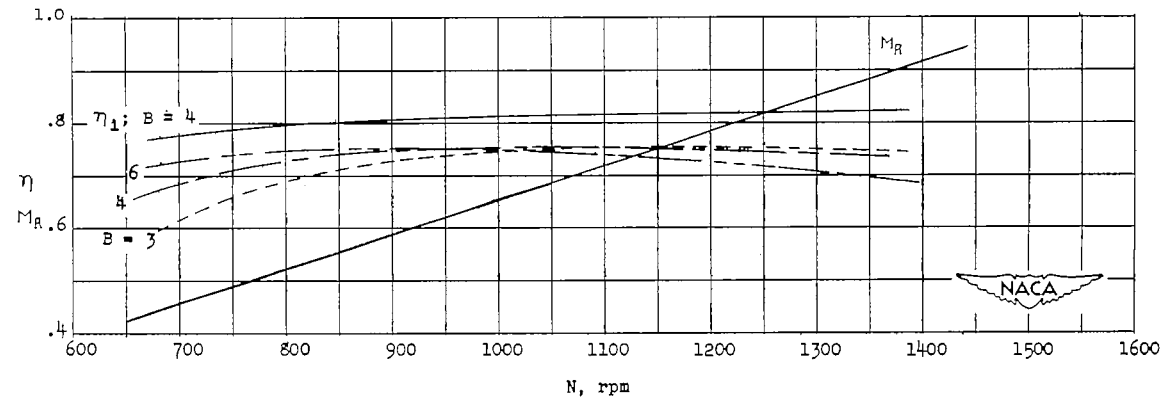

(c) D = 14.0; V = 100 mph.

Figure 9.- Propeller efficiency and tip Mach number at sea level. Single rotation; 1,000 horsepower; activity factor, 120 per blade.

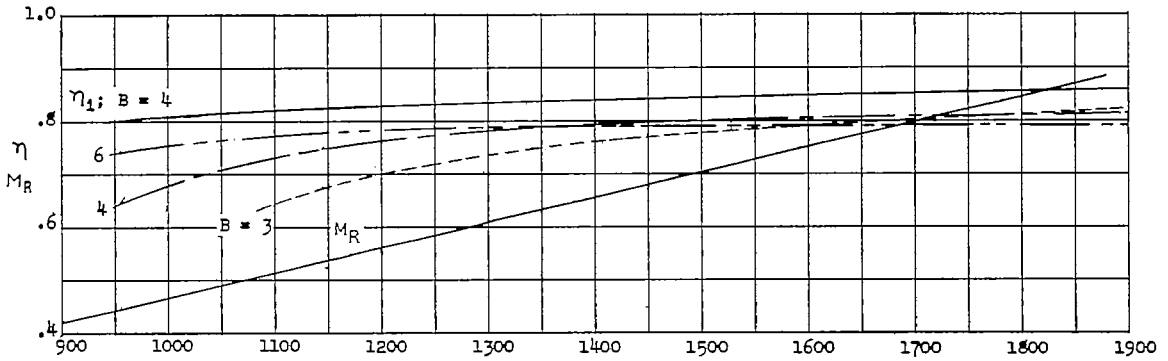

(d) D = 10.0; V = 150 mph.

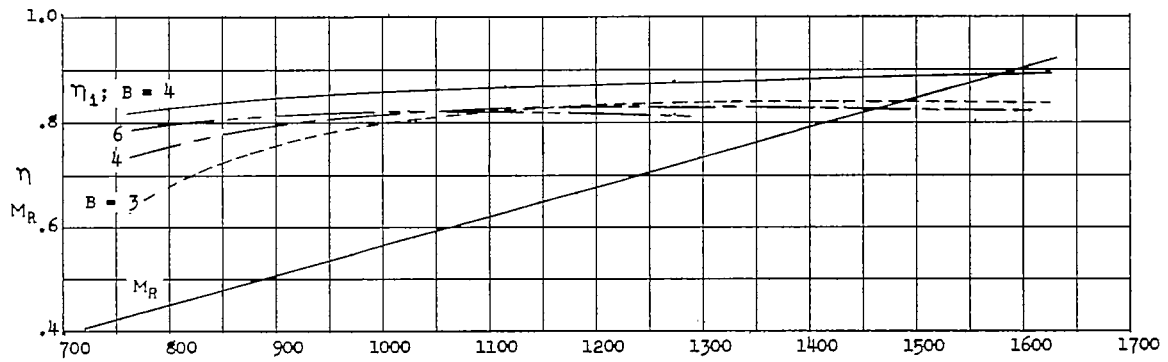

(e) D = 12.0; V = 150 mph.

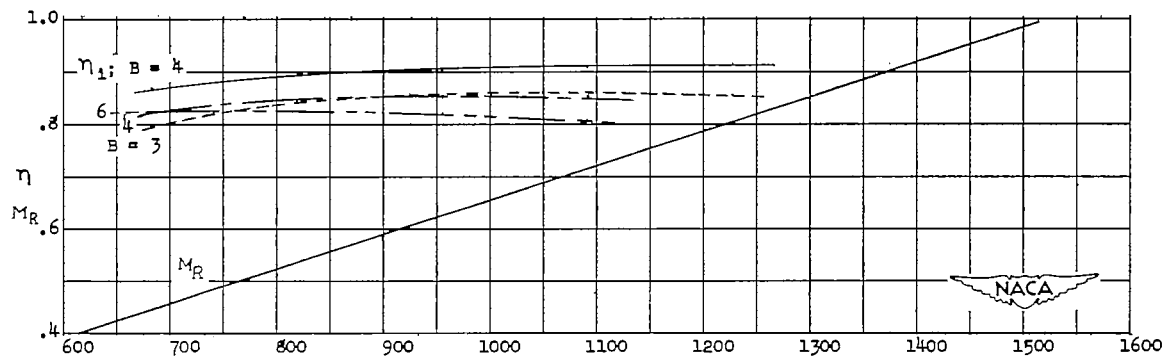

(f) D = 14.0; V = 150 mph.

Figure 9.- Continued.

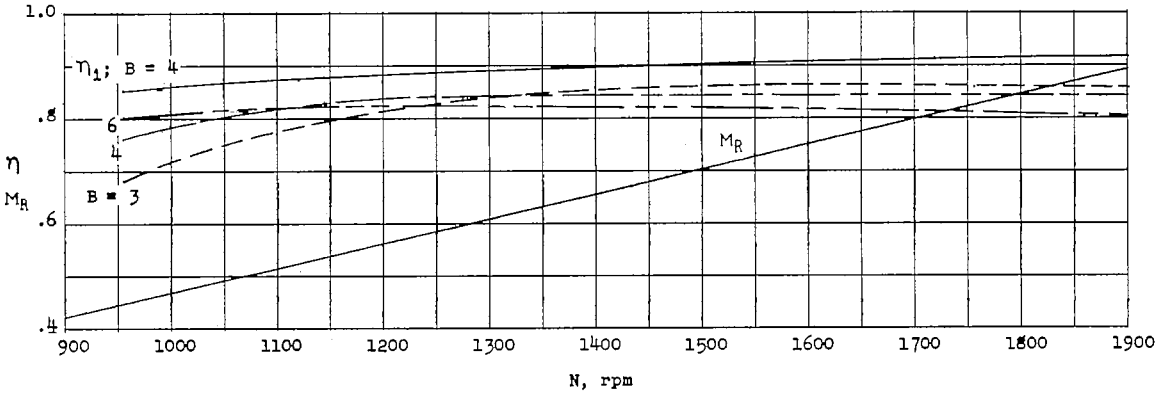

(g) D = 10.0; V = 200 mph.

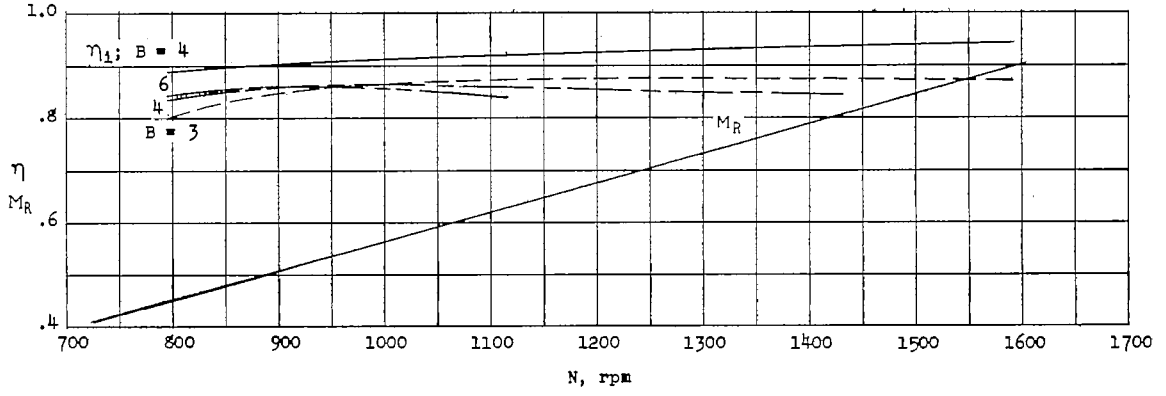

(h) D = 12.0; V = 200 mph.

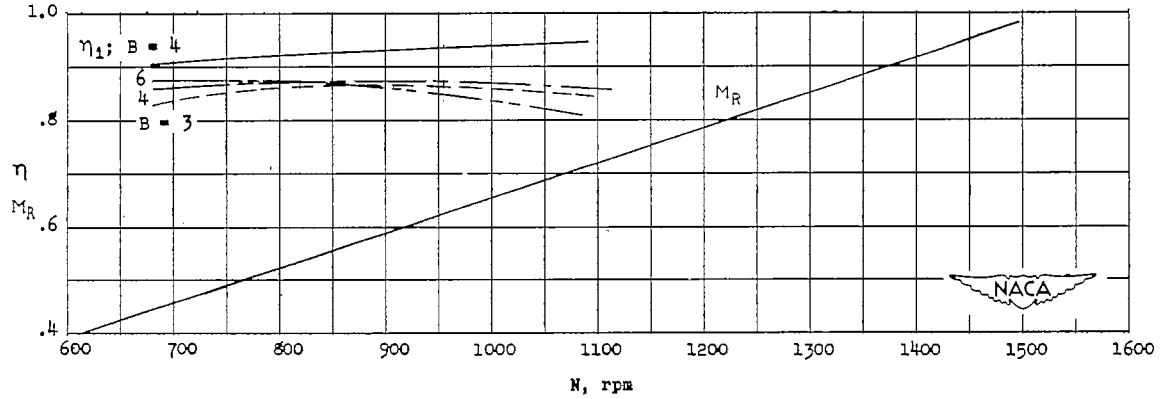

(i) D = 14.0; V = 200 mph.

Figure 9.- Continued.

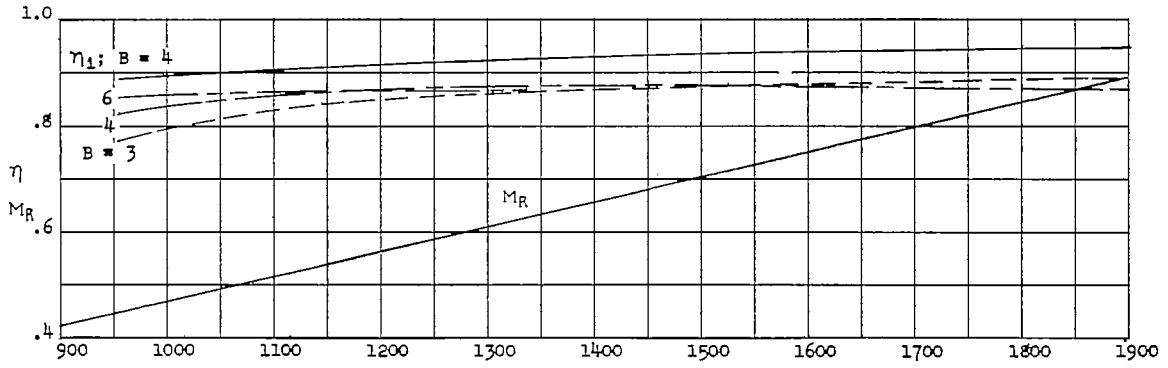

(j) D = 10.0; V = 250 mph.

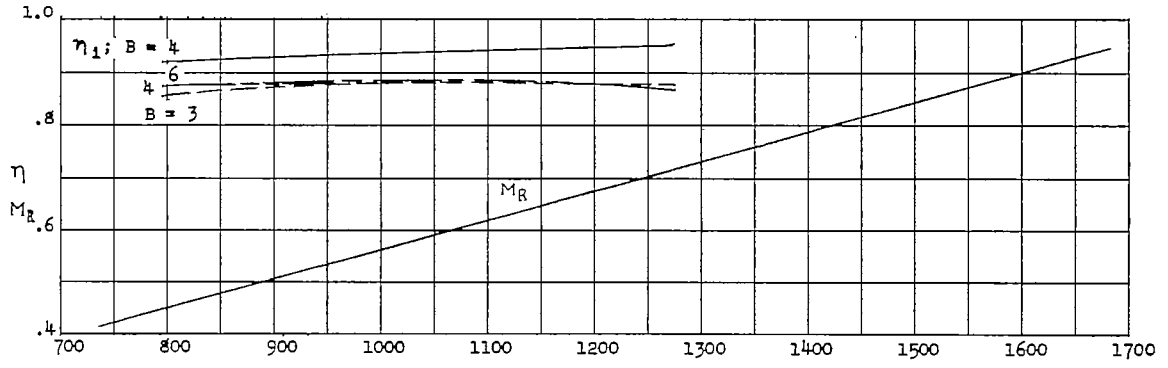

(k) D = 12.0; V = 250 mph.

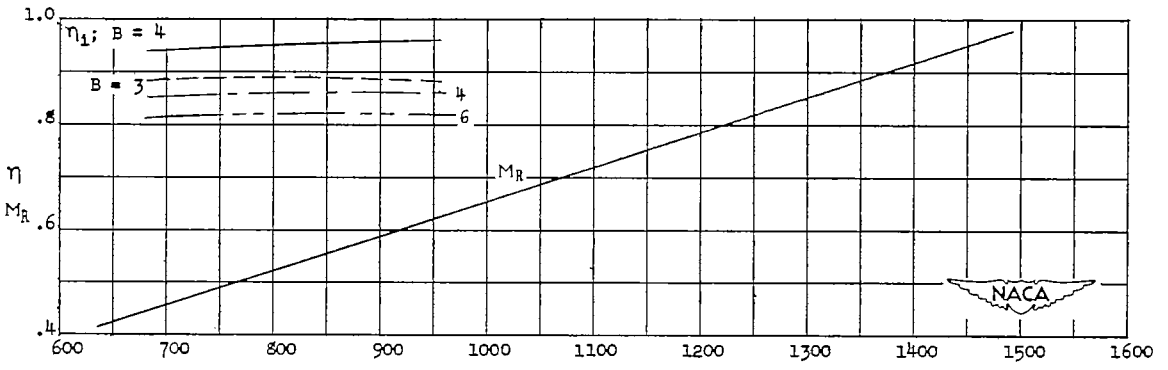

(l) D = 14.0; V = 250 mph.

Figure 9.- Concluded.

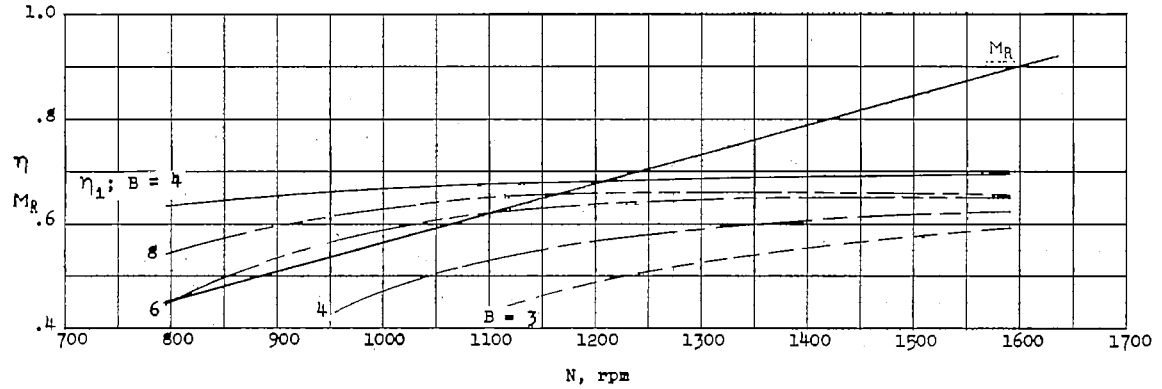

(a) D = 12.0; V = 100 mph.

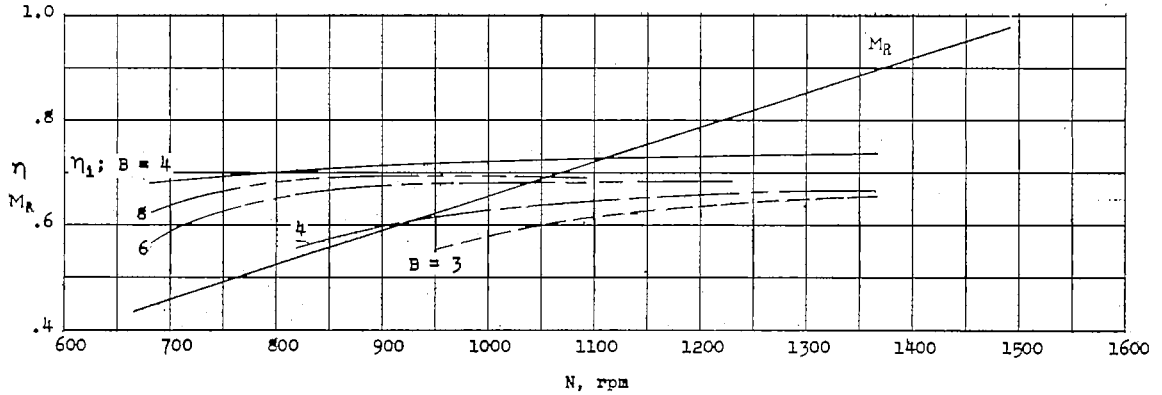

(b) D = 14.0; V = 100 mph.

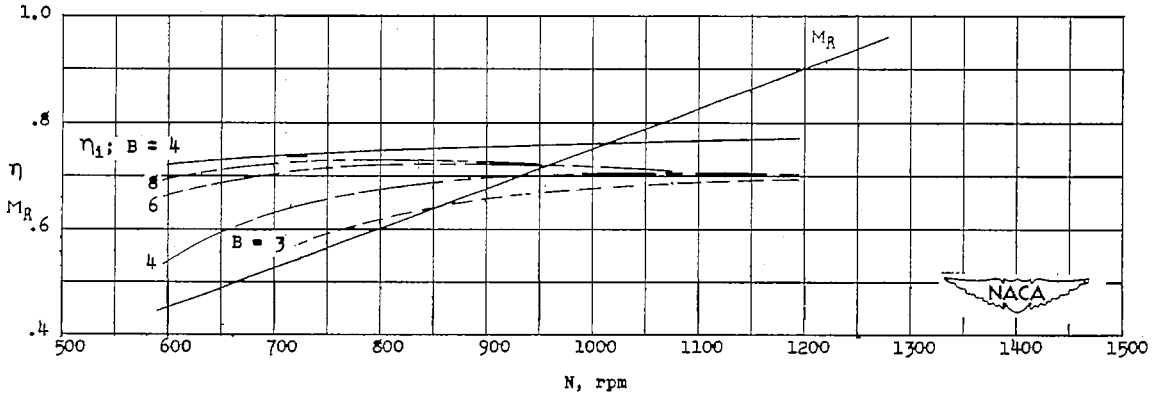

(c) D = 16.0; V = 100 mph.

Figure 10.- Propeller efficiency and tip Mach number at sea level. Single rotation; 2,000 horsepower; activity factor, 120 per blade.

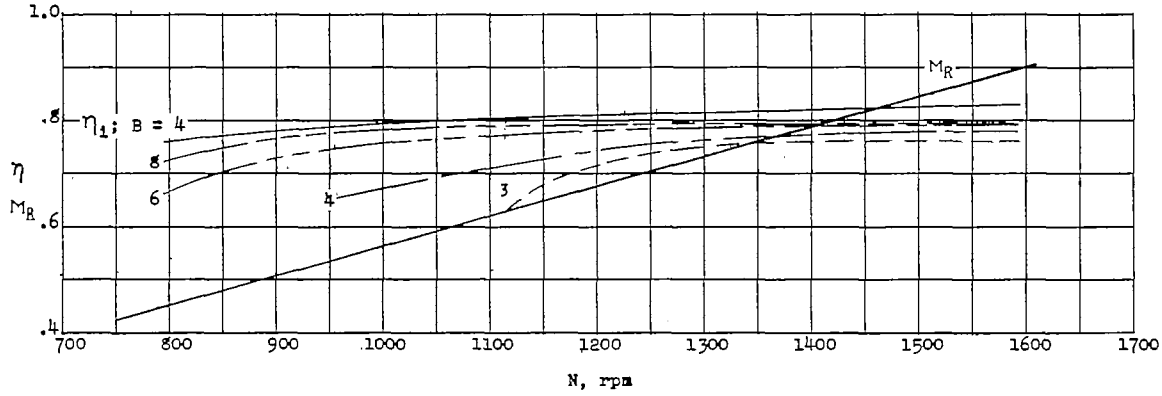

(d) D = 12.0; V = 150 mph.

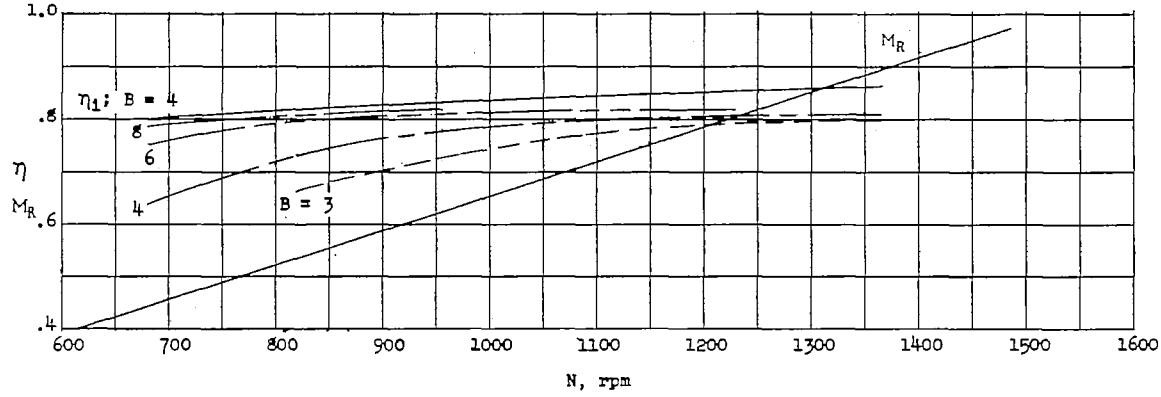

(e) D = 14.0; V = 150 mph.

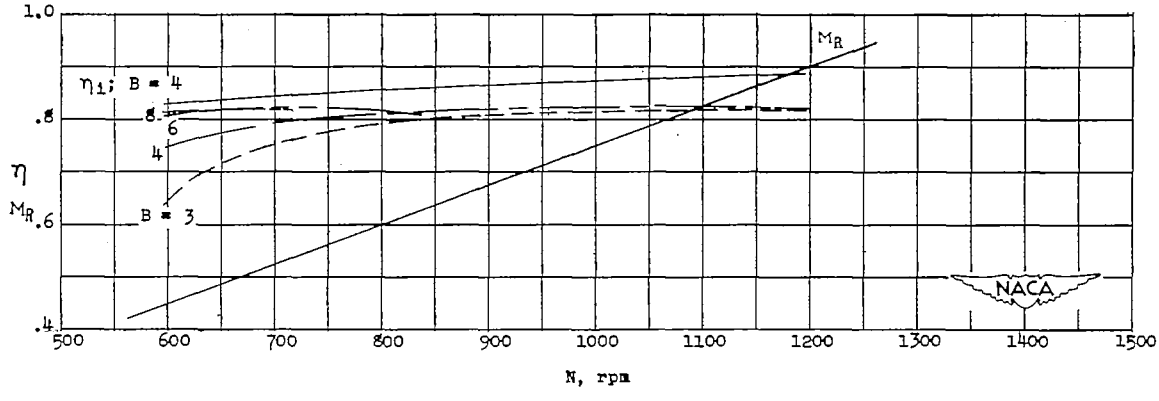

(f) D = 16.0; V = 150 mph.

Figure 10.- Continued.

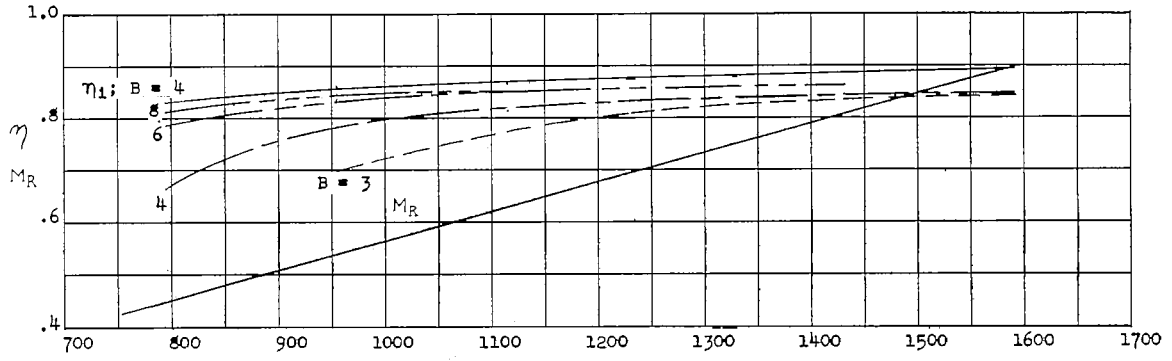

(g) D = 12.0; V = 200 mph.

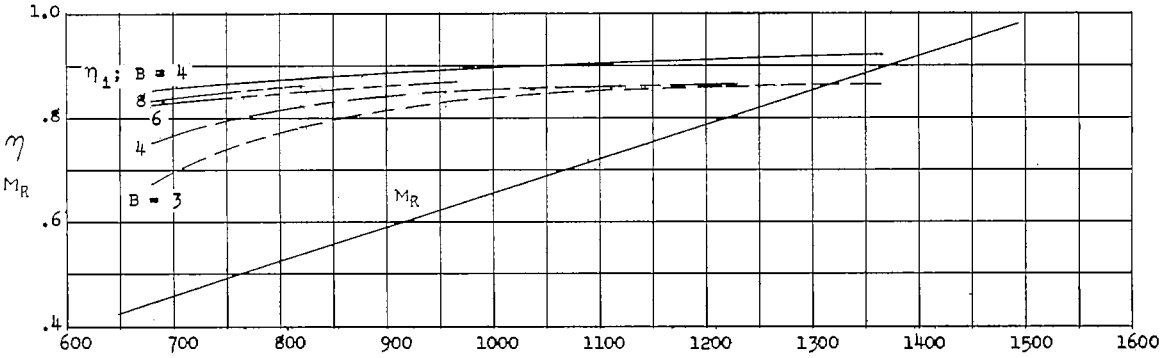

(h) D = 14.0; V = 200 mph.

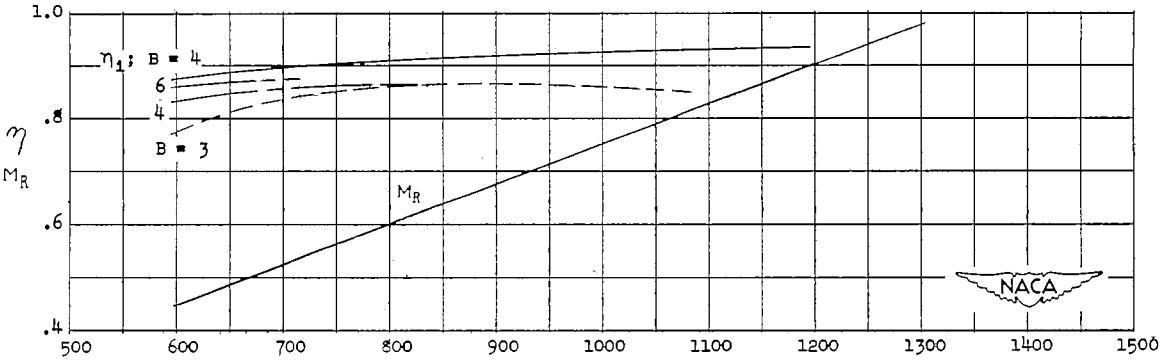

(i) D = 16.0; V = 200 mph.

Figure 10.- Continued.

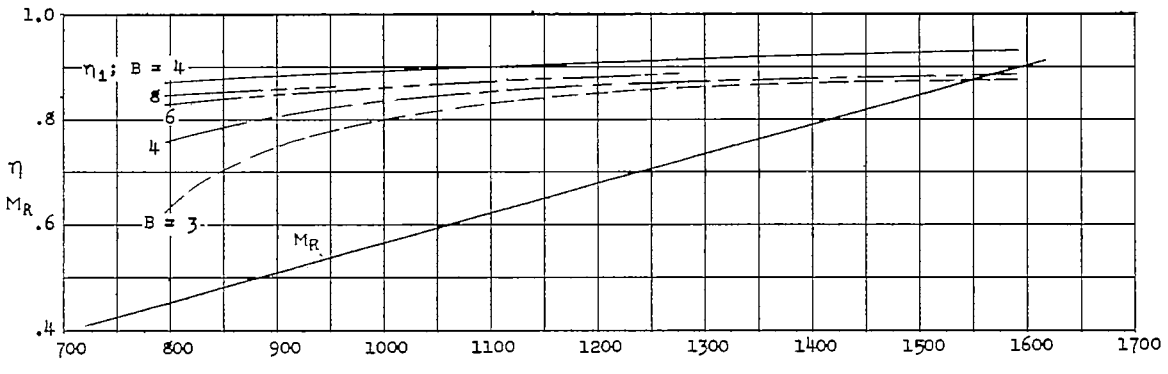

(j) D = 12.0; V = 250 mph.

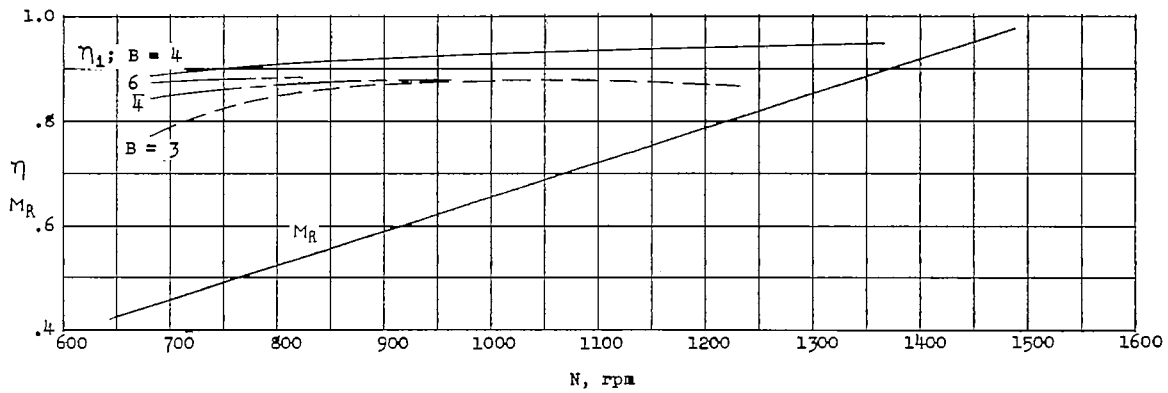

(k) D = 14.0; V = 250 mph.

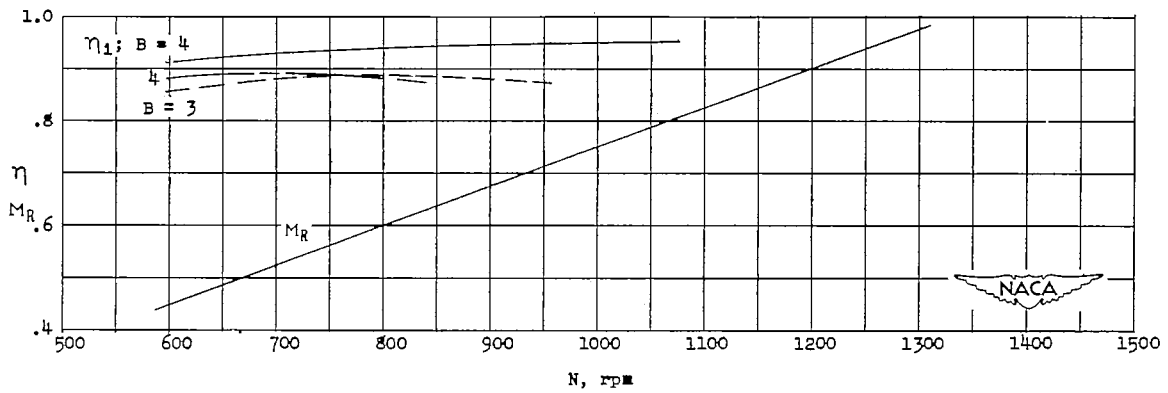

(l) D = 16.0; V = 250 mph.

Figure 10.- Concluded.

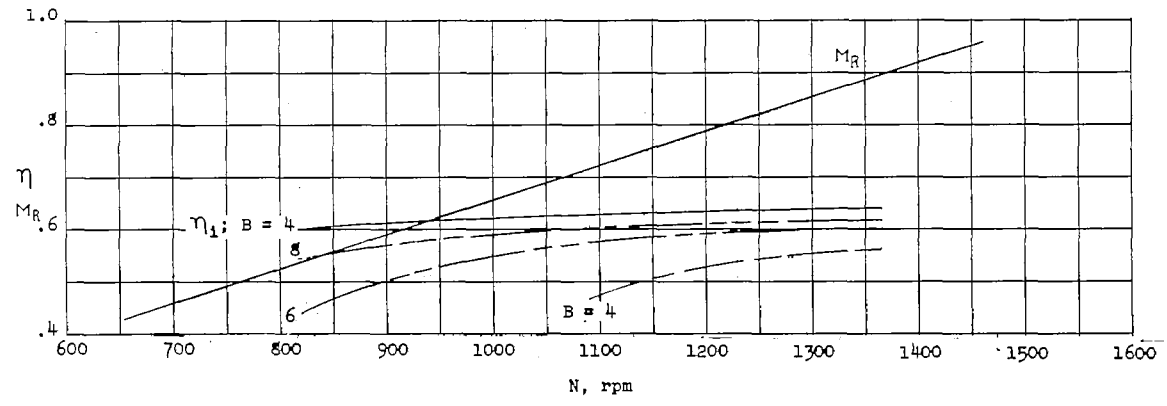

(a) D = 14.0; V = 100 mph.

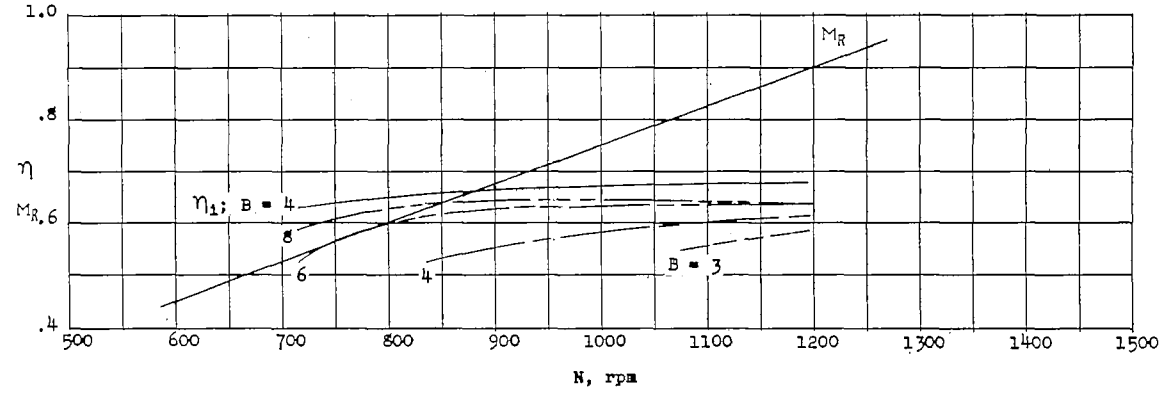

(b) D = 16.0; V = 100 mph.

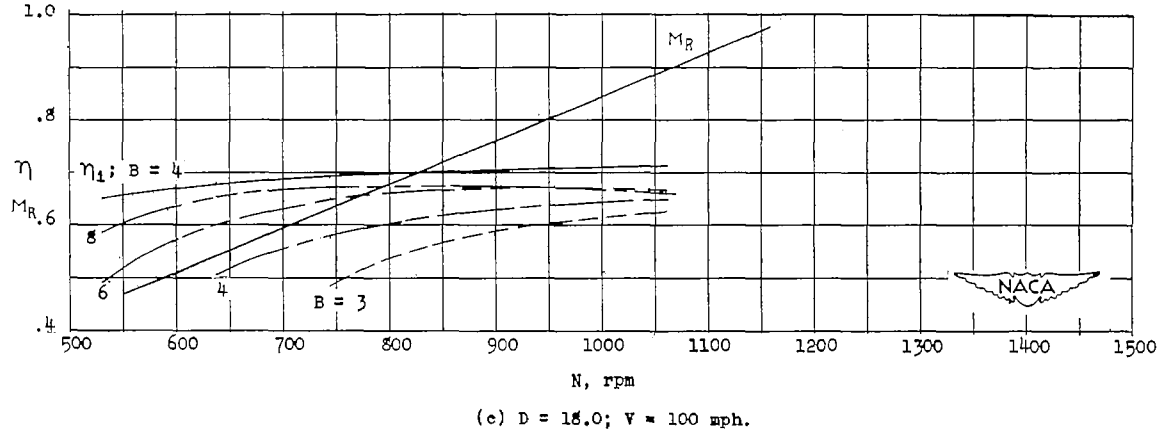

(c) D = 18.0; V = 100 mph.

Figure 11.- Propeller efficiency and tip Mach number at sea level. Single rotation; 4,000 horsepower; activity factor, 120 per blade.

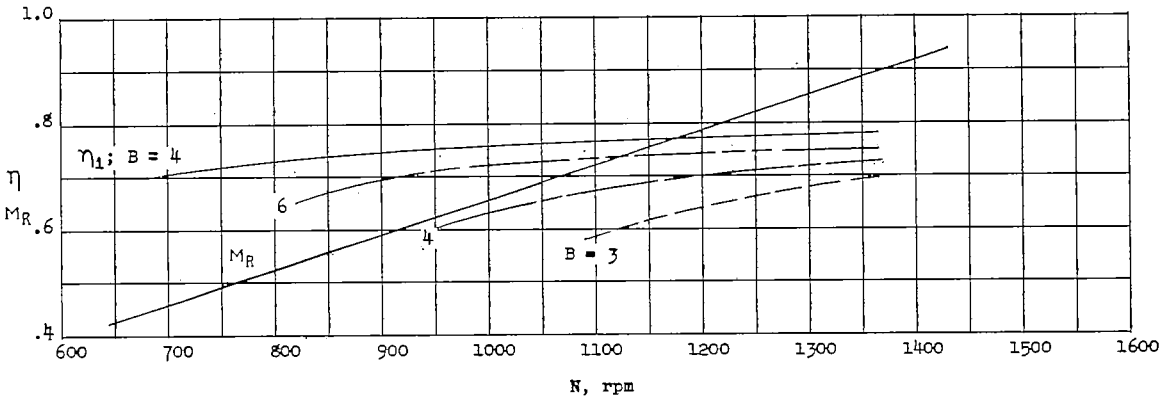

(d) D = 14.0; V = 150 mph.

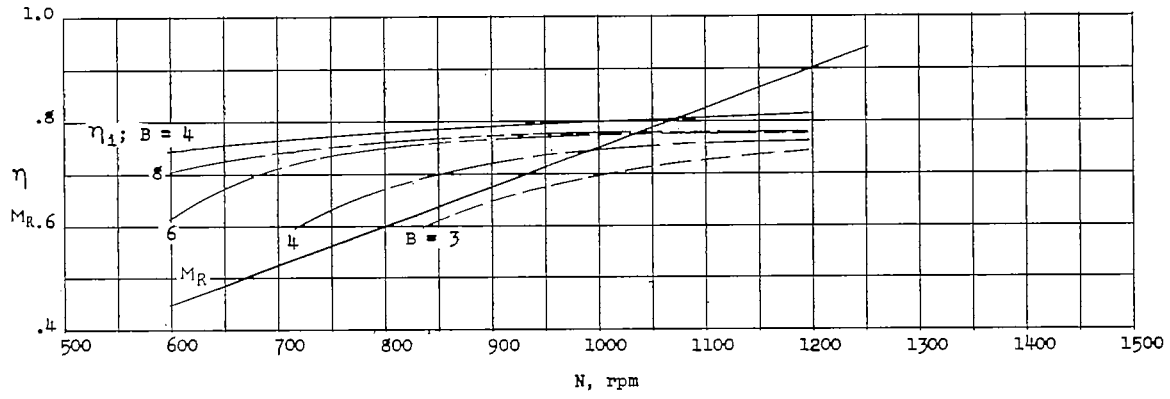

(e) D = 16.0; V = 150 mph.

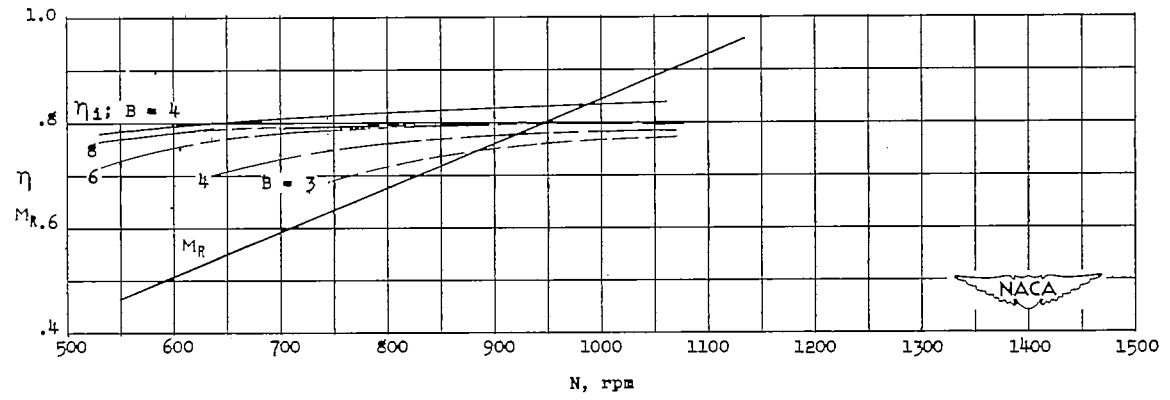

(f) D = 18.0; V = 150 mph.

Figure 11.- Continued.

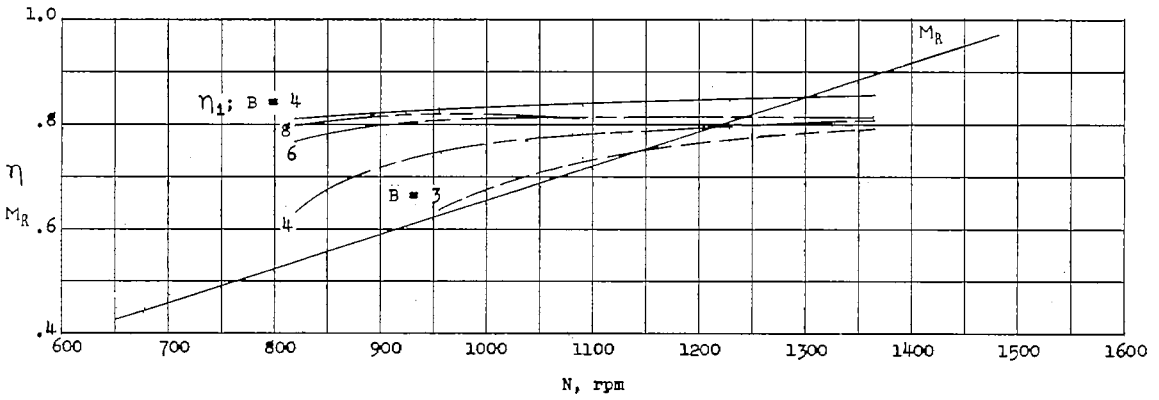

(g) D = 14.0; V = 200 mph.

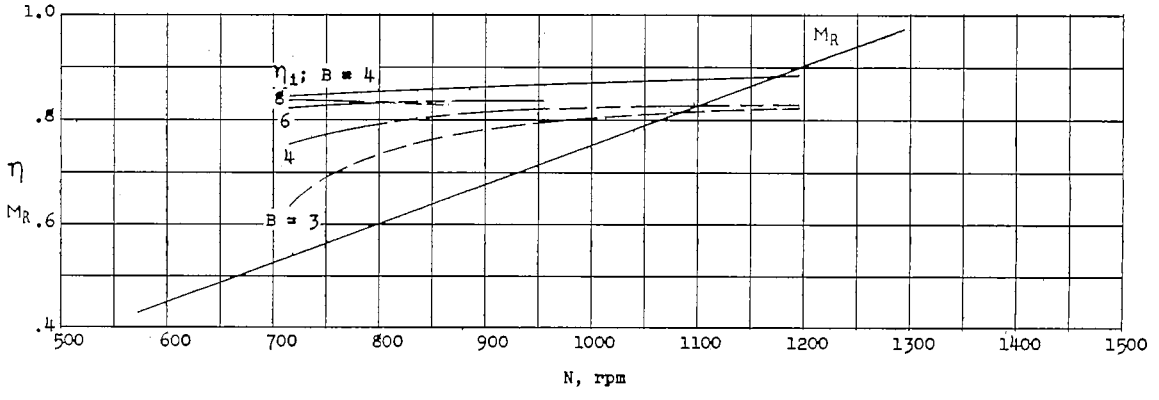

(h) D = 16.0; V = 200 mph.

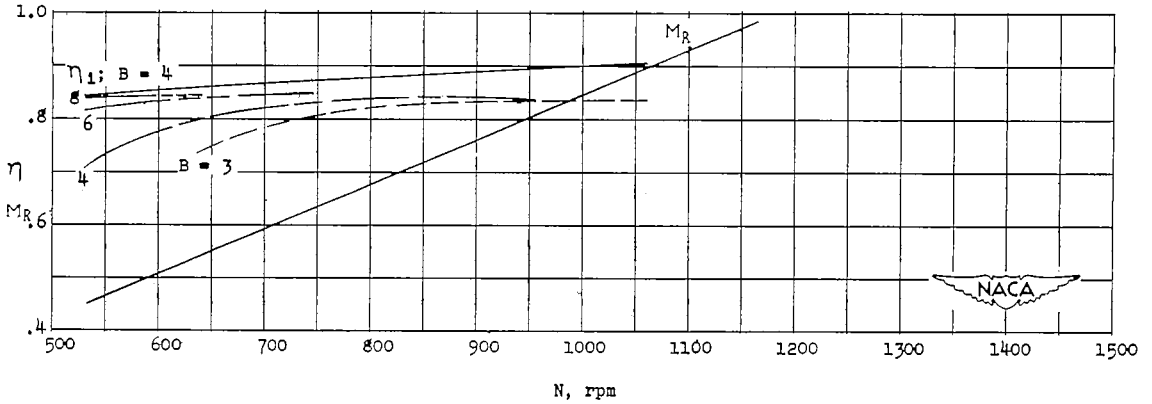

(i) D = 18.0; V = 200 mph.

Figure 11.- Continued.

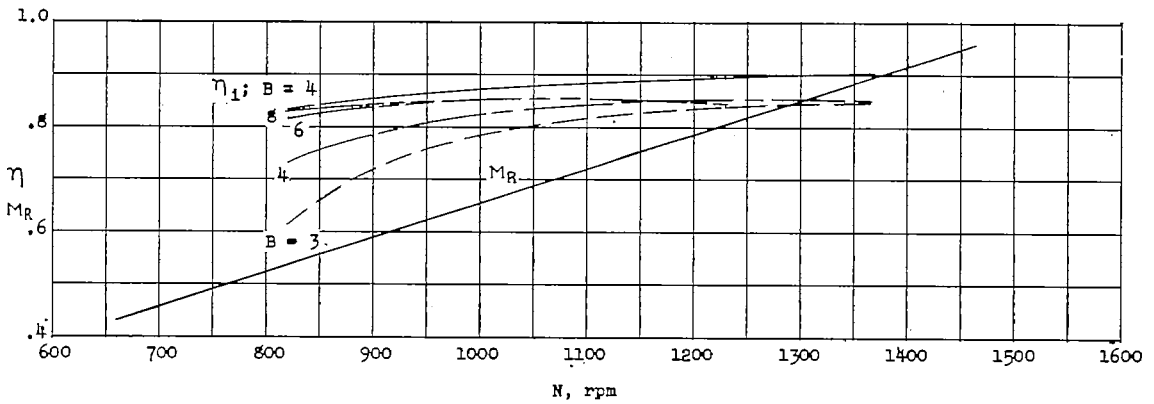

(j) D = 14.0; V = 250 mph.

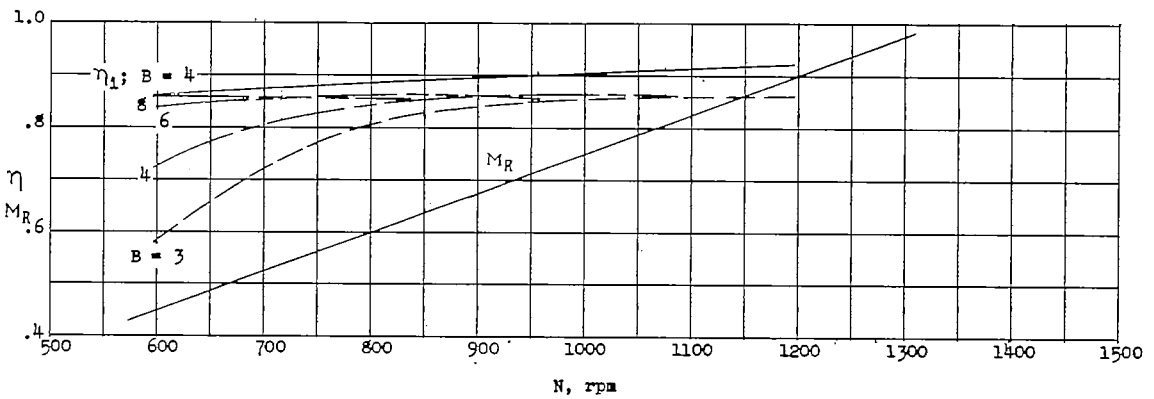

(k) D = 16.0; V = 250 mph.

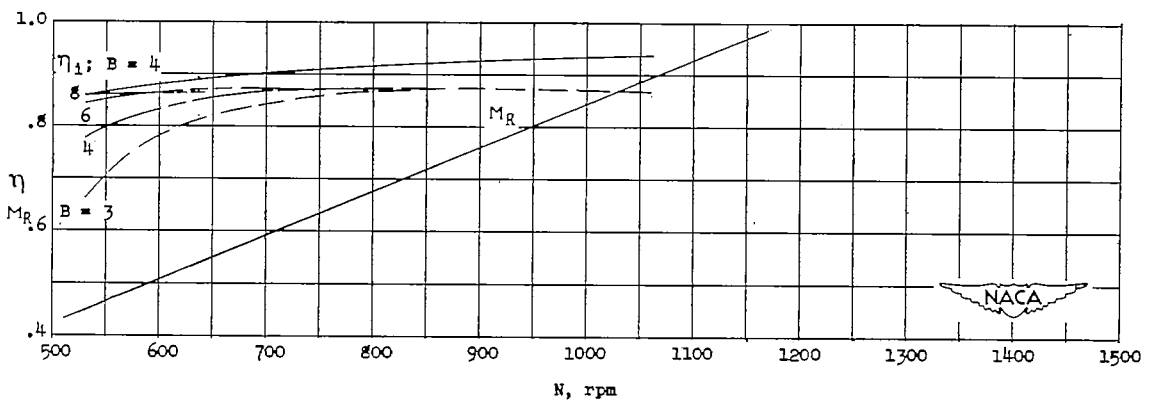

(l) D = 18.0; V = 250 mph.

Figure 11.- Concluded.

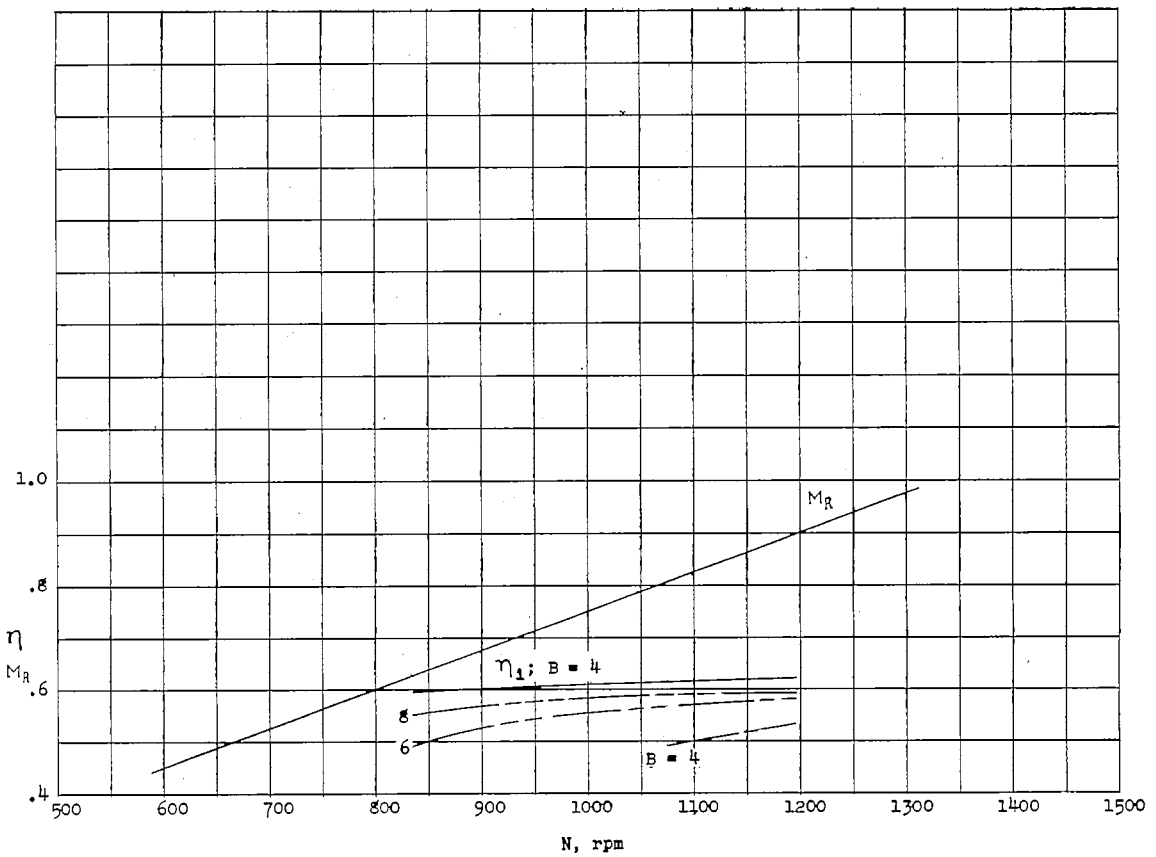

(a) D = 16.0; V = 100 mph.

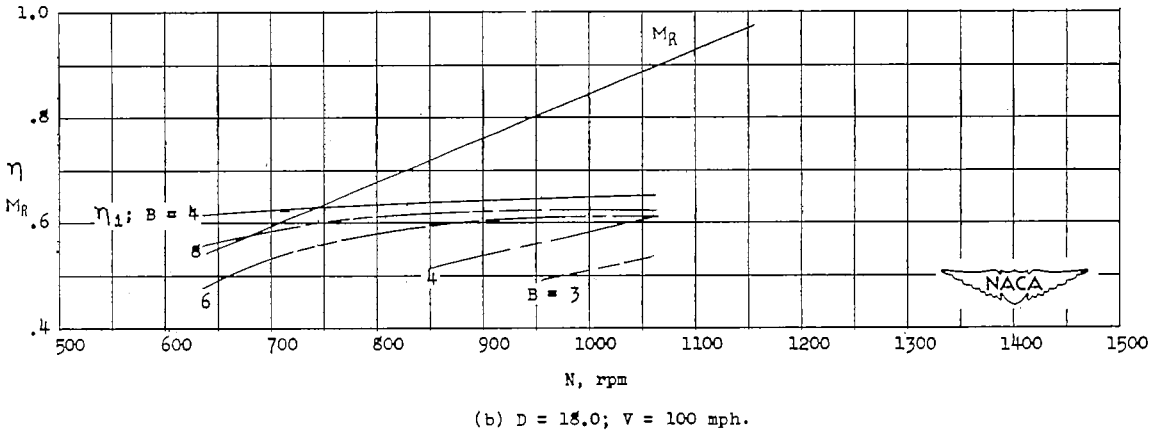

(b) D = 18.0; V = 100 mph.

Figure 12.- Propeller efficiency and tip Mach number at sea level. Single rotation; 6,000 horsepower; activity factor, 120 per blade.

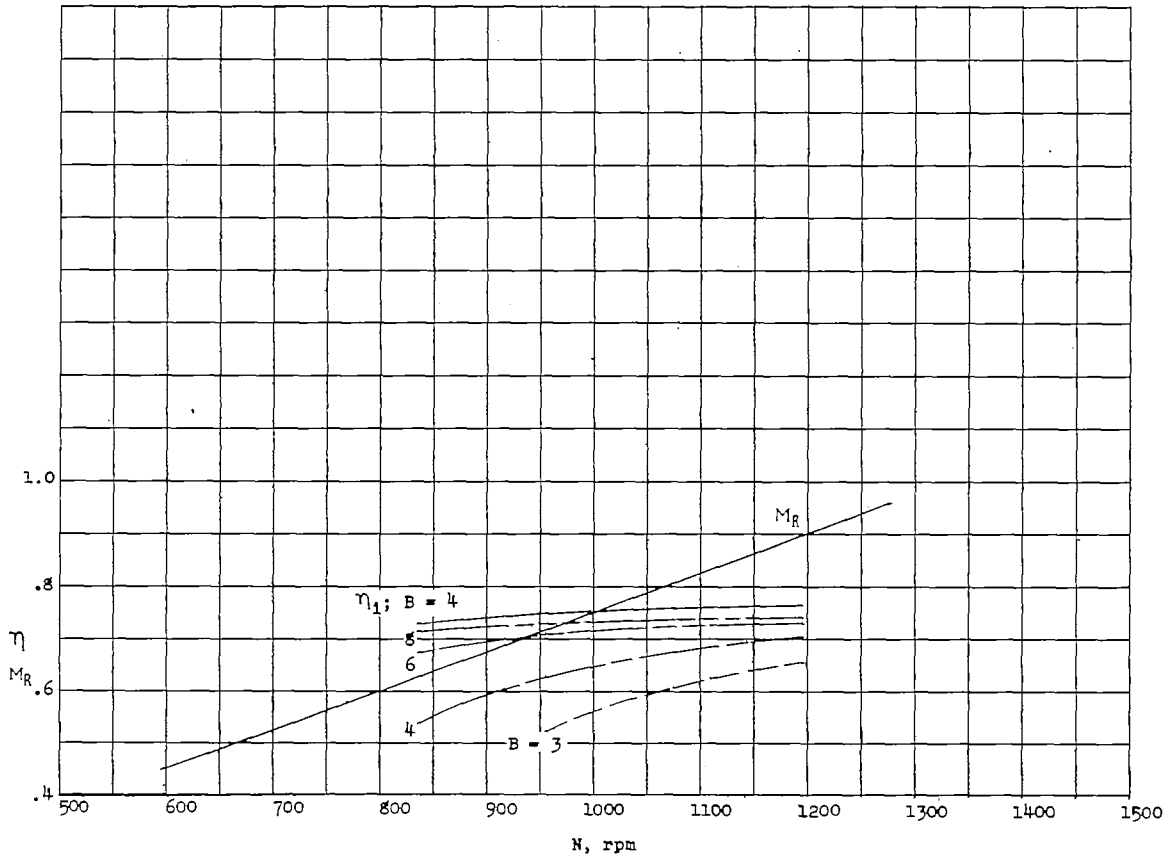

(c) D = 16.0; V = 150 mph.

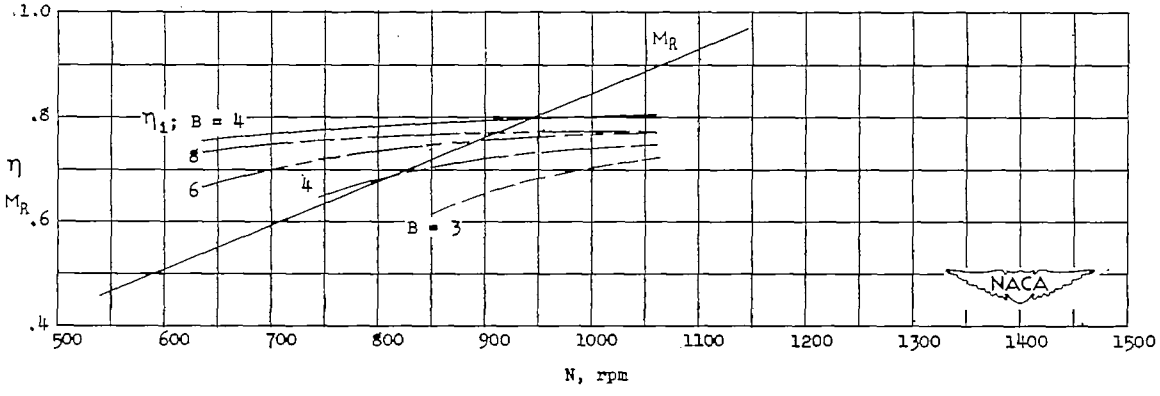

(d) D = 18.0; V = 150 mph.

Figure 12.- Continued.

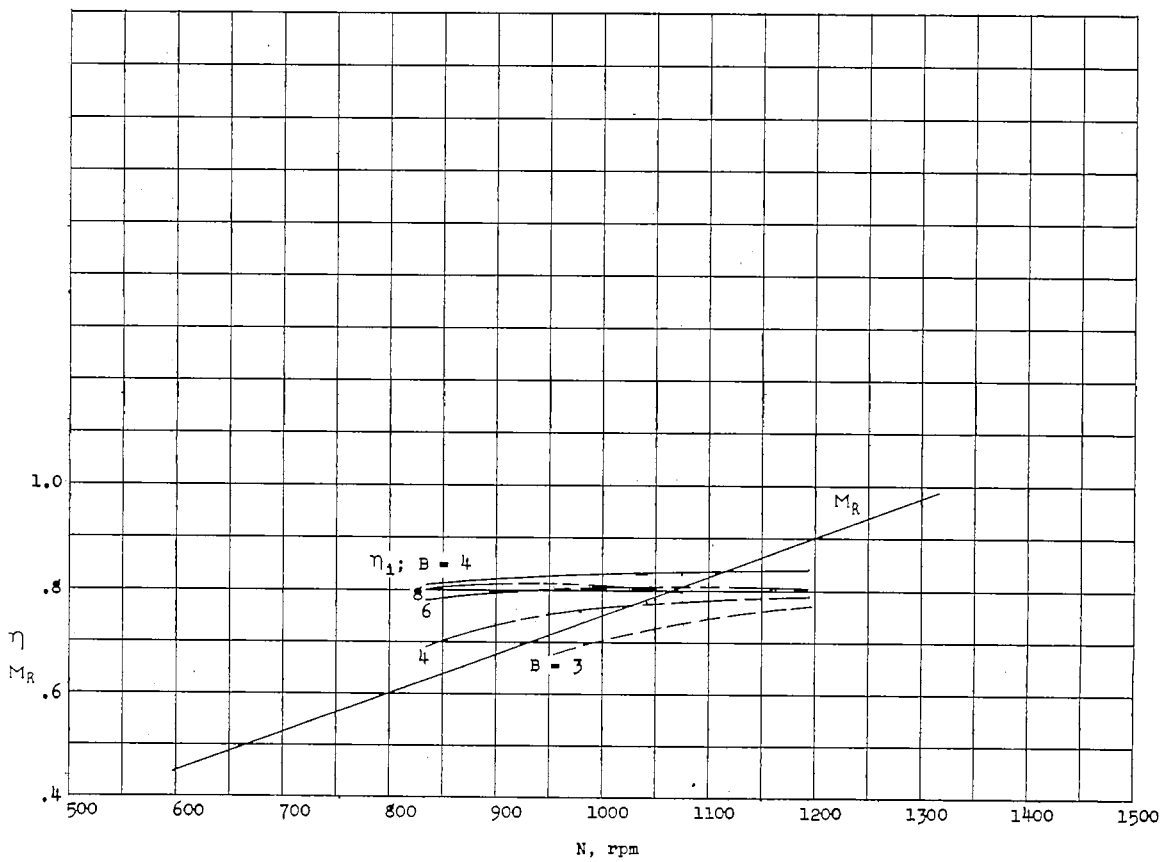

(e) D = 16.0; V = 200 mph.

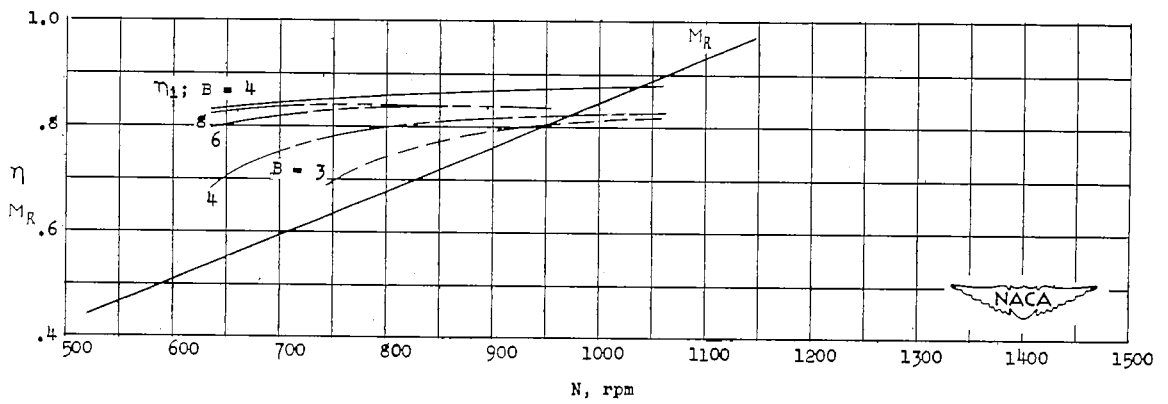

(f) D = 18.0; V = 200 mph.

Figure 12.- Continued.

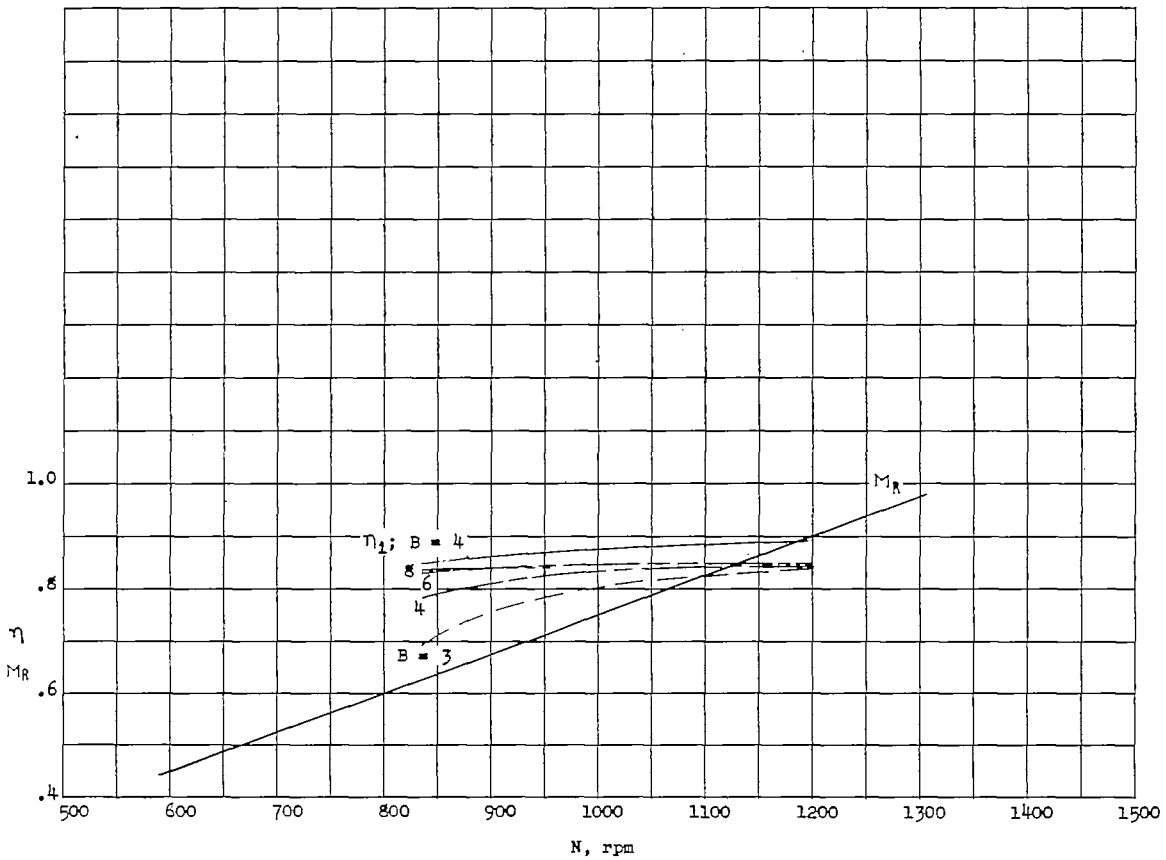

(g) D = 16.0; V = 250 mph.

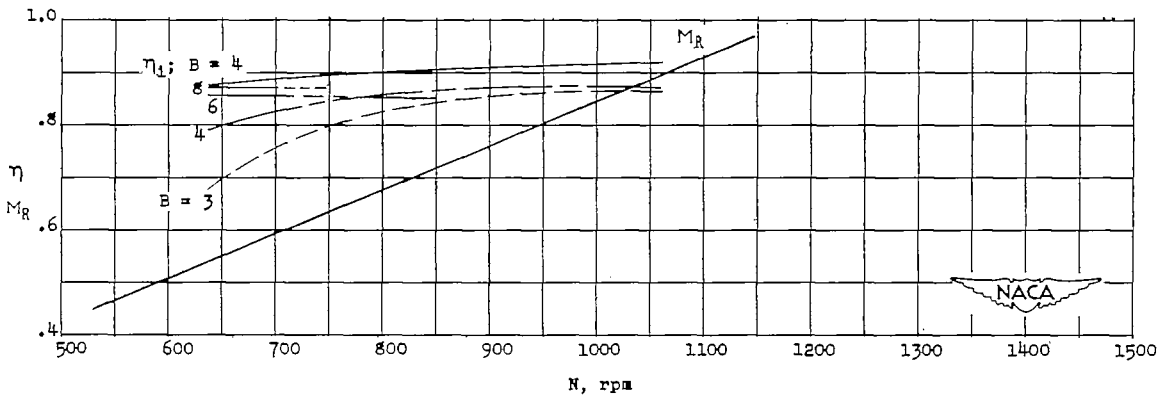

(h) D = 18.0; V = 250 mph.

Figure 12.- Concluded.

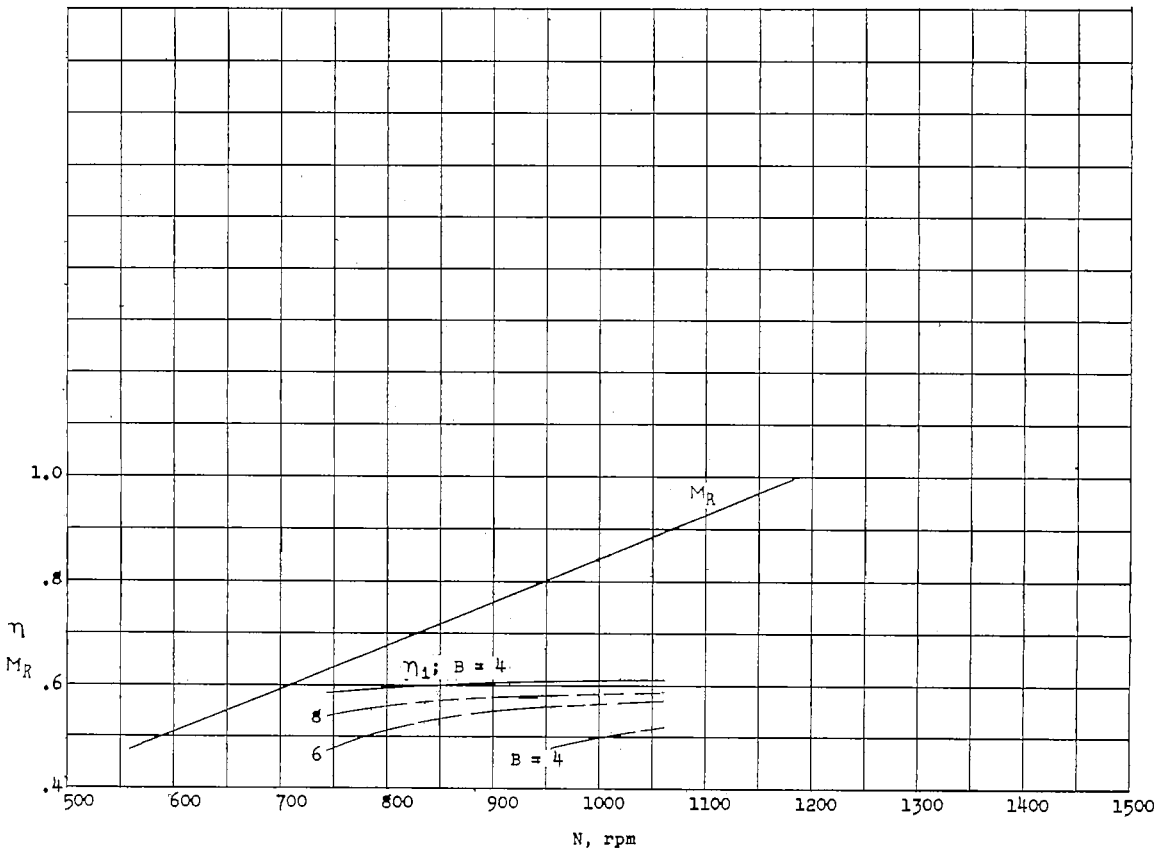

(a) D = 15.0; V = 100 mph.

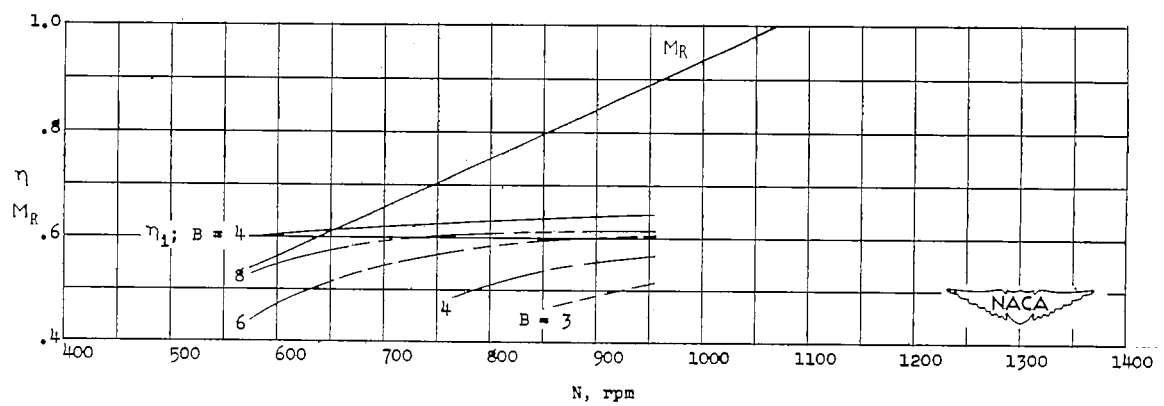

(b) D = 20.0; V = 100 mph.

Figure 13.- Propeller efficiency and tip Mach number at sea level. Single rotation; 8,000 horsepower; activity factor, 120 per blade.

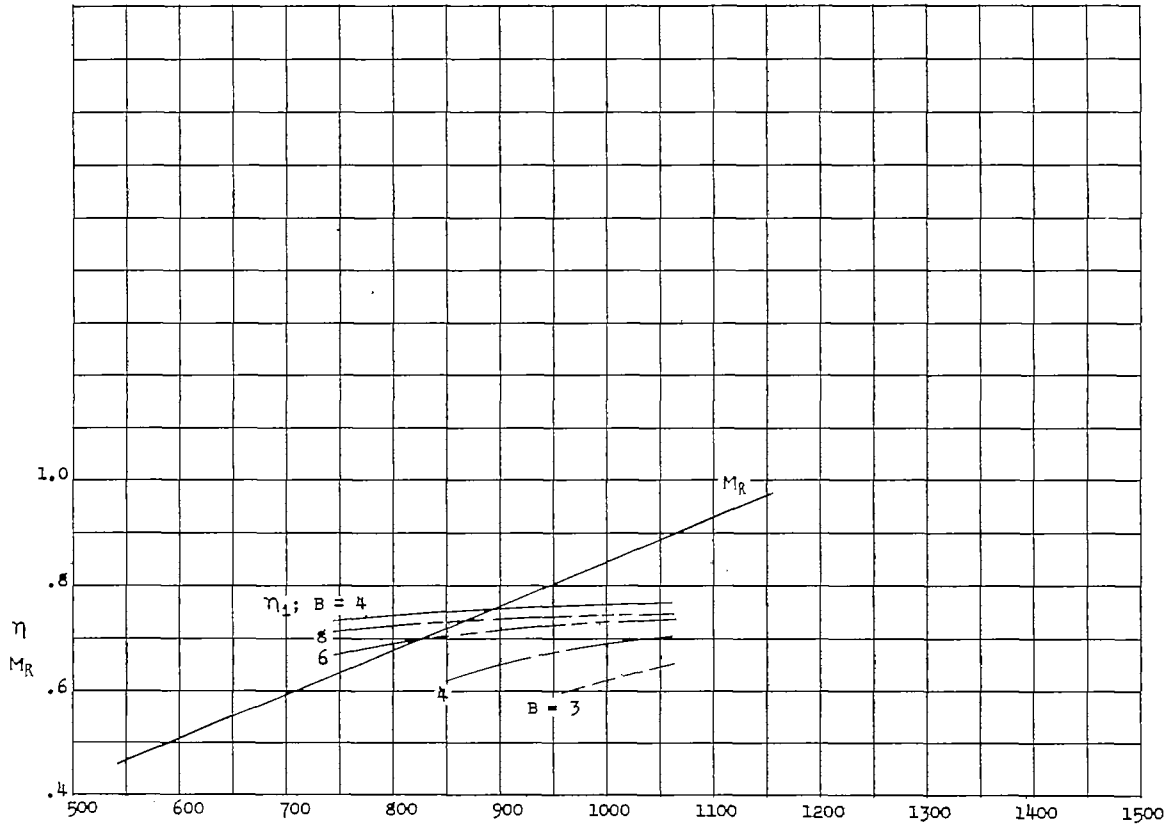

(c) D = 18.0; V = 150 mph.

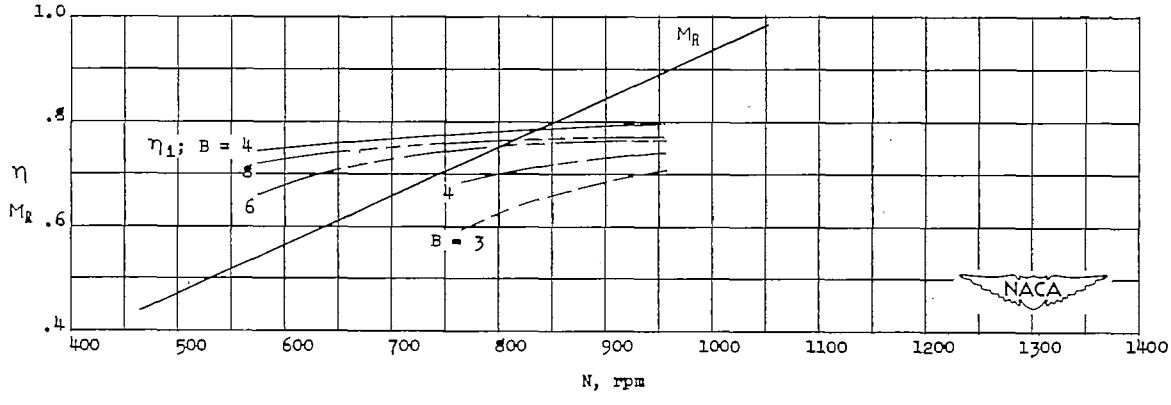

(d) D = 20.0; V = 150 mph.

Figure 13.- Continued.

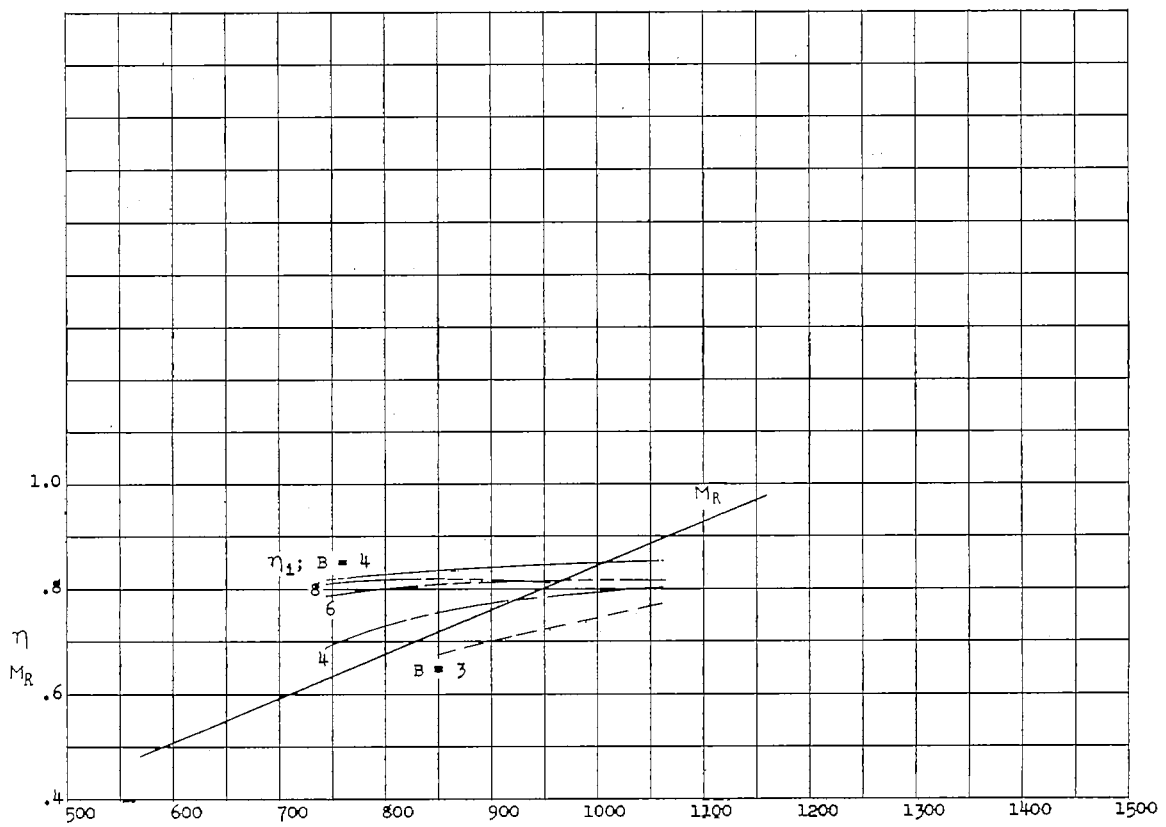

(e) D = 18.0; V = 200 mph.

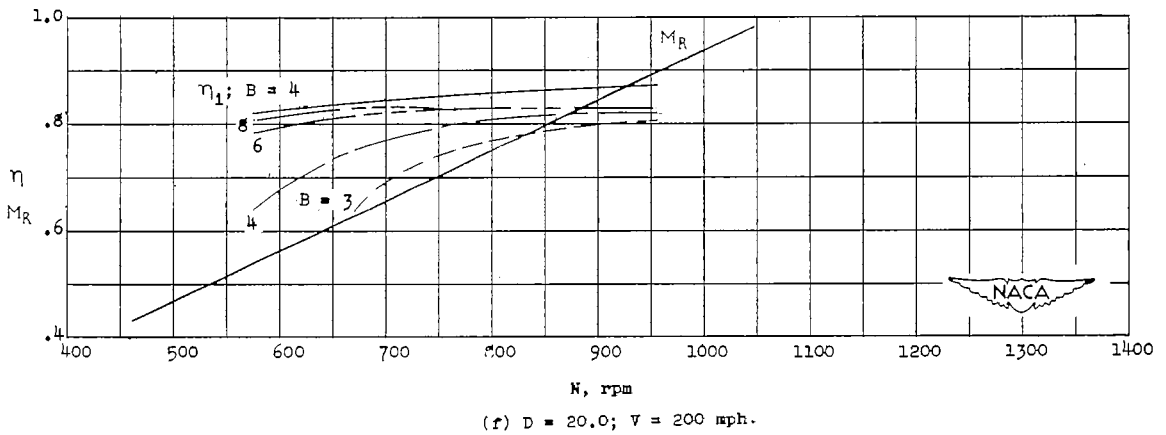

(f) D = 20.0; V = 200 mph.

Figure 13.- Continued.

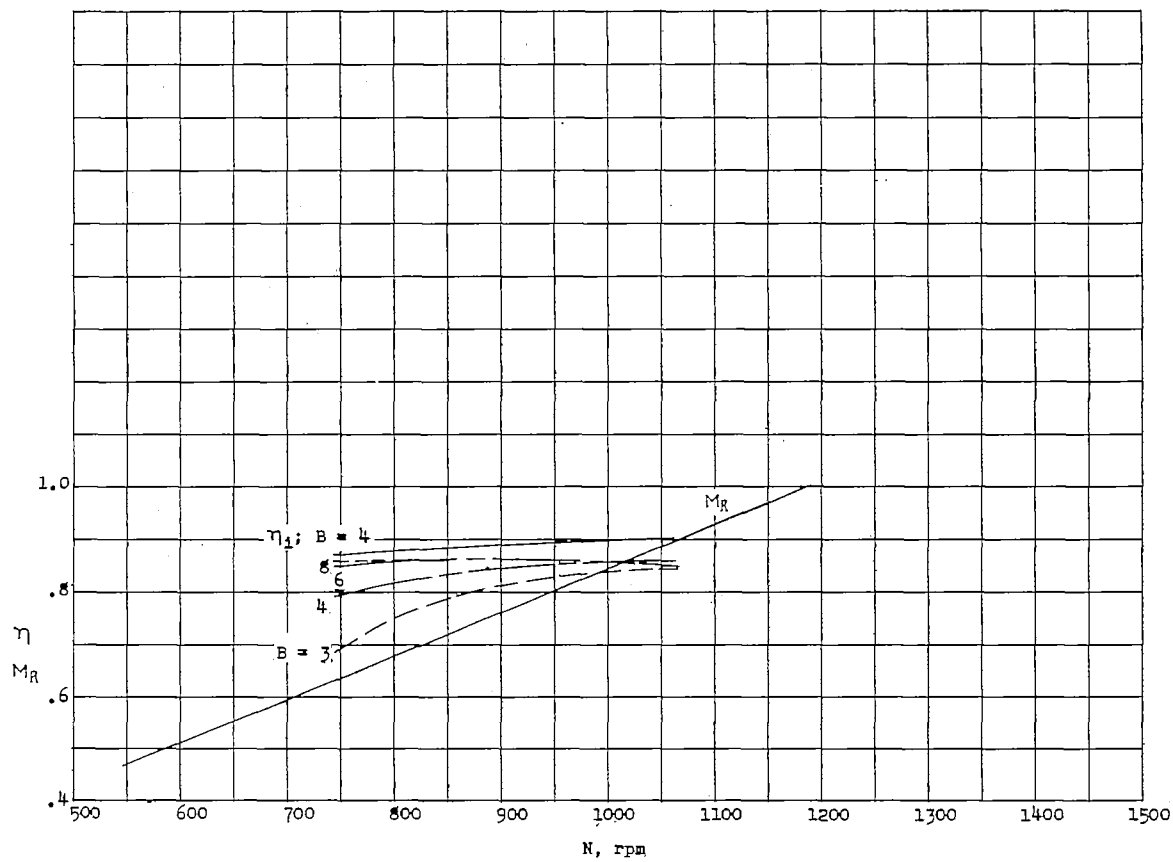

(g) D = 18.0; V = 250 mph.

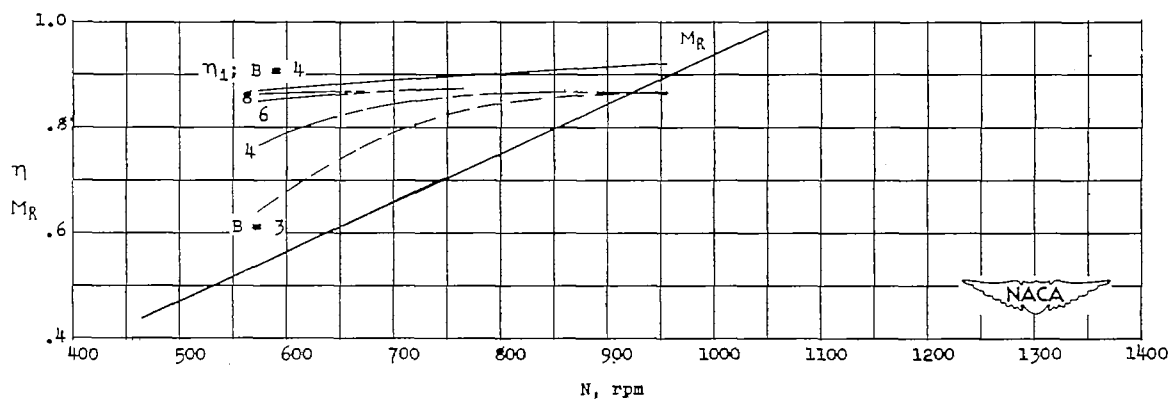

(h) D = 20.0; V = 250 mph.

Figure 13.- Concluded.

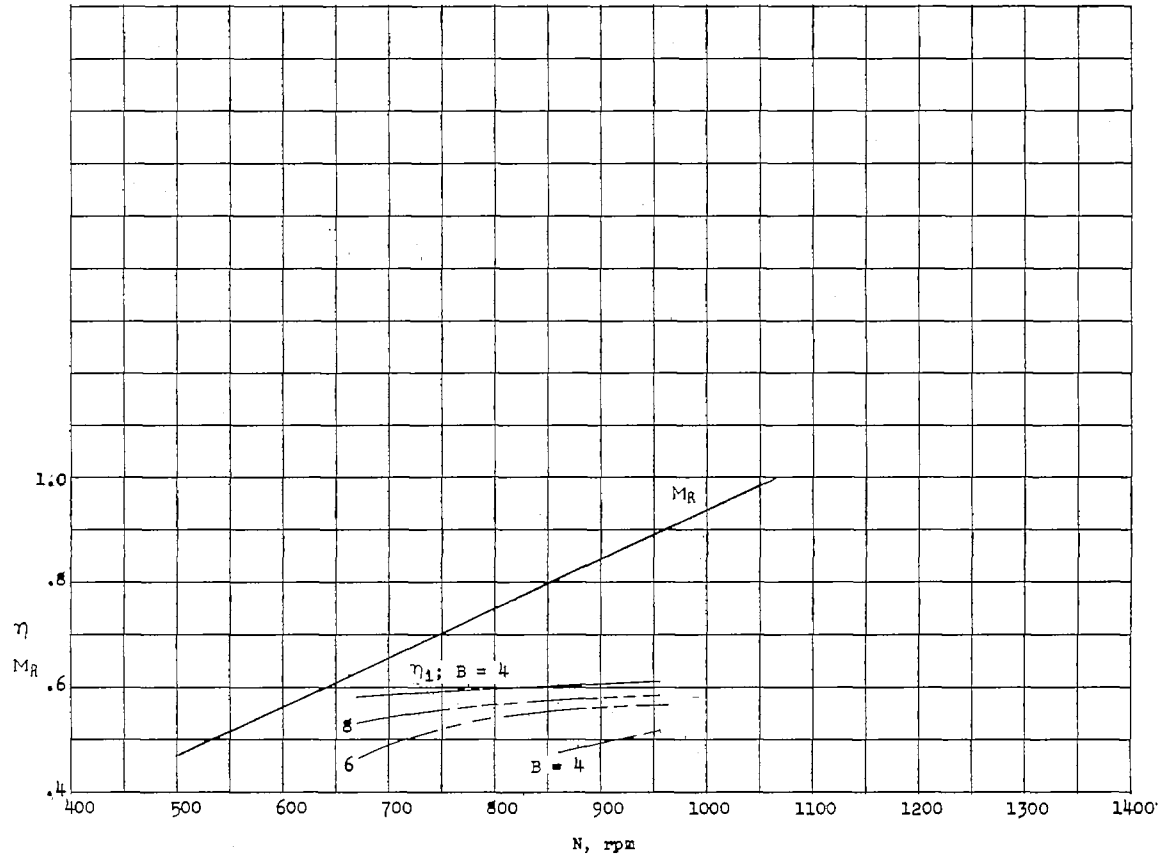

(a) D = 20.0; V = 100 mph.

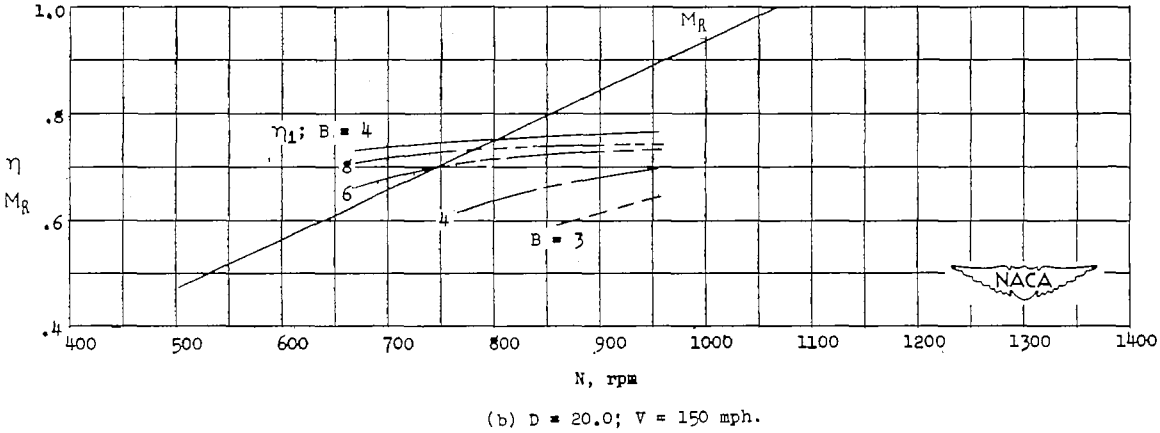

(b) D = 20.0; V = 150 mph.

Figure 14.- Propeller efficiency and tip Mach number at sea level. Single rotation; 10,000 horsepower; activity factor, 120 per blade.

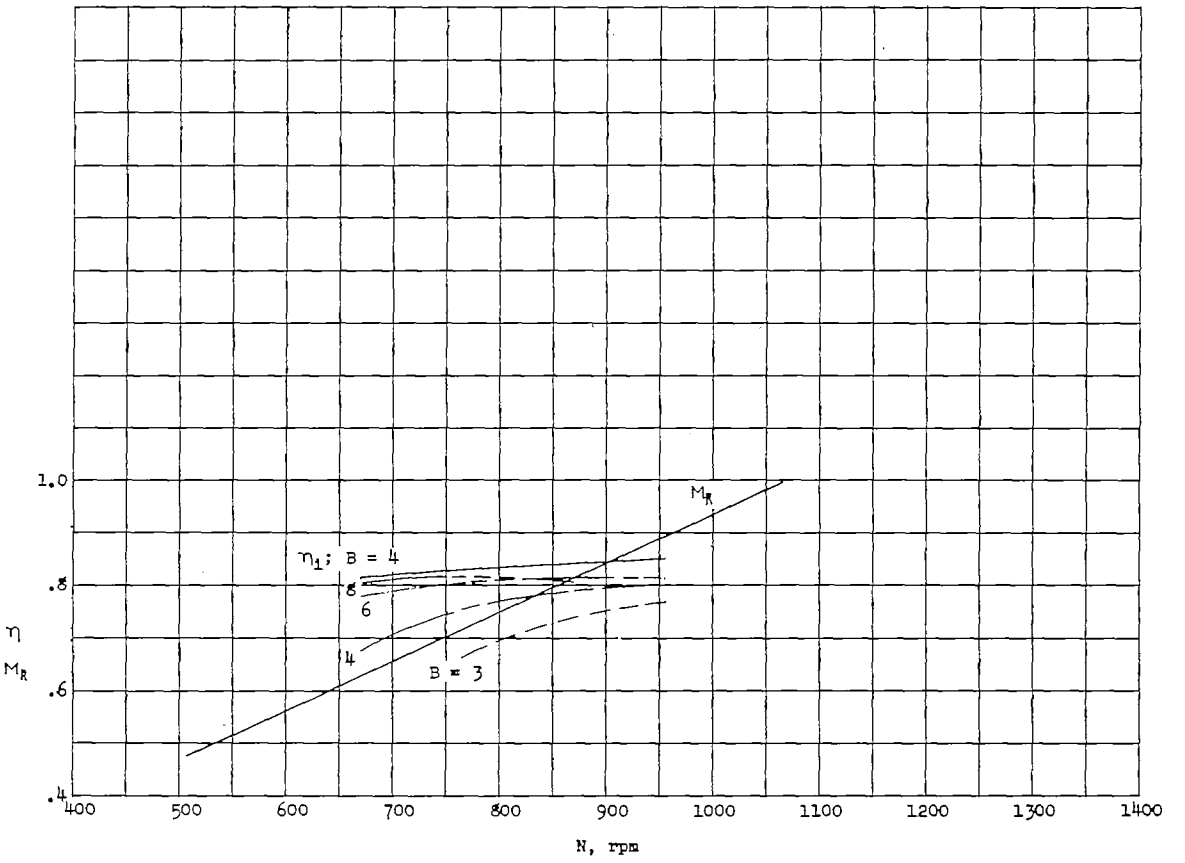

(c) D = 20.0; V = 200 mph.

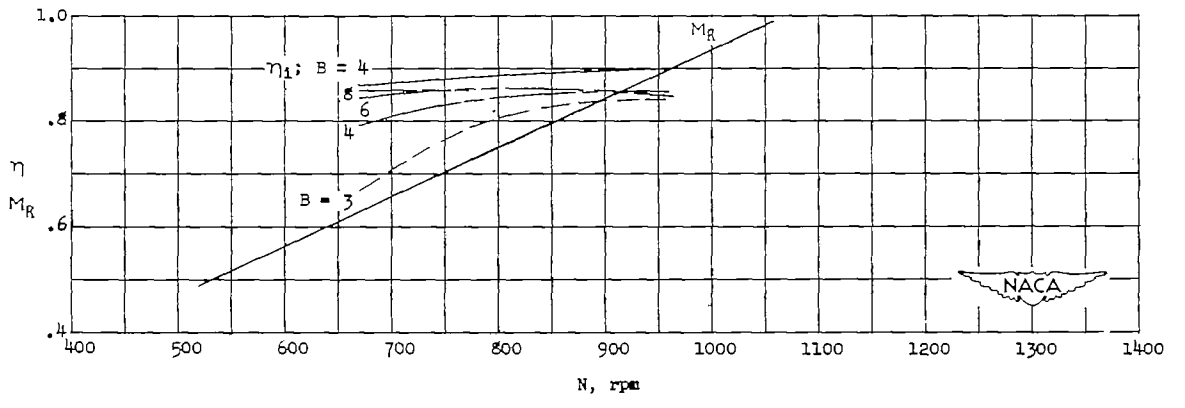

(d) D = 20.0; V = 250 mph.

Figure 14.- Concluded.

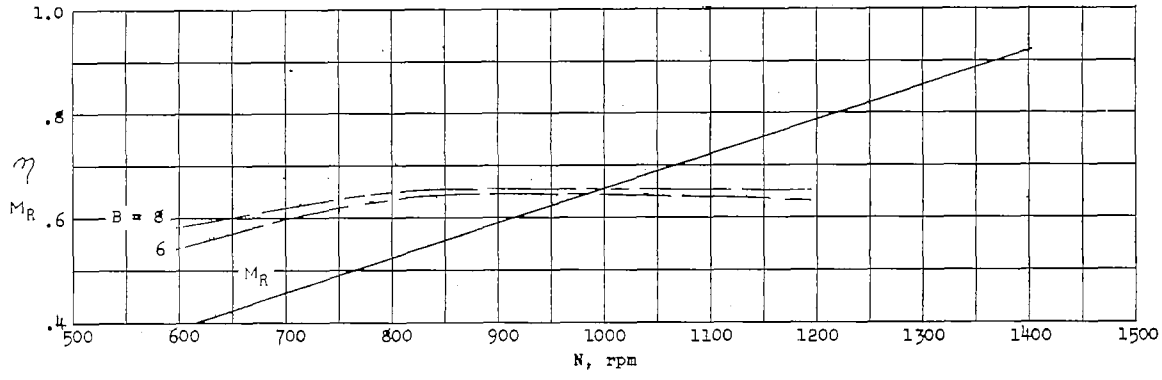

(a) D = 14.0; V = 100 mph; η_a = 0.695.

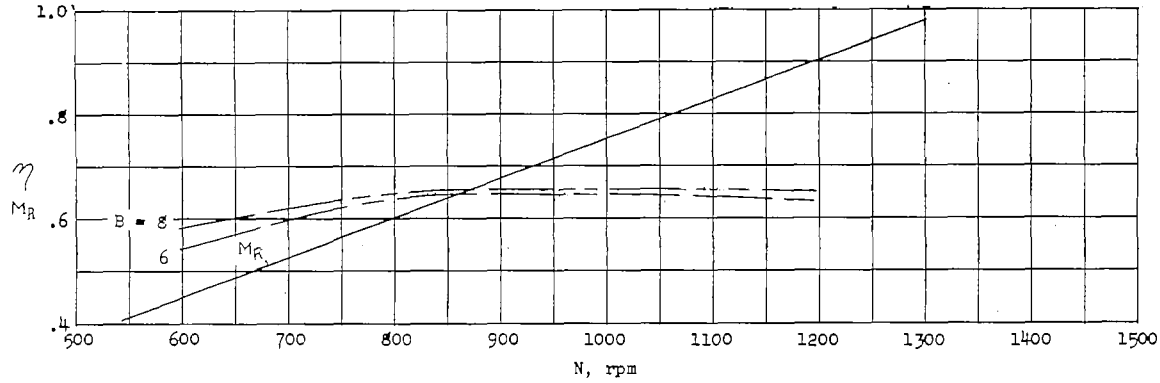

(b) D = 16.0; V = 100 mph; η_a = 0.725.

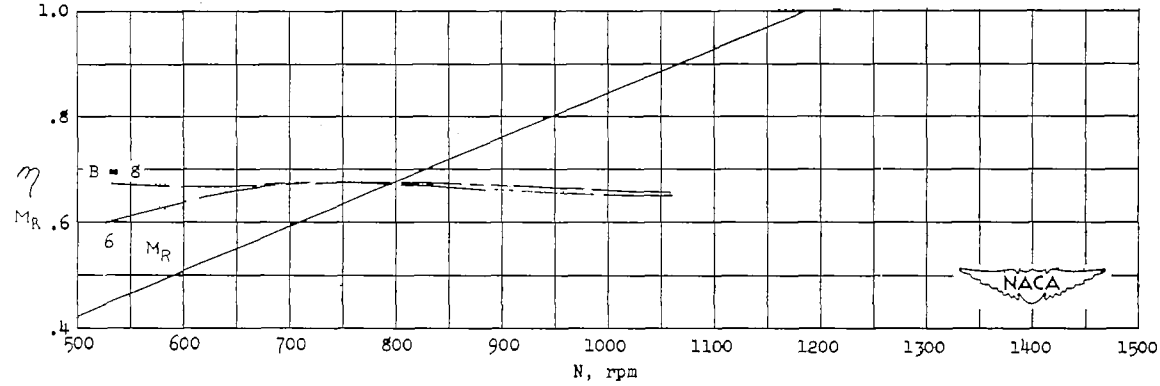

(c) D = 18.0; V = 100 mph; η_a = 0.758.

Figure 15.- Propeller efficiency and tip Mach number at sea level. Dual rotation; 4,000 horsepower; activity factor, 120 per blade.

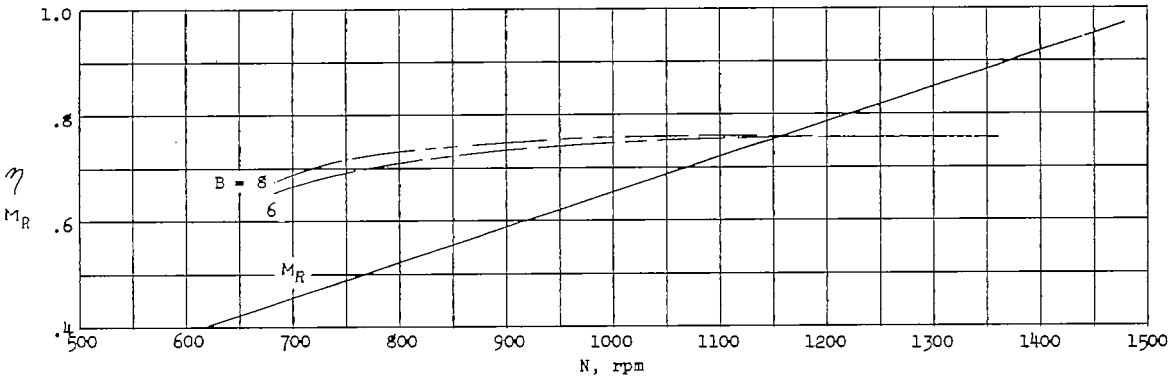

(d) D = 14.0; V = 150 mph; η_a = 0.835.

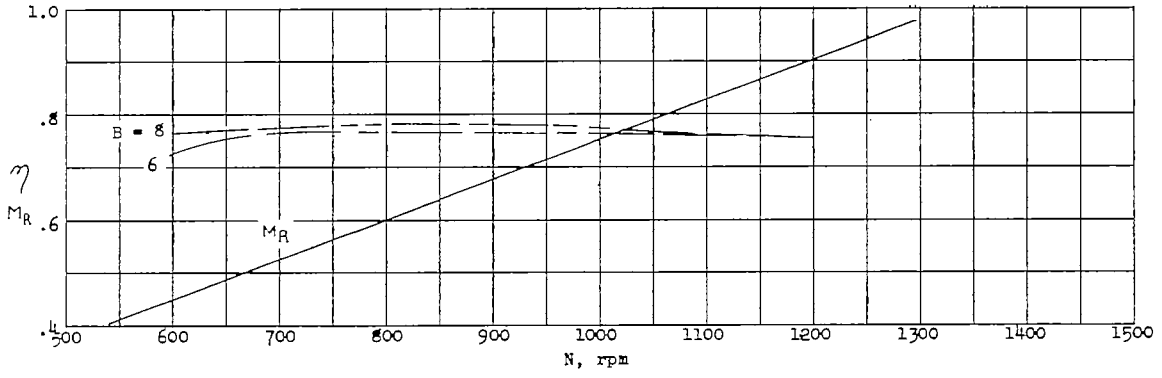

(e) D = 16.0; V = 150 mph; η_a = 0.860.

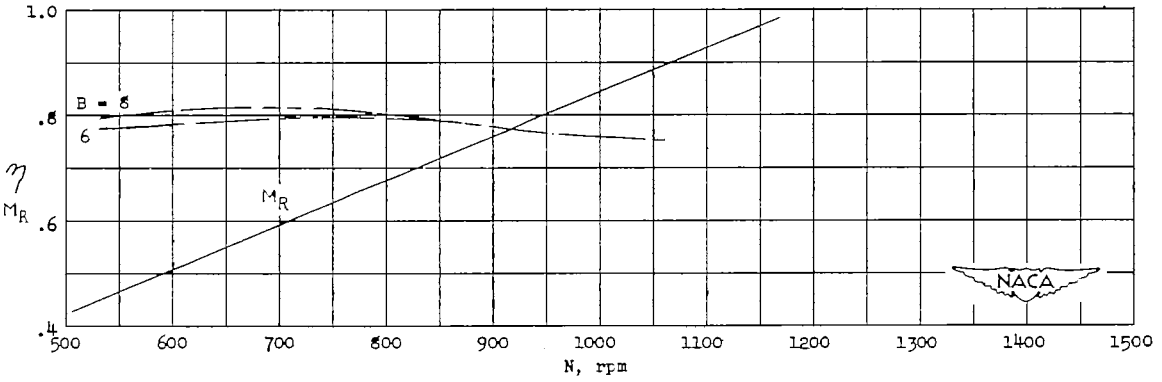

(f) D = 18.0; V = 150 mph; η_a = 0.875.

Figure 15.- Continued.

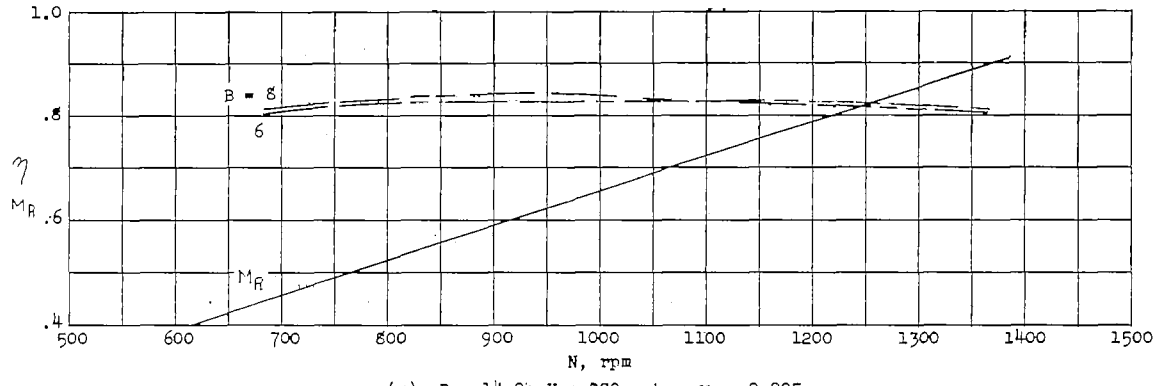

(g) D = 14.0; V = 200 mph; η_a = 0.905.

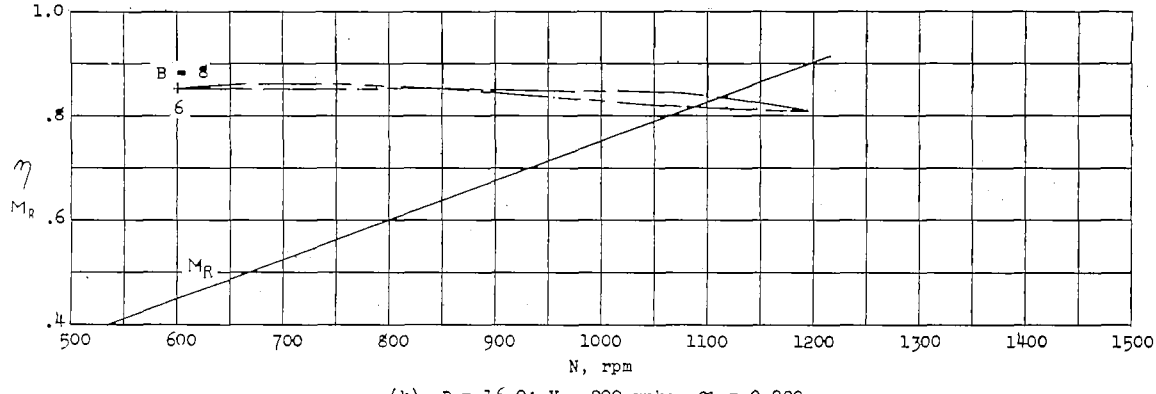

(h) D = 16.0; V = 200 mph; η_a = 0.920.

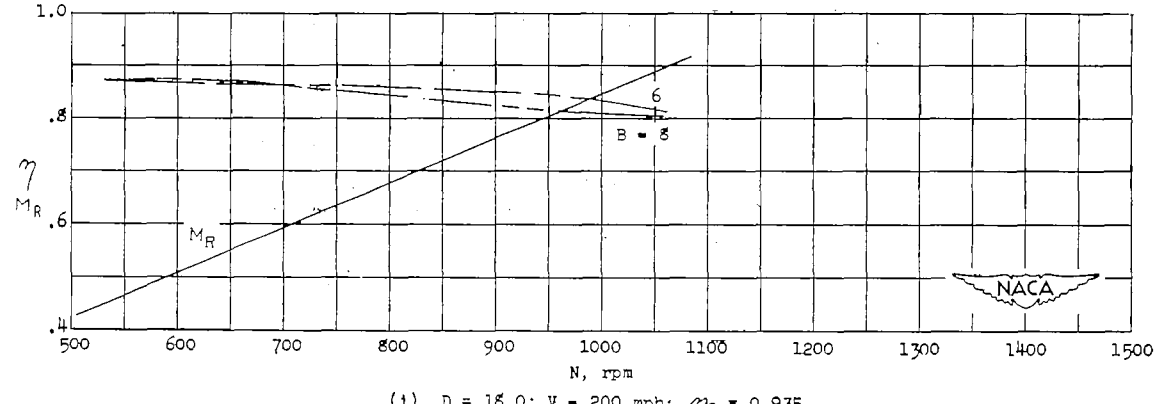

(i) D = 18.0; V = 200 mph; η_a = 0.935.

Figure 15.- Continued.

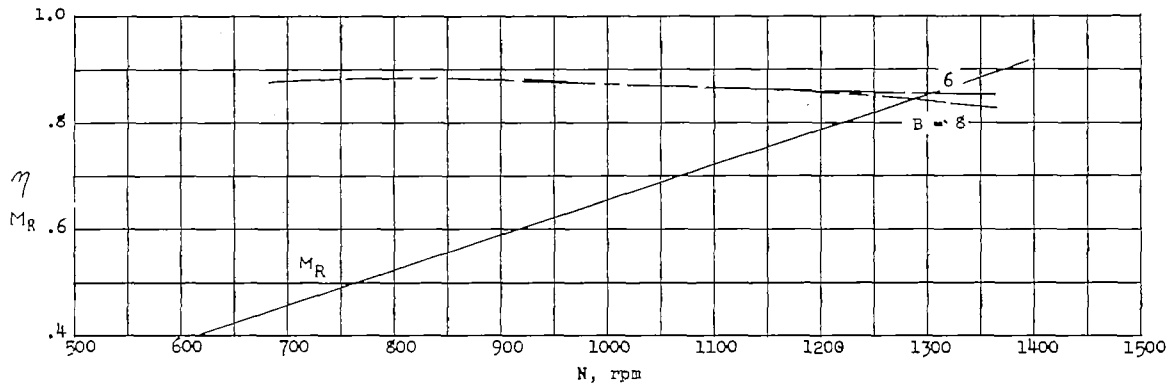

(j) D = 14.0; V = 250 mph; η_a = 0.945.

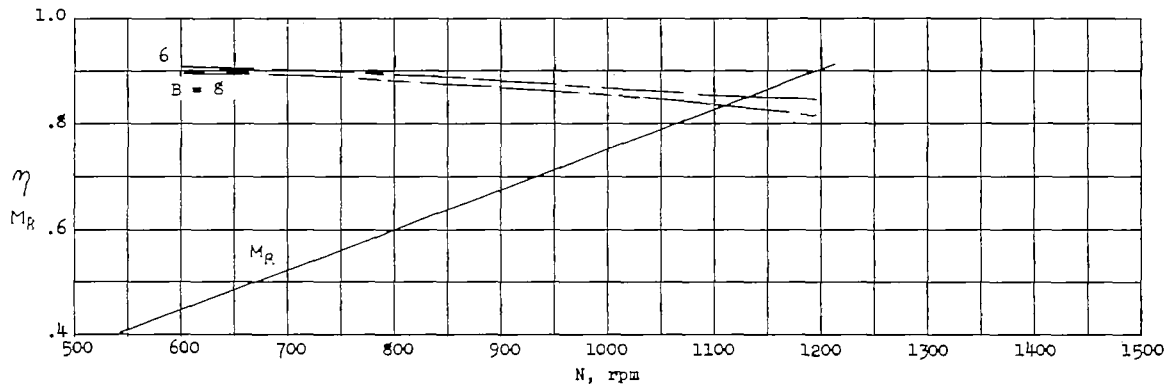

(k) D = 16.0; V = 250 mph; η_a = 0.955.

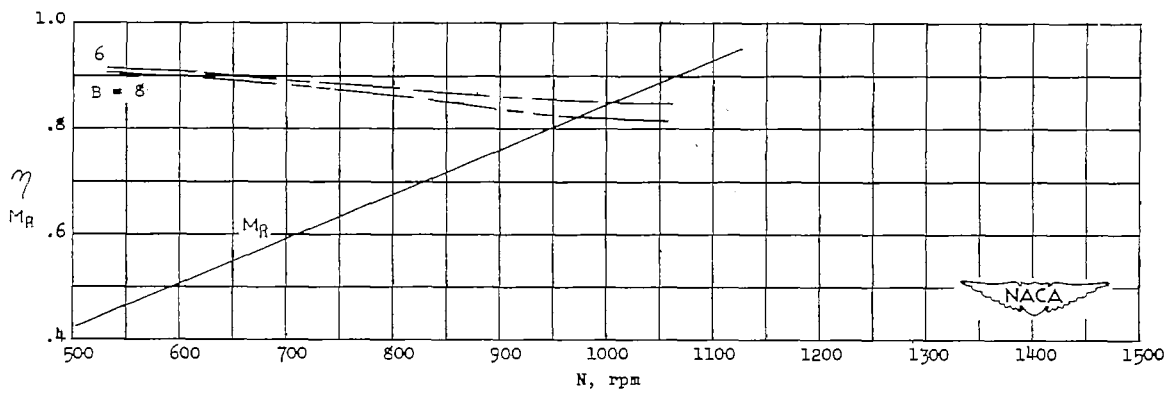

(l) D = 18.0; V = 250 mph; η_a = 0.960.

Figure 15.- Concluded.

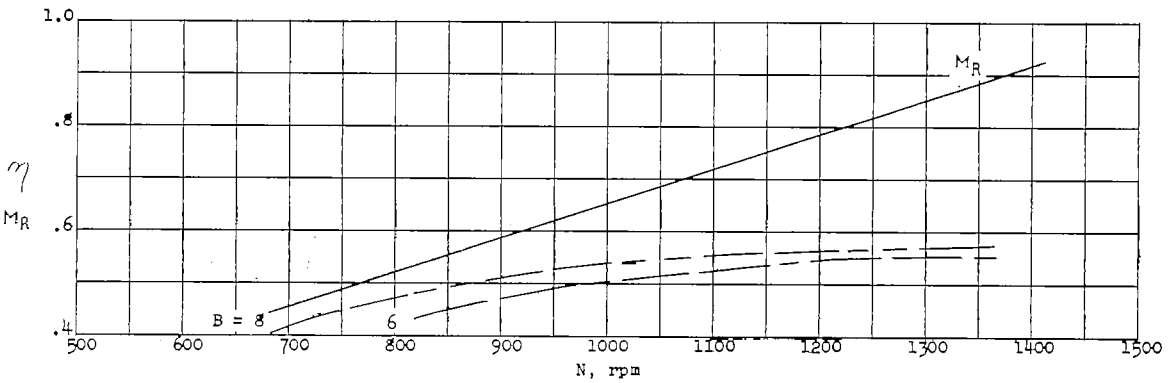

(a) D = 14.0; V = 100 mph; η_a = 0.635.

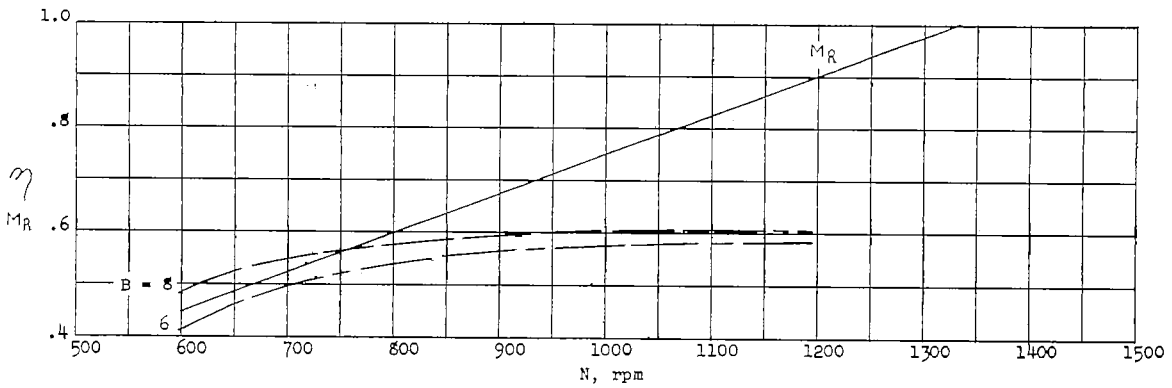

(b) D = 16.0; V = 100 mph; η_a = 0.670.

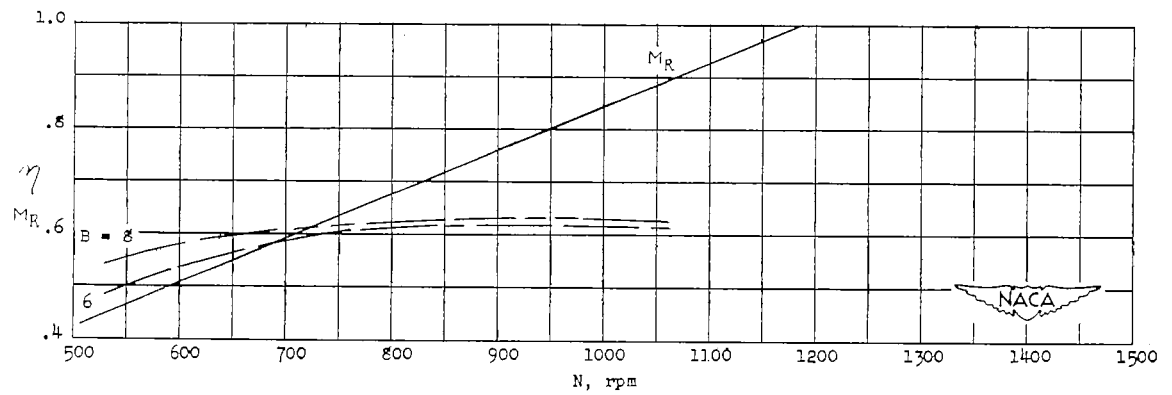

(c) D = 18.0; V = 100 mph; η_a = 0.705.

Figure 16.- Propeller efficiency and tip Mach number at sea level. Dual rotation; 6,000 horsepower; activity factor, 120 per blade.

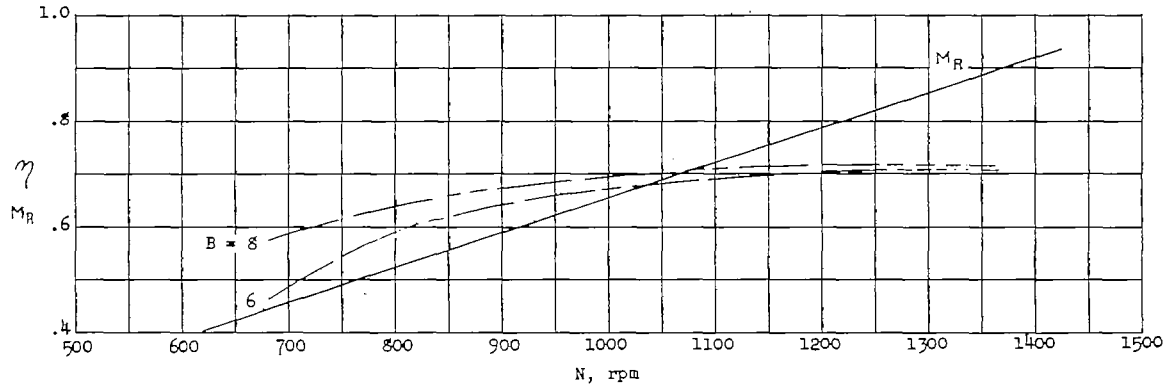

(d) D = 14.0; V = 150 mph; η_a = 0.792.

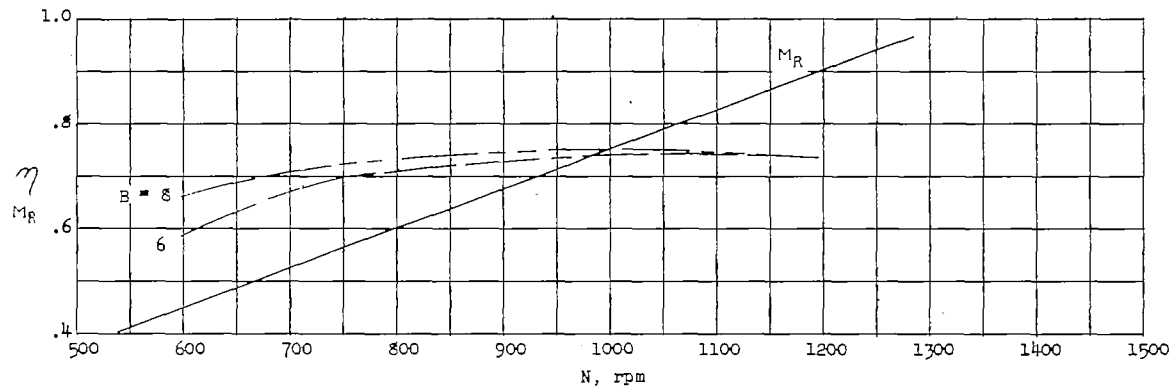

(e) D = 16.0; V = 150 mph; η_a = 0.820.

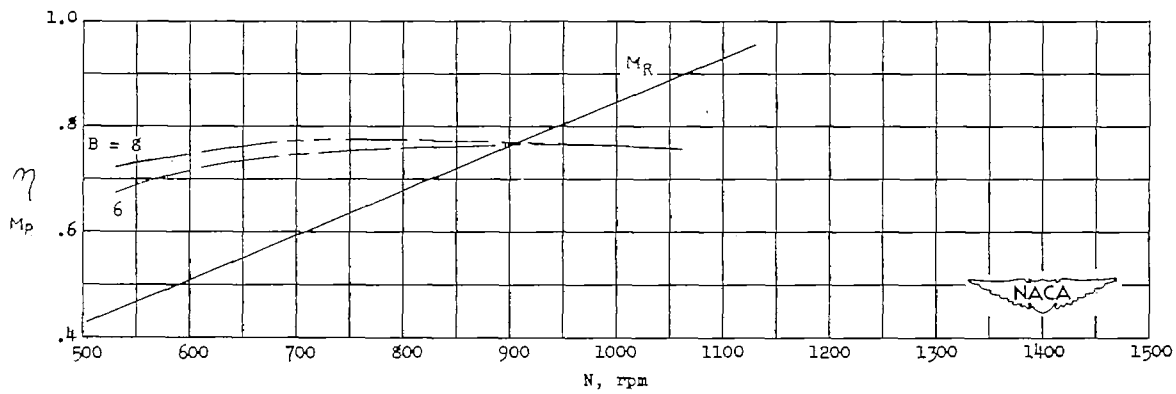

(f) D = 18.0; V = 150 mph; η_a = 0.840.

Figure 16.- Continued.

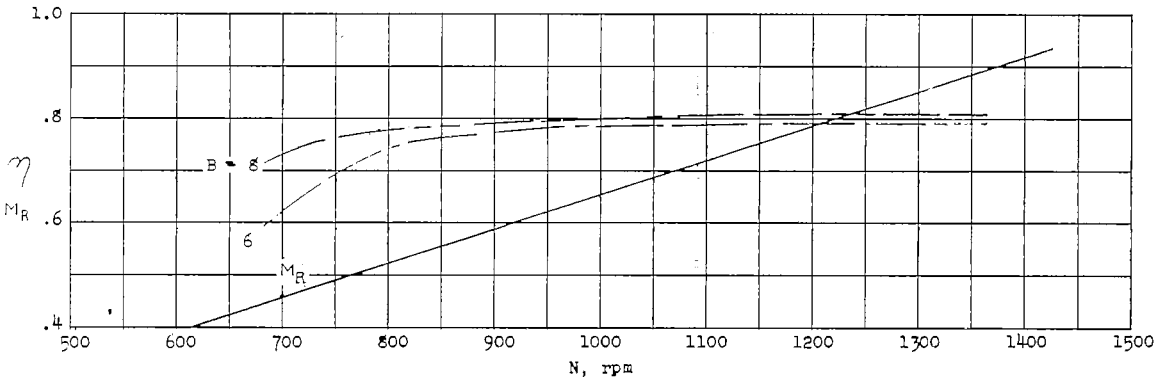

(g) D = 14.0; V = 200 mph; η_a = 0.878.

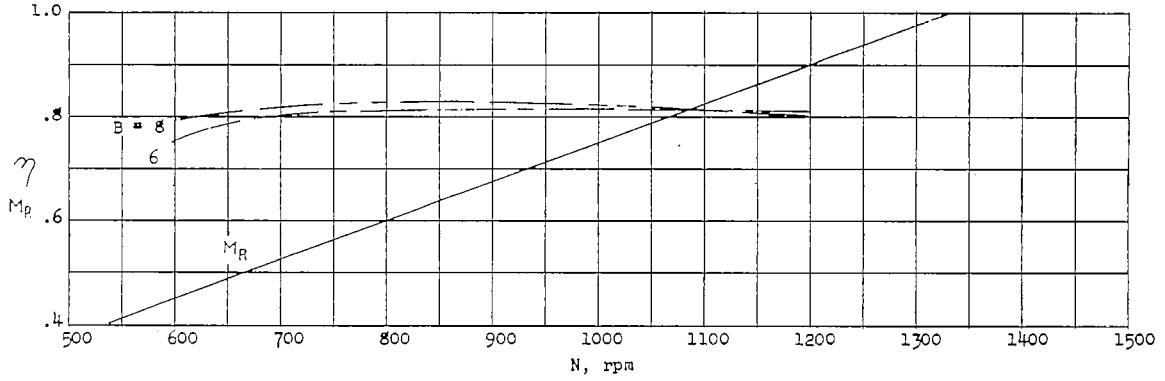

(h) D = 16.0; V = 200 mph; η_a = 0.895.

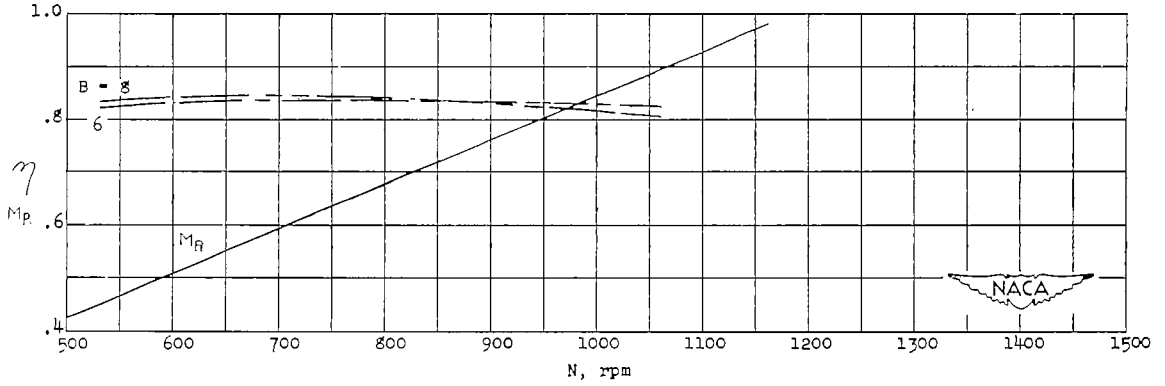

(i) D = 18.0; V = 200 mph; η_a = 0.910.

Figure 16.- Continued.

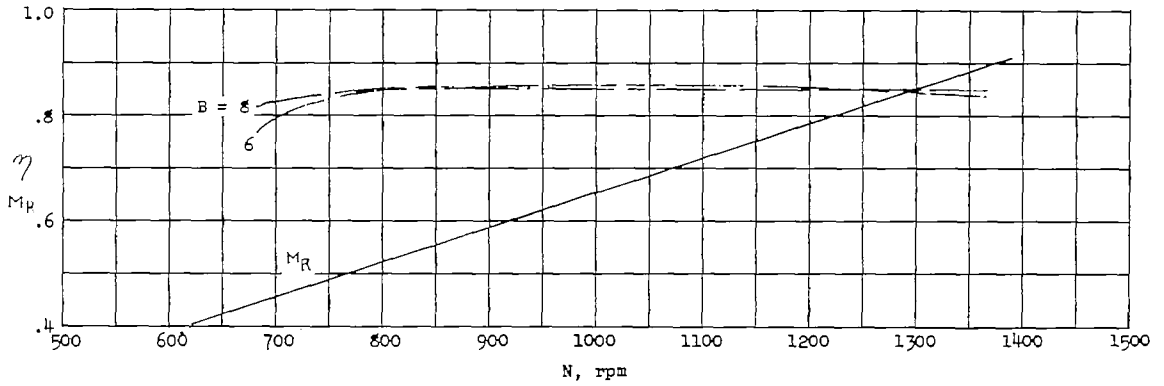

(j) D = 14.0; V = 250 mph; η_a = 0.920.

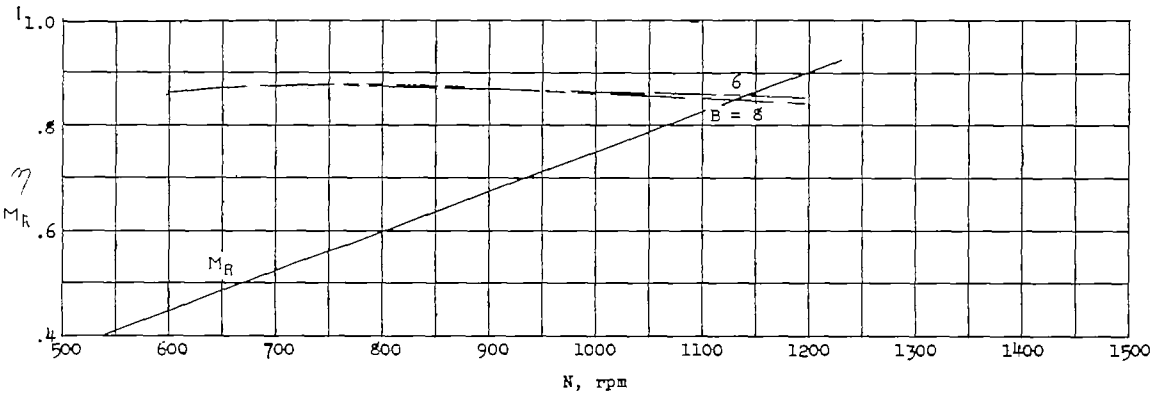

(k) D = 16.0; V = 250 mph; η_a = 0.939.

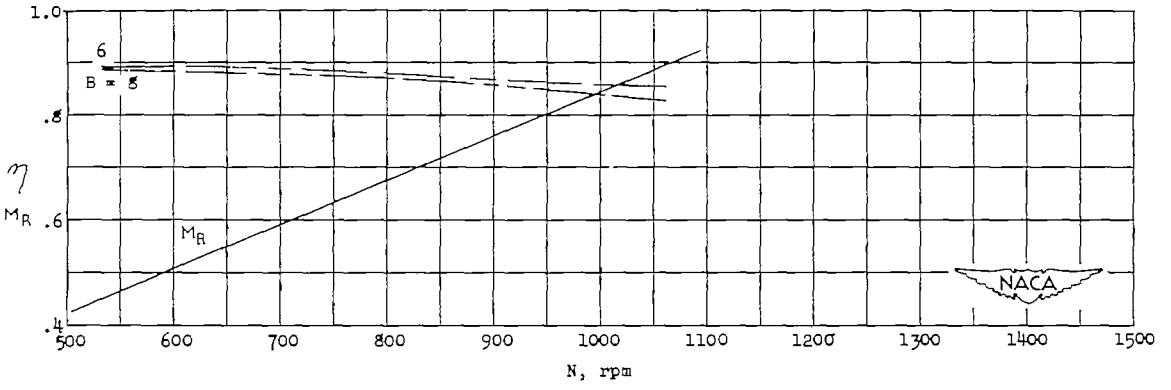

(l) D = 18.0; V = 250 mph; η_a = 0.950.

Figure 16.- Concluded.

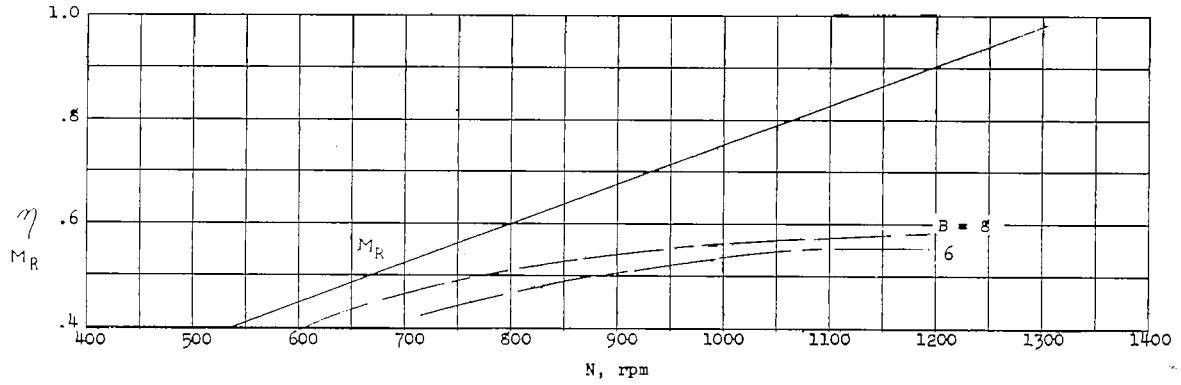

(a) D = 16.0; V = 100 mph; η_a = 0.635.

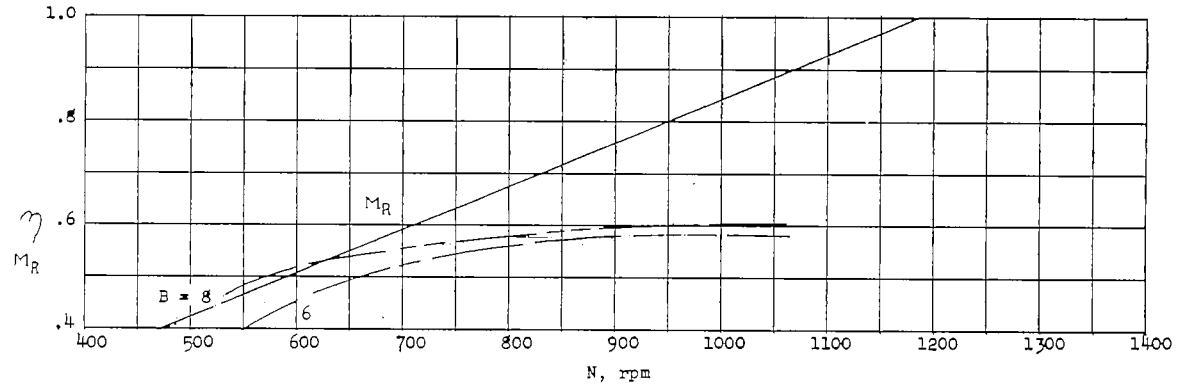

(b) D = 18.0; V = 100 mph; η_a = 0.665.

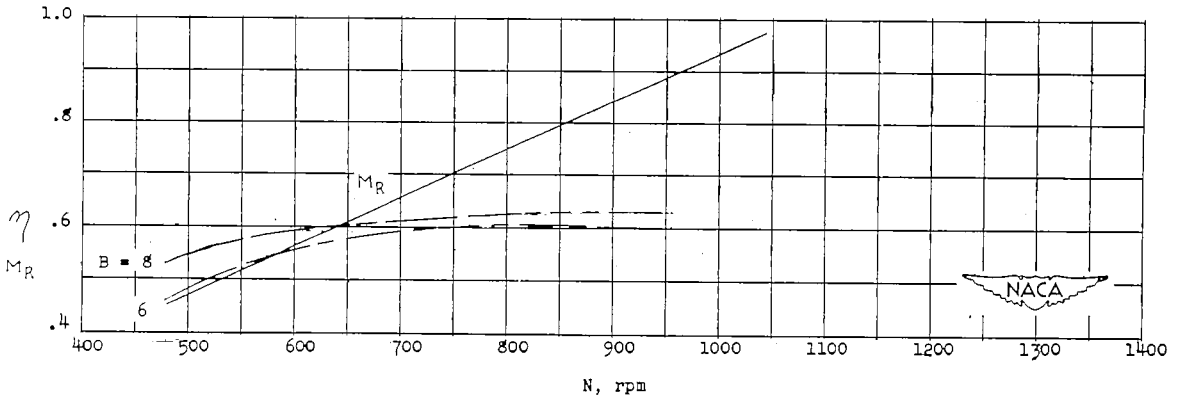

(c) D = 20.0; V = 100 mph; η_a = 0.695.

Figure 17.- Propeller efficiency and tip Mach number at sea level. Dual rotation; 8,000 horsepower; activity factor, 120 per blade.

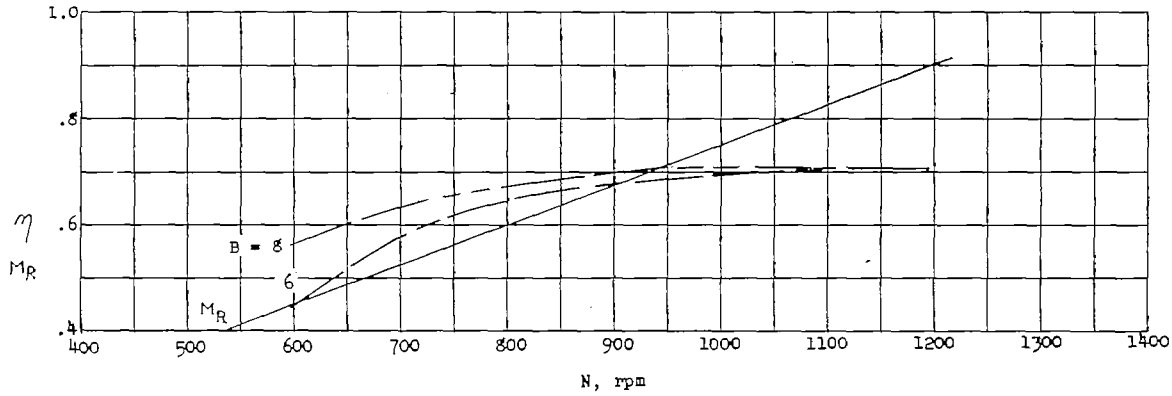

(d) D = 16.0; V = 150 mph; η_a = 0.790.

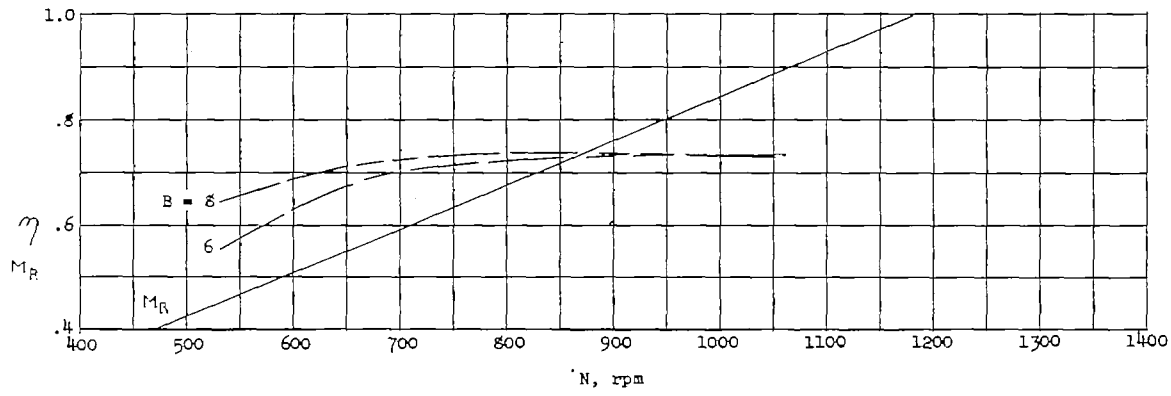

(e) D = 18.0; V = 150 mph; η_a = 0.815.

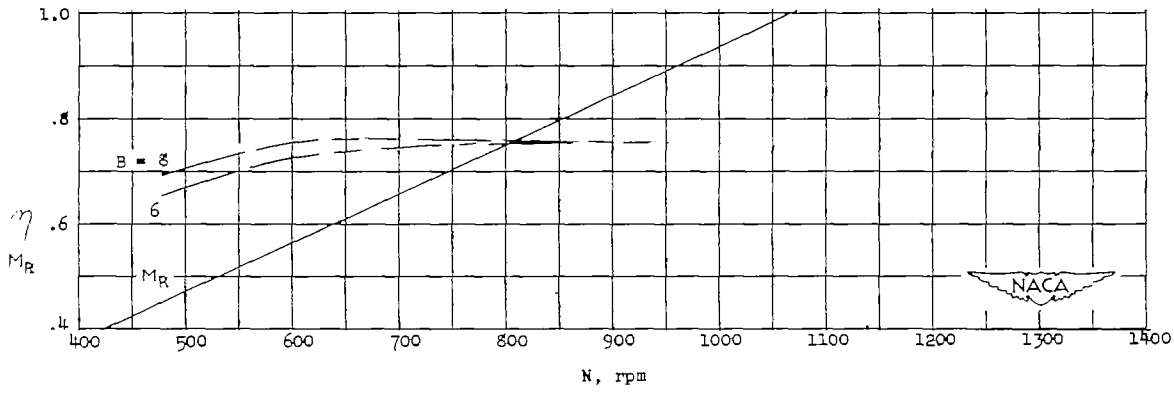

(f) D = 20.0; V = 150 mph; η_a = 0.839.

Figure 17.- Continued.

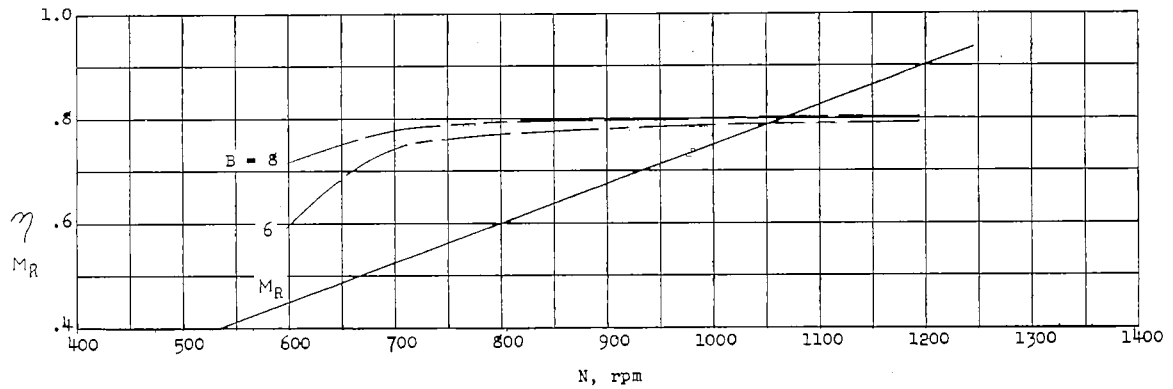

(g) D = 16.0; V = 200 mph; η_a = 0.871.

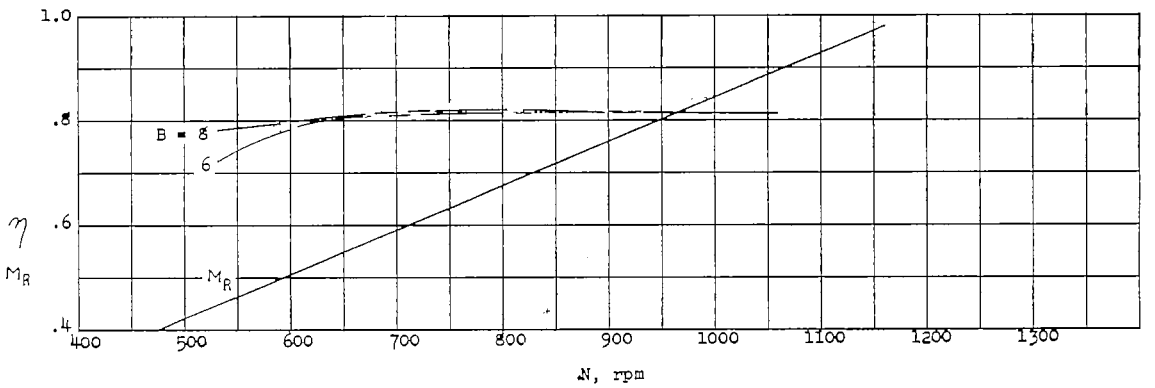

(h) D = 18.0; V = 200 mph; η_a = 0.890.

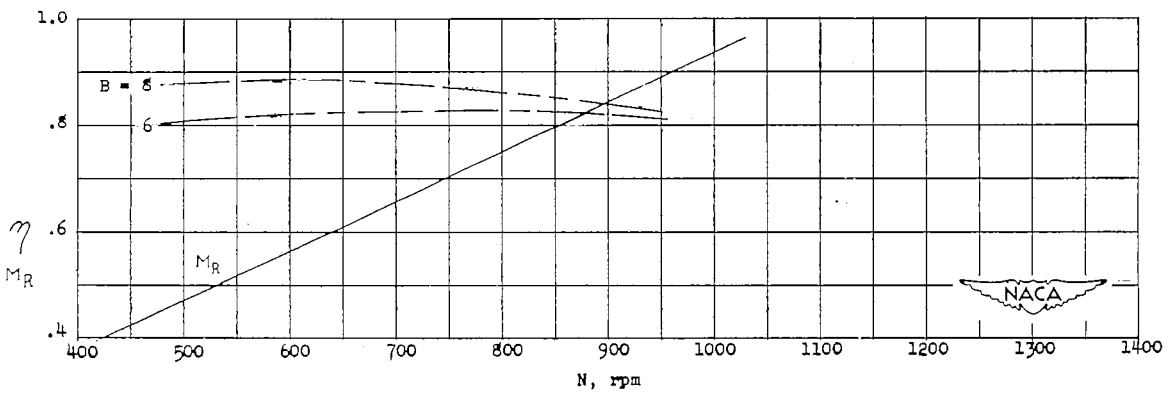

(i) D = 20.0; V = 200 mph; η_a = 0.908.

Figure 17.- Continued.

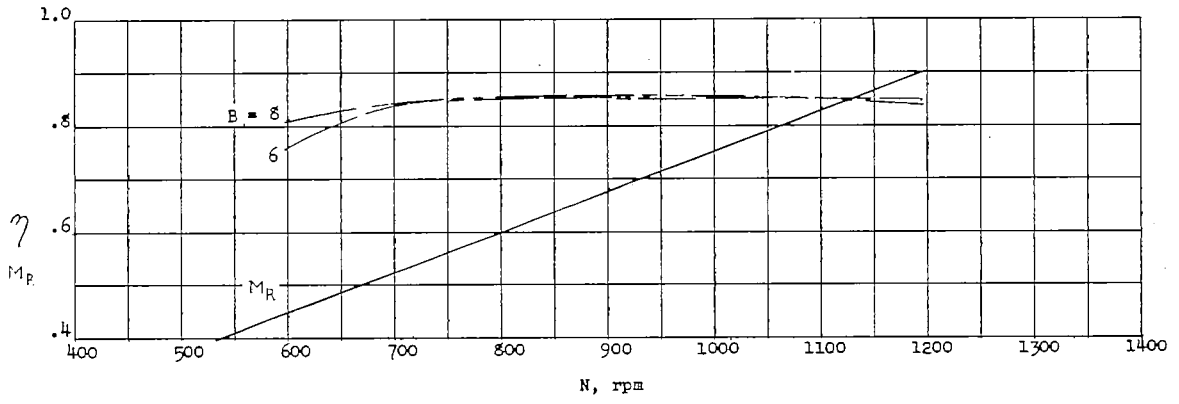

(j) D = 16.0; V = 250 mph; η_a = 0.920.

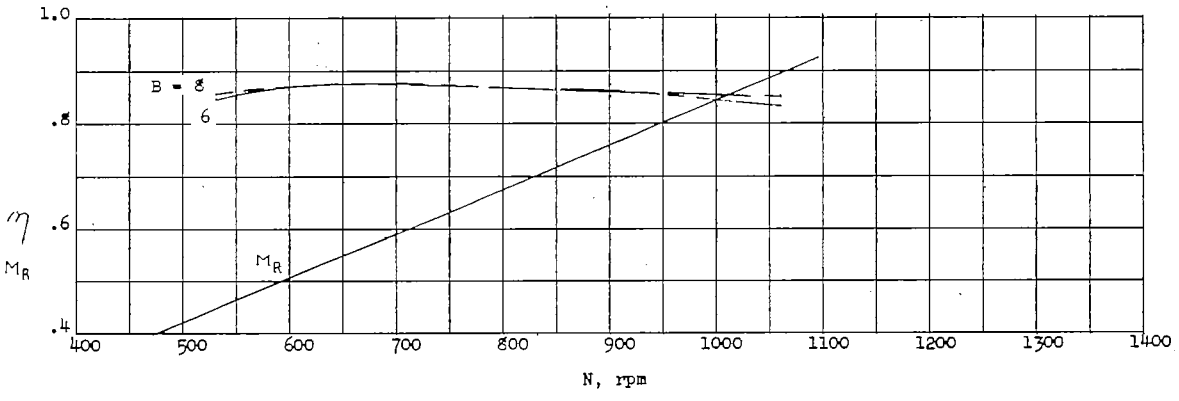

(k) D = 18.0; V = 250 mph; η_a = 0.935.

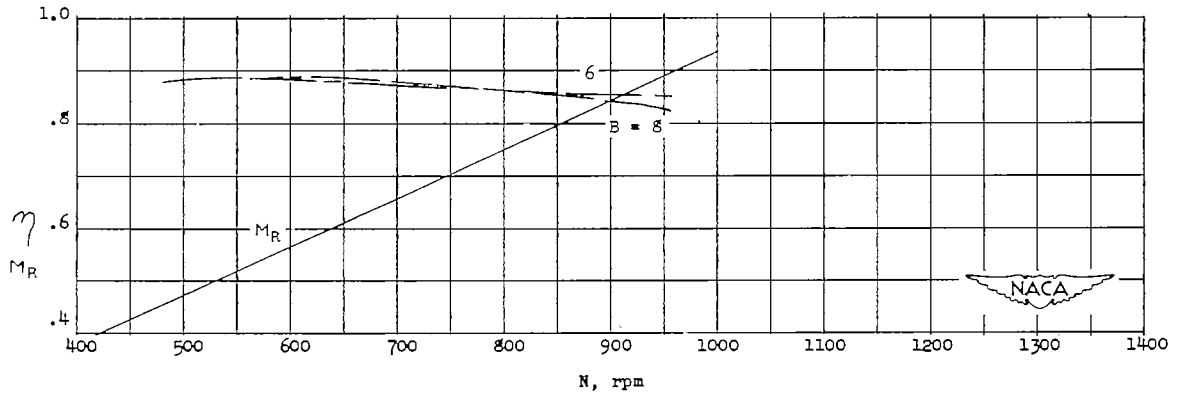

(l) D = 20.0; V = 250 mph; η_a = 0.945.

Figure 17.- Concluded.

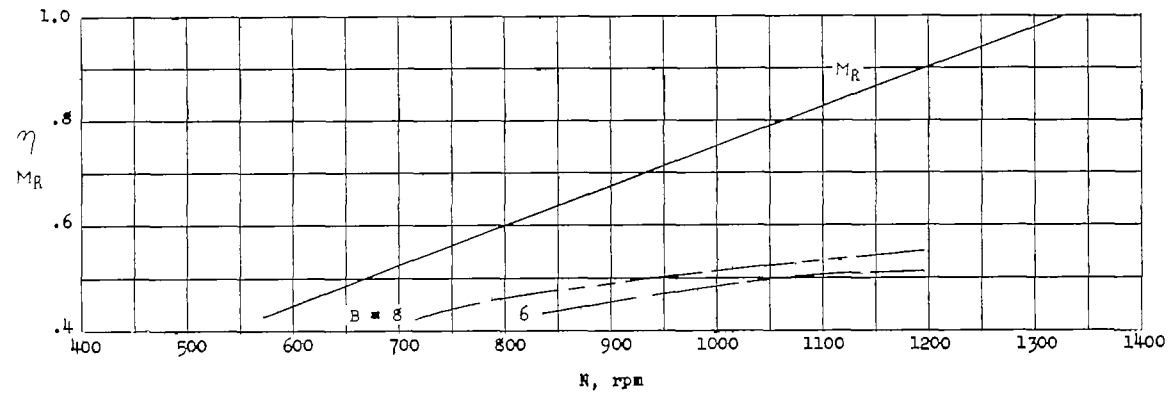

(a) D = 16.0; V = 100 mph; η_a = 0.600.

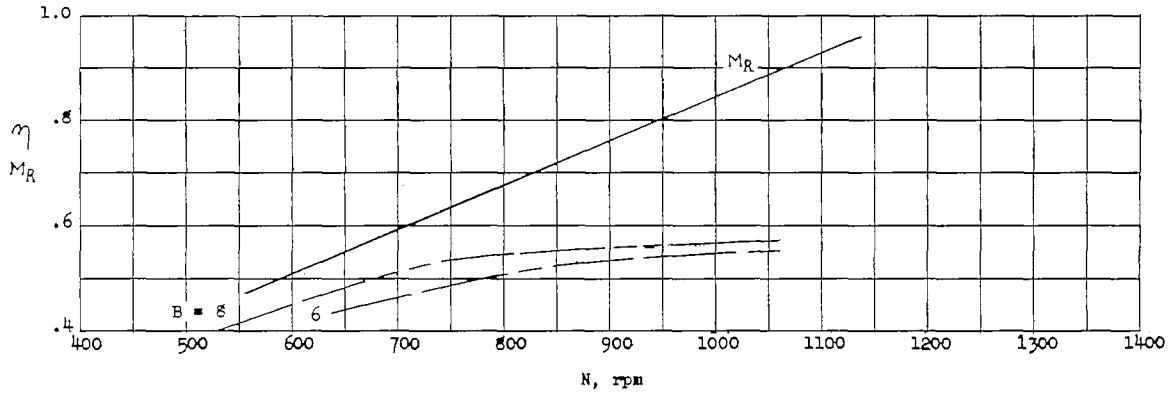

(b) D = 18.0; V = 100 mph; η_a = 0.635.

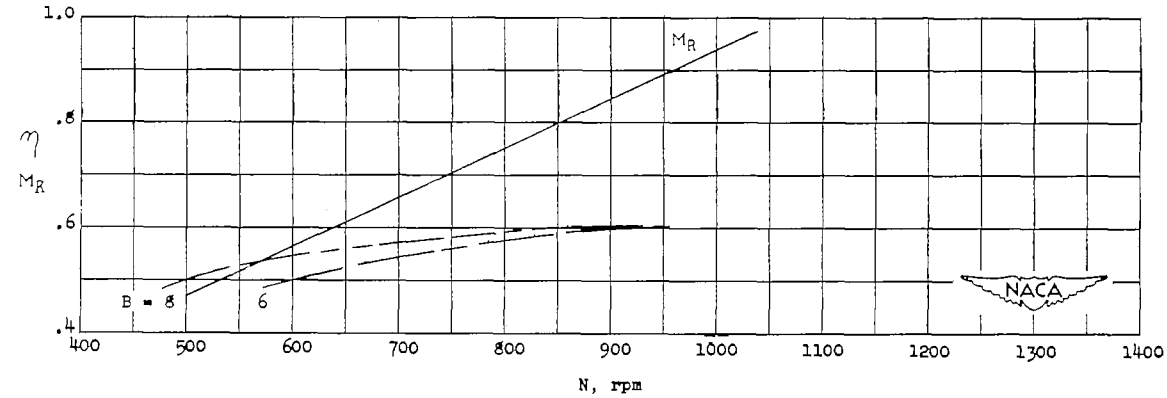

(c) D = 20.5; V = 100 mph; η_a = 0.661.

Figure 18.- Propeller efficiency and tip Mach number at sea level. Dual rotation; 10,000 horsepower; activity factor, 120 per blade.

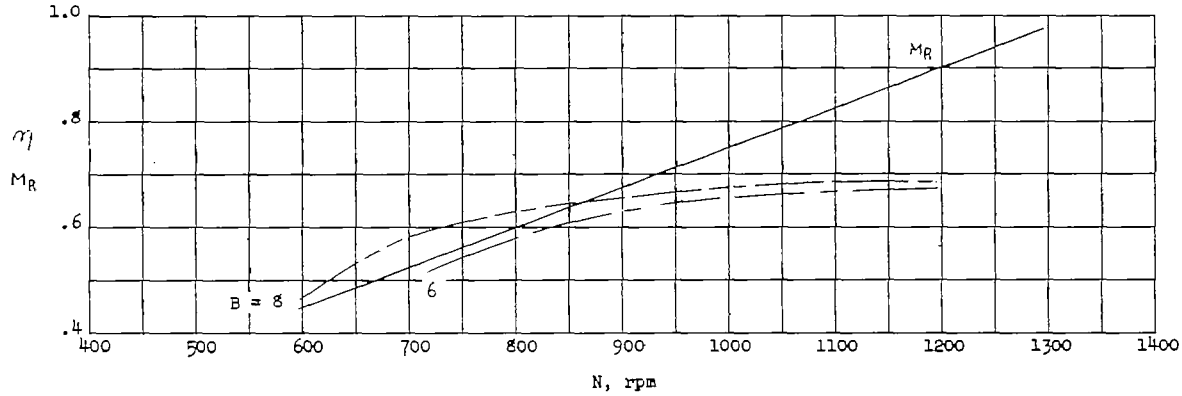

(d) D = 16.0; V = 150 mph; η_a = 0.765.

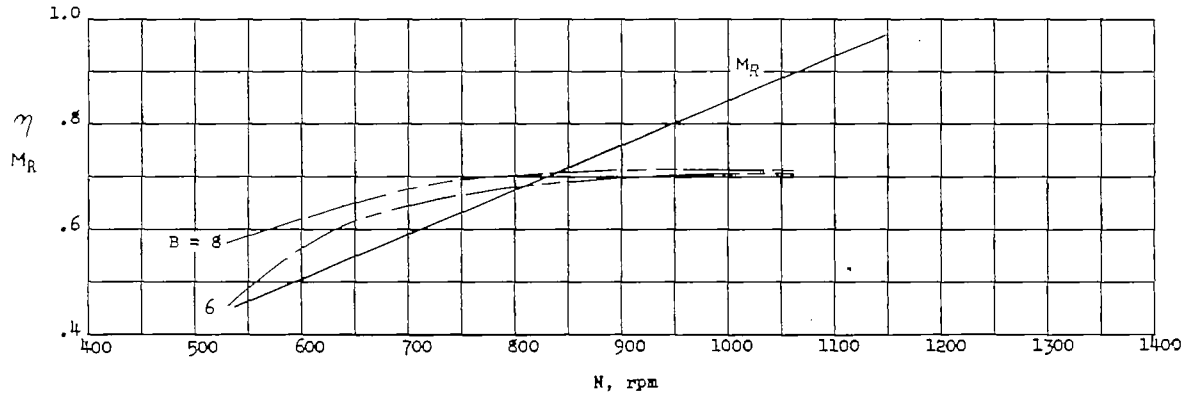

(e) D = 18.0; V = 150 mph; η_a = 0.790.

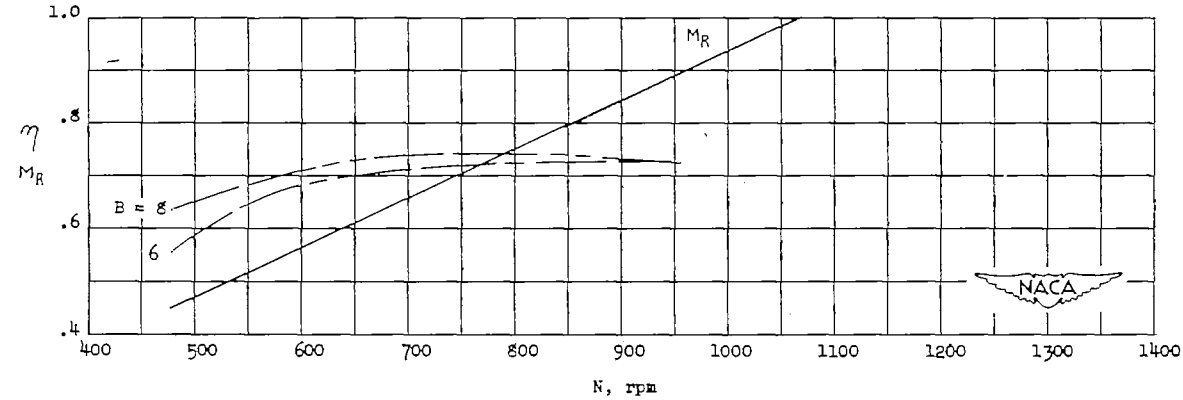

(f) D = 20.0; V = 150 mph; η_a = 0.815.

Figure 18.- Continued.

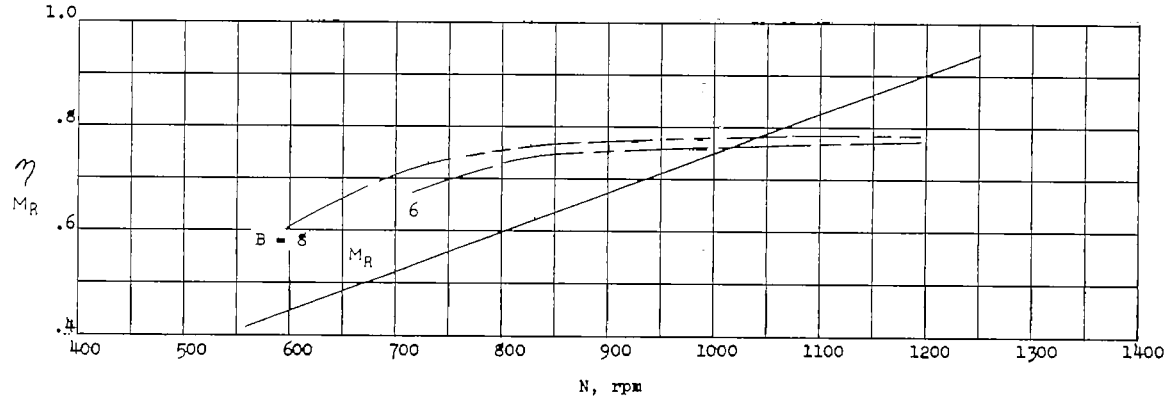

(g) D = 16.0; V = 200 mph; η_a = 0.855.

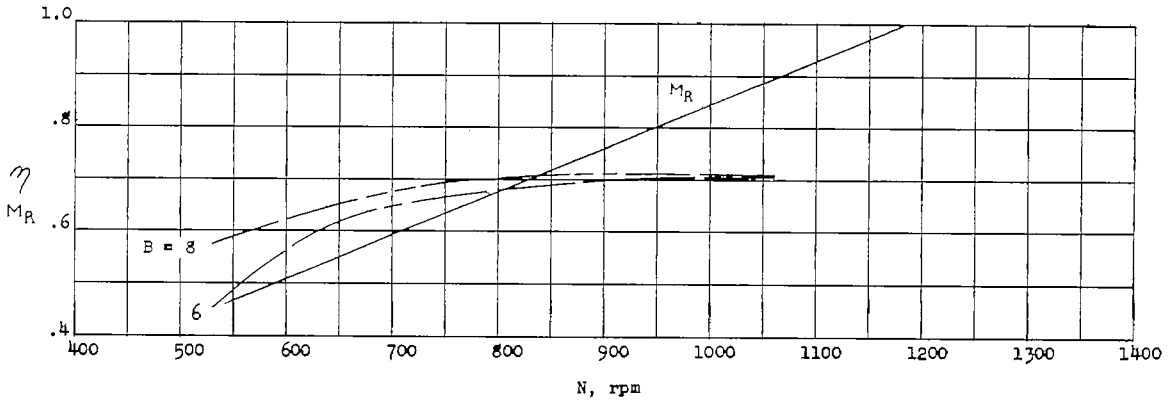

(h) D = 18.0; V = 200 mph; η_a = 0.878.

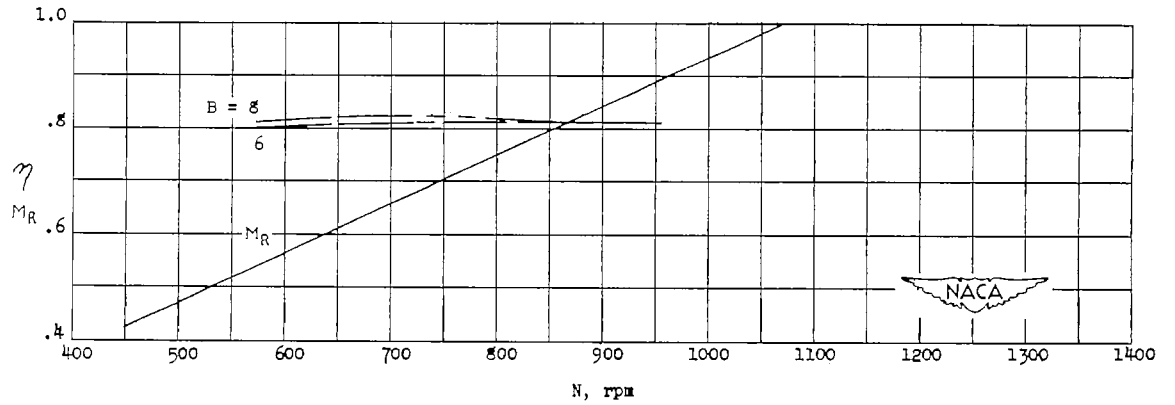

(i) D = 20.0; V = 200 mph; η_a = 0.890.

Figure 18.- Continued.

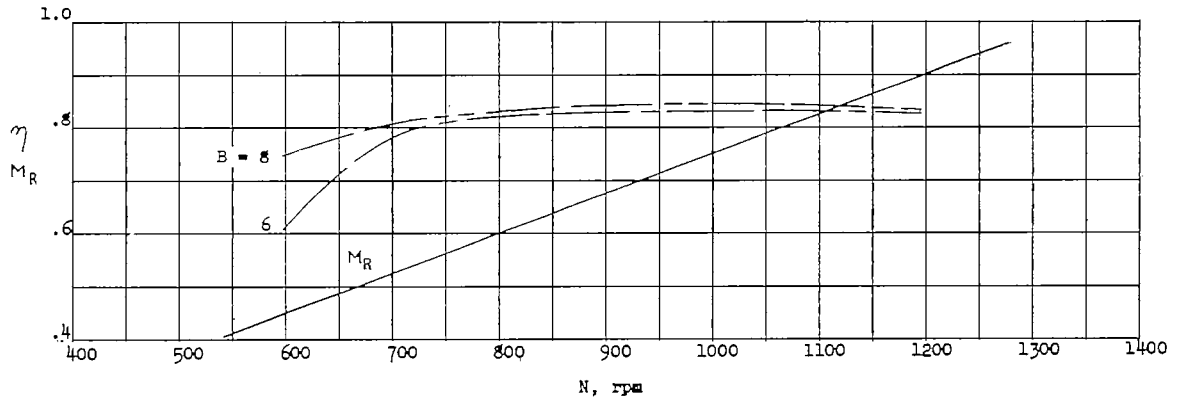

(j) D = 16.0; V = 250 mph; η_a = 0.909.

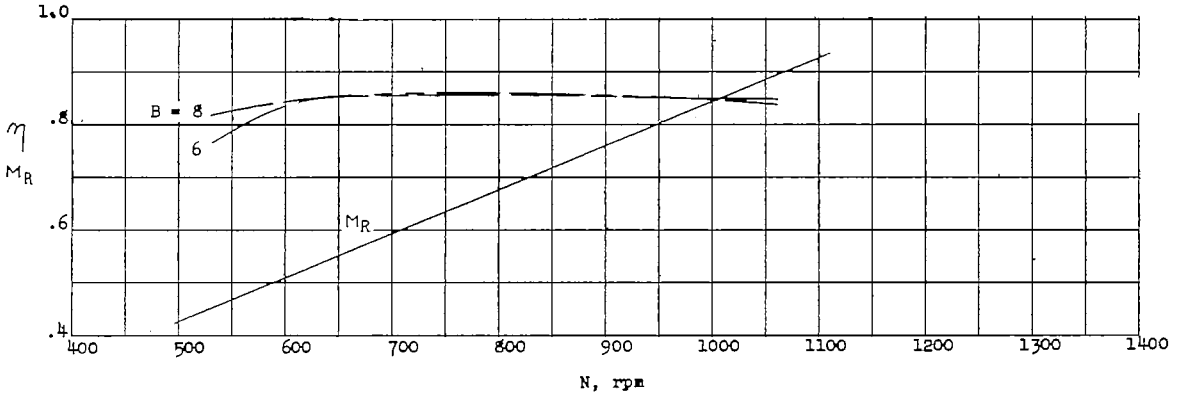

(k) D = 18.0; V = 250 mph; η_a = 0.920.

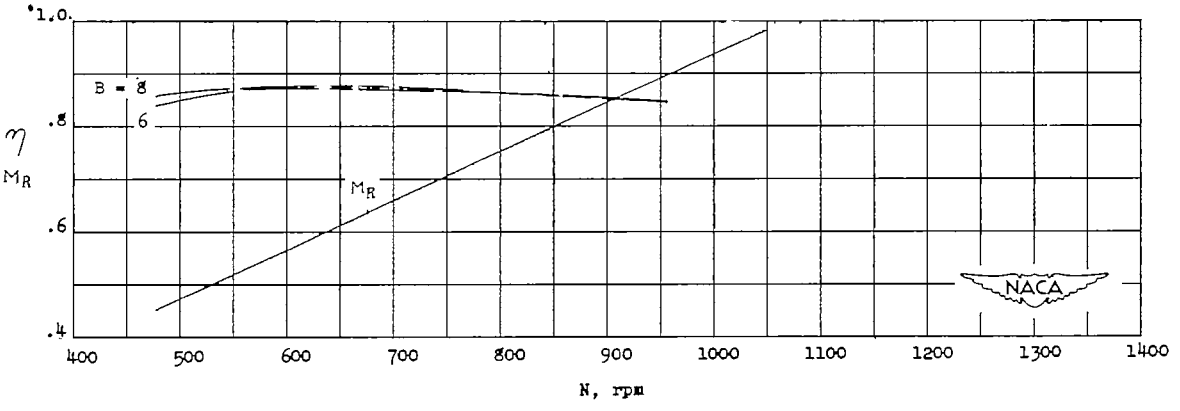

(l) D = 20.0; V = 250 mph; η_a = 0.932.

Figure 18.- Concluded.

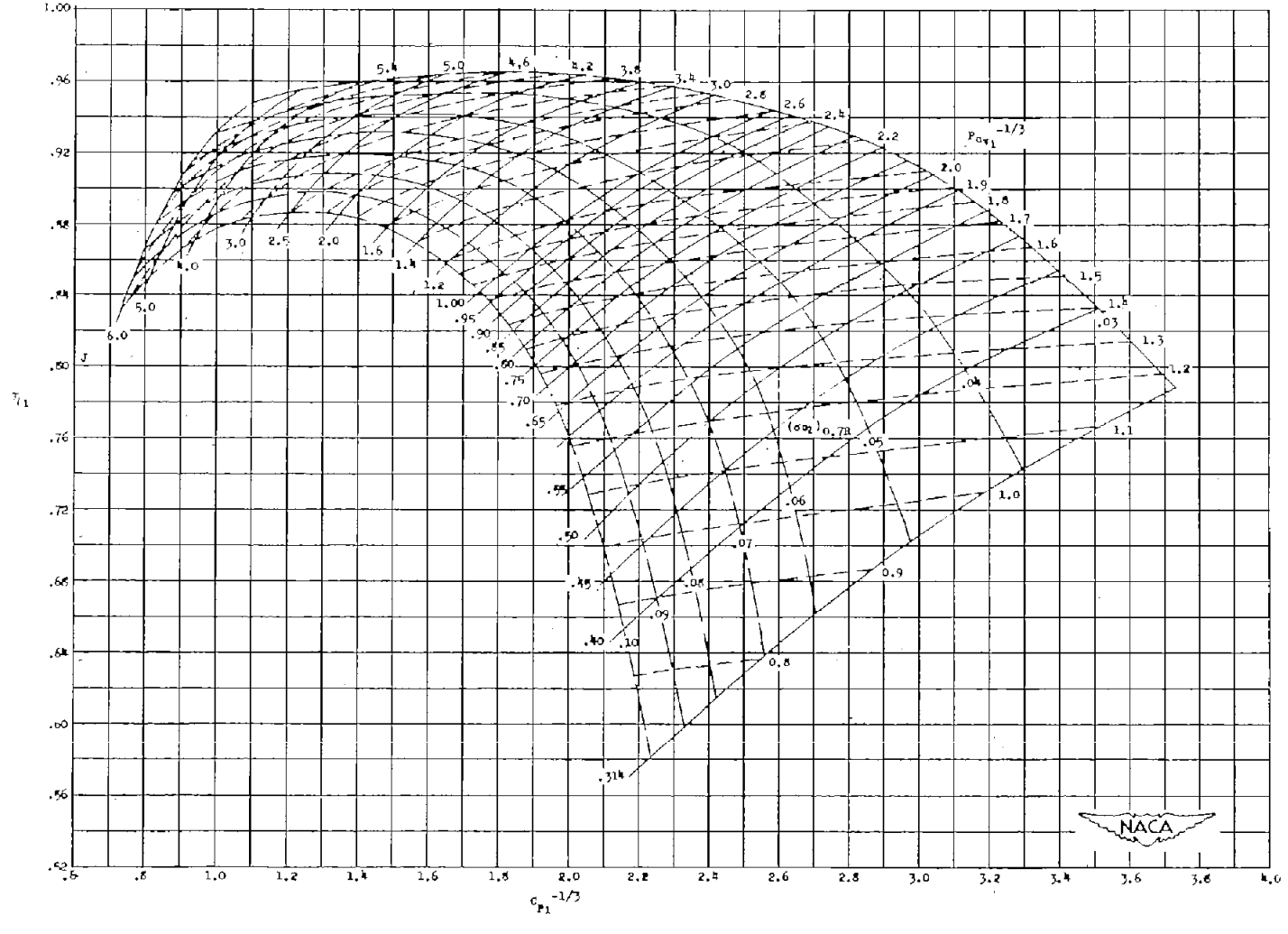

(a) Three-blade propellers..

Figure 19.- Propeller performance charts. Without drag.

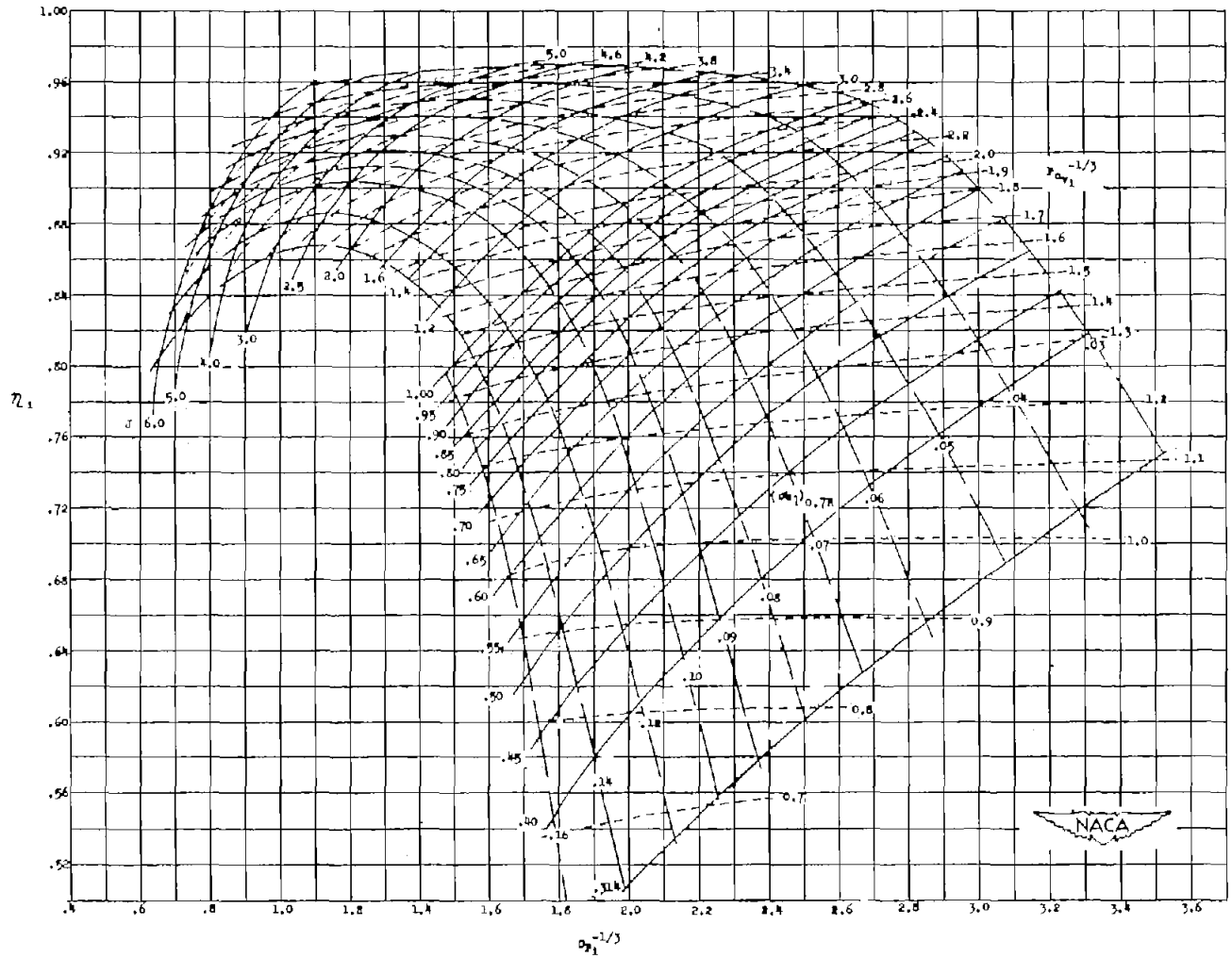

(b) Four-blade propellers.

Figure 19.- Continued.

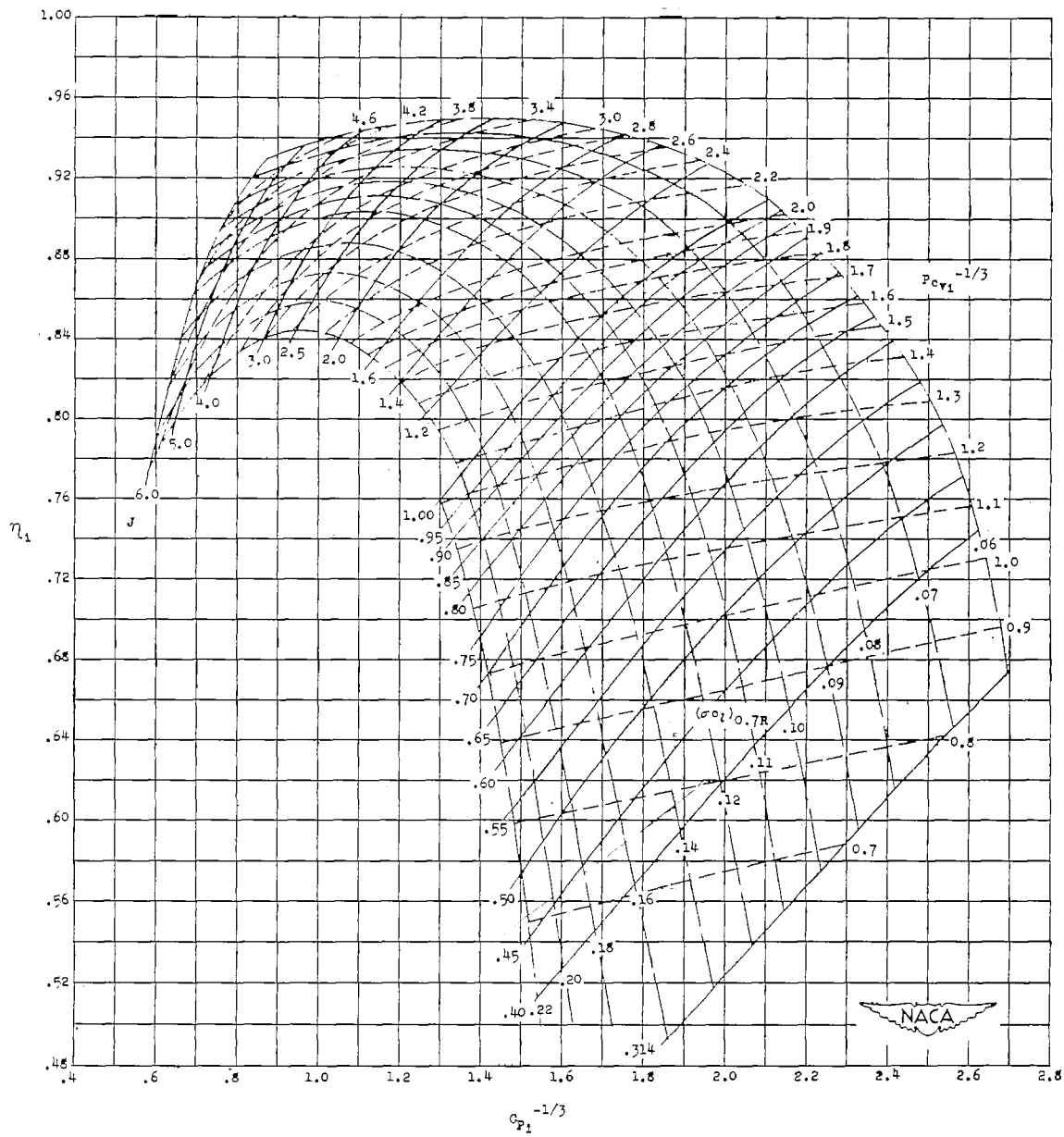

(c) Six-blade propellers.

Figure 19.- Continued.

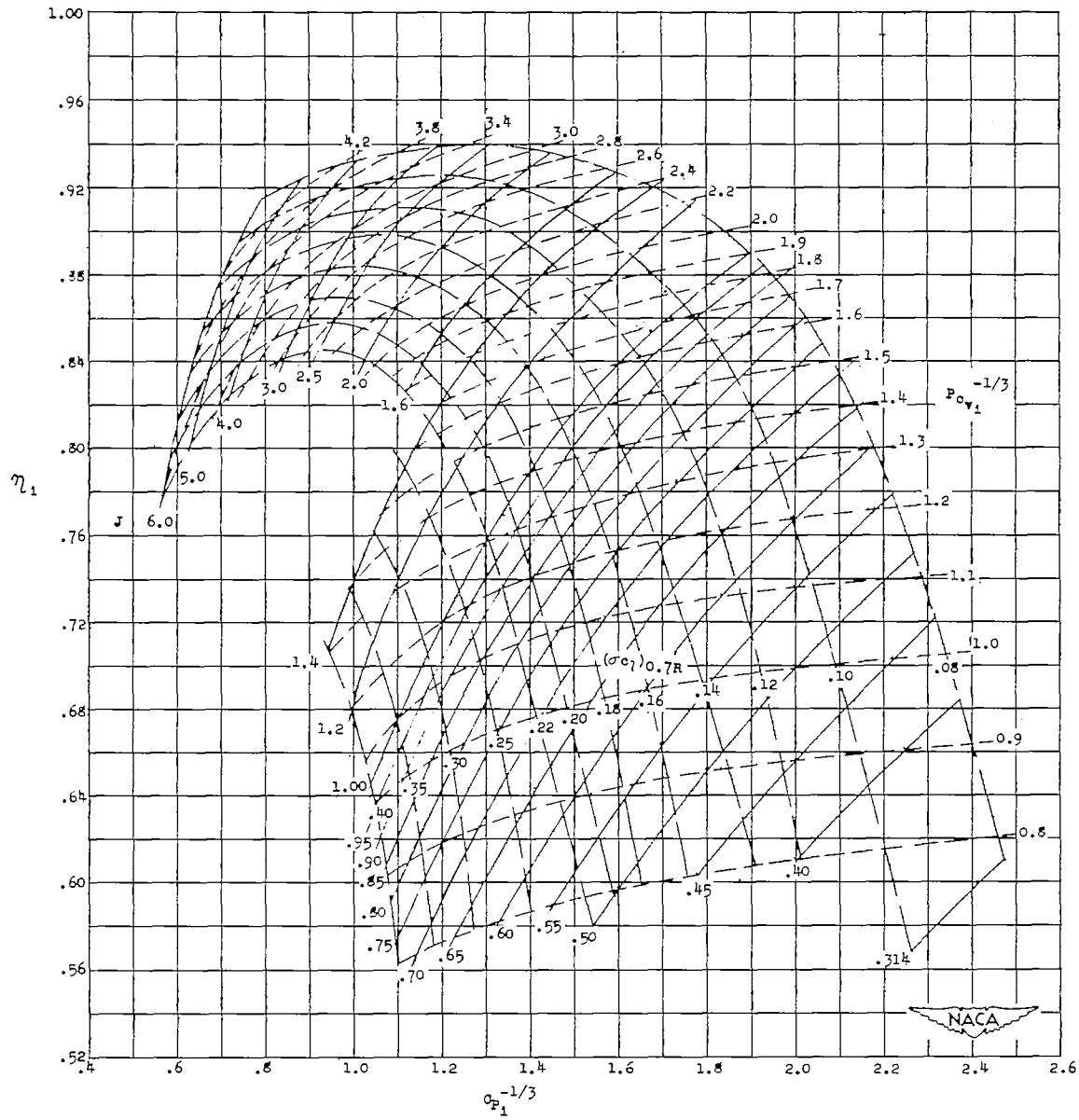

(d) Eight-blade propellers.

Figure 19.- Concluded.

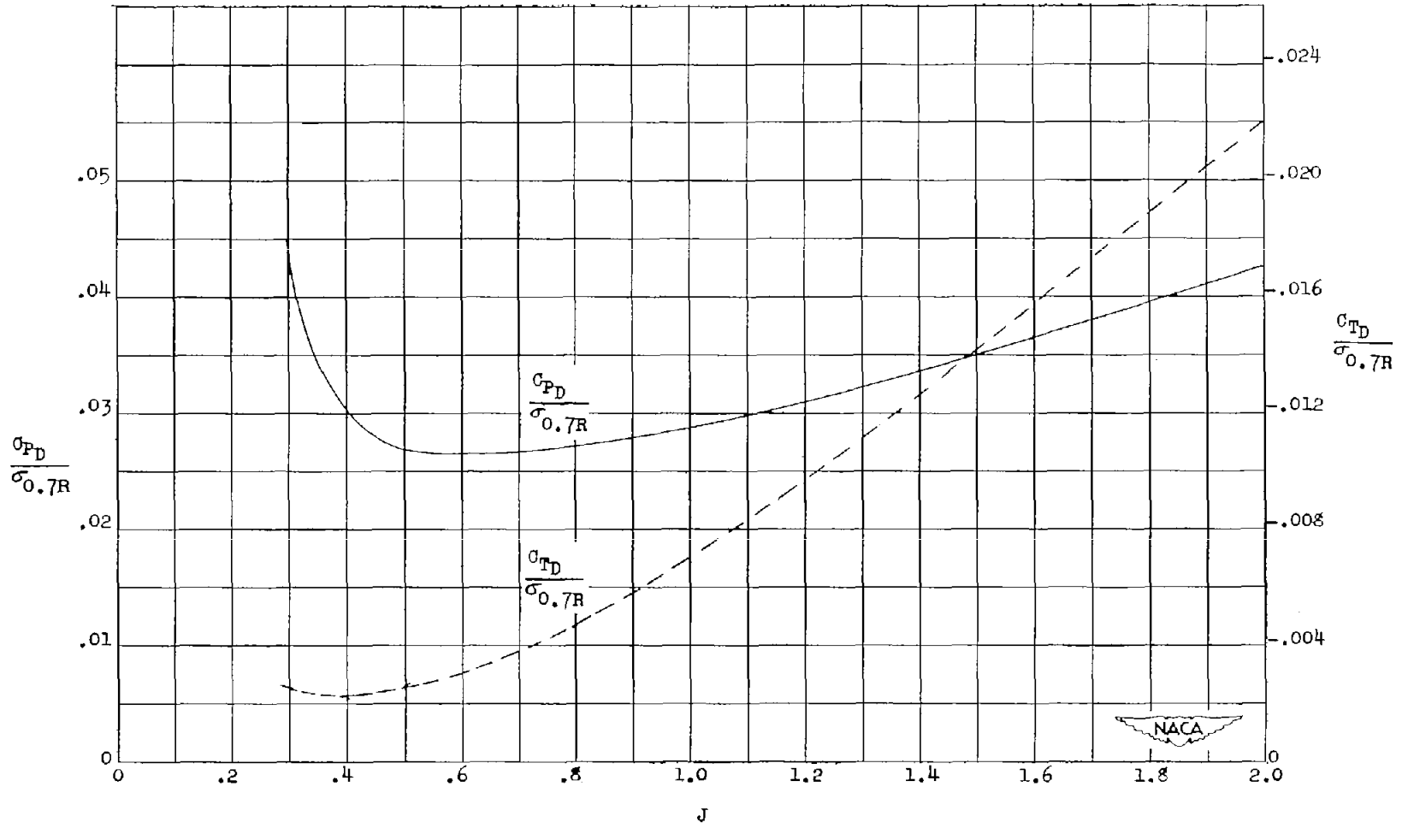

Figure 20.- Variation with advance ratio of thrust and power coefficients due to drag for typical transport propellers in terms of the propeller solidity at the 0.7R station. Curves apply to lift-coefficient range in which the drag coefficient remains approximately constant.

NACA-Langley - 7-10-53 - 1000